POLITECNICO DI TORINO
Repository ISTITUZIONALE

Density measurements in subcooled water at pressures up to 400 MPa

Original
Density measurements in subcooled water at pressures up to 400 MPa / Romeo, Raffaella. - (2016).

Availability:
This version is available at: 11583/2652785 since: 2016-10-11T17:50:21Z

Publisher:
Politecnico di Torino

Published
DOI:10.6092/polito/porto/2652785

Terms of use:
Altro tipo di accesso

This article is made available under terms and conditions as specified in the corresponding bibliographic description in the repository

Publisher copyright

(Article begins on next page)

04 August 2020

Politecnico di Torino

Department of Applied Science and Technology, DISAT

Ph.D. in Physics

Density measurements in subcooled water at pressures up to 400 MPa

Doctoral candidate:
Raffaella Romeo

Supervisor
Prof. Fabrizio Pirri

Tutors:
Dr Salvatore Lorefice
Dr Simona Lago

XXVIII Cycle
2013 - 2016

"It doesn't matter how beautiful your theory is, it doesn't matter how smart you are. If it doesn't agree with experiment, it's wrong."
Richard P. Feynman

Contents

List of Figures

List of Tables

Introduction

Besides being a vital substance for the known form of life, water affects every aspect of our lives: from climate and oceanography (it is the major component on Earth surface) to agriculture and public health. As one of the Aristotelian elements, water has long been central in the scientific thought. Its properties have a remarkable influence on the physical and chemical processes that are essential for life.

Despite many applications in industry and science, water is still pretty unknown and continuously under study, since it is a complex fluid with several anomalies, e.g. at atmospheric pressure the temperature of its maximum density is 4 °C. Even in the crystalline state it has many anomalies: water has thirteen known polymorphs, of which nine (ices II, III, V, VI, VII, VIII, X, XI and ordinary hexagonal ice, Ih) are stable, and four are metastable (ices IV, IX, XII and cubic ice, Ic).

Considering only atmospheric pressure states, the stable liquid range is limited by the equilibrium melting (0 °C) and boiling points (100 °C). However, liquid water can exist even outside the range of stability (below the melting temperature and above the boiling temperature) in precarious equilibrium, the so called "metastable states".

The thermodynamic states of liquid water below the normal freezing point (supercooled water) and above the normal boiling point (superheated water) are called metastable: at atmospheric pressure water can exist in the liquid state (stable and metastable) in the temperature range from -41 °C to 280 °C [1].

Metastability occurs when there is an energy barrier against nucleation of the stable phase. In homogeneous nucleation (i.e. nucleation as intrinsic properties of the system), a new phase is formed when some fluctuations overcome the free energy barrier and forms a nucleus of a critical size [2]. Supercooled water can be maintained if the sample is extremely pure, so that heterogeneous nucleation is avoided, if it is not subjected to vibration or an abrupt change in temperature.

At very low pressures, cooled and supercooled water is of interest in meteorology and atmospheric science: in cirrus and orographic wave clouds droplets of supercooled water have been observed at ambient pressure. The study of the microphysical properties, such as droplets size or the minimum

temperature before the droplets freeze that influence the rate of homogeneous nucleation [3], allows to understand ice nucleation mechanisms for cloud models simulating rain, hail, and cloud electrification. Incorporation of these changes in global circulation models will probably produce substantial changes in our understanding of the way that aerosols, clouds and precipitation are affecting the global climate [4].

In cryobiology supercooled water states can be used for the preservation of cells, proteins and organs [5]. For example, a recent study presented a method to extend organs storage with metabolic reduction, by using supercooling as a preservation technique. It was demonstrated that transplanted organs, such as livers, can be preserved for up to four days, thereby tripling the viable preservation duration with a higher survival rate after transplantation, with respect to the conventional technique [6]. Furthermore, at very high pressures (up to 300 MPa), different ices can be obtained during freezing processes (ice I and III).

Moreover, supercooled water can be exploited in food industry, in particular in the storage, thawing and deep freezing processes. For example, the presence of metastable supercooled liquid could allow large thermal gradients to be employed in the freezing process, permitting very reduced times, and greater amounts of ice instantaneously formed upon depressurization, thus avoiding tissues damage, maintaining quality and nutritional value of foods [7, 8].

However, this particular region of the water phase diagram needs to be accurately studied because of the lacking of accurate experimental data of the thermodynamic properties. Indeed, experimental measurements of subcooled water in literature are very few and their uncertainties, in some cases, are not clear [9]. Experimental measurements, especially of density, are also necessary because they form the basis to implement a fundamental equation of state, from which all thermodynamic properties can be calculated. Nowadays, the current international reference equation of state ("IAPWS Formulation 1995 for the Thermodynamic Properties of Ordinary Water Substance for general and Scientific Use" [10]), provided by the International Association for Properties of Water and Steam (IAPWS), not valid in the liquid metastable region. The density measure of water under 273 K and at pressures up to 400 MPa is one of the needs of IAPWS, to improve the equation of cooled water and to extend the equation to metastable states.

The purpose of this thesis project is to measure with high accuracy the density of cooled and supercooled water, i.e. in stable and metastable states, in the temperature range of (243 and 283) K, and at high pressures, from (140 to 400) MPa. The experimental work presented in this thesis was carried out at the *Istituto Nazionale di Ricerca Metrologica* (INRiM) laboratories of Turin, Italy. Furthermore, the paramount goal of performing accurate

experimental measurements is clear in the development of equation of state. With this aim, a complementary activity, consisting of the implementation of a fundamental equation of state, from experimental measurements, was carried out at the *National Institute of Standards and Technology* (NIST) in Boulder, Colorado. Two alkanes, *n*-hexadecane ($C_{16}H_{34}$) and *n*-docosane ($C_{22}H_{46}$), were chosen as first approach in this field, since they do not present several complexities like water, and above all are missing of the equation of state formulation even if are of interest in industrial field (e.g. aviation).

The thesis is divided into five chapters: the first four chapters refer to the experimental activity carried out at INRiM, while the last chapter concern the activity conducted at NIST. Chapter 1 introduces an overview about the measure of density at high pressures, with particular attention on the state of the art about experimental cooled water density. Furthermore, the principle of the measurement method used for this work is explained. In Chapter 2 the experimental apparatus designed and realized at INRiM, to measure subcooled water density, is presented. Chapter 3 explains how the volume and the amount of liquid were determined and reports the analysis of the uncertainty in detail. In Chapter 4, the experimental results are reported. The obtained results are analyzed by comparing them with the reference equation of state of the International Association for the Properties of Water and Steam (IAPWS), with the recent equation developed by Holten *et al.* [11] and with the previous experimental values of water density performed in the temperature and pressure range under study available in the literature.

Chapter 5 introduces the development of the equation of state starting from experimental data: two alkanes were studied, i.e. *n*-hexadecane and *n*-docosane.

Chapter 1

Density measurement

In this chapter, the main experimental methods commonly used to measure density of fluid at high pressure are reviewed. In particular, the attention is focused on the isochoric method that resulted the more adaptable method to study subcooled water at high pressure. Finally, the principle of the experiment used in this work is explained.

1.1 High pressure density measurement

The knowledge of the density is required to develop fundamental equations of state, custody transfer of fluids, industrial process design and implementation. The measurement of density at ambient conditions is an established analytical procedure, while there are still many problems in performing measurements at high pressure. The appropriate choice of measuring method or instrument is usually determined by the physical state of the sample to be tested, by the accuracy required and by the available sample quantity. However, experimental difficulties arise in many processes, where the influence of pressure, temperature and composition should be considered. Nowadays, the main standard methods used for high pressure measurements are:

- hydrostatic balance densimeter;
- vibrating tube densimeter;
- pycnometry;
- isochoric $p\rho T$ method.

In the following paragraphs, a brief description of the methods and measuring principles is reported.

1.1.1 Hydrostatic balance densimeter with magnetic suspension

The working method is based on the Archimedes' buoyancy principle: the upward buoyant force exerted on a body, the sinker, which is usually a sphere or cylinder of glass or metal of known mass and volume, immersed in a fluid is equal to the weight of the fluid that the body displaces. The fluid density, ρ, is expressed by

$$\rho = \frac{m_\mathrm{s} - m_\mathrm{s}^*}{V_\mathrm{s}} \tag{1.1}$$

where m_s is the "true" mass of the sinker weighted in vacuum, m_s^* is the "apparent" mass of the sinker immersed in the liquid sample and V_s is the volume of the sinker.

With this method, the density is obtained directly thus calibration fluids are not required. A combination of the Achimedes principle with magnetic suspension allows to reach wide-ranging measurements. A magnetic suspension coupling transmits the weight of the sinker to the analytical balance, and separates the fluid, which may be at extremes of temperature and pressure, from the balance at ambient conditions [12]. The coupling consists of a permanent magnet connected by a thin wire to the sinker support, an electro-magnet attached to the weighting hook on the underside of the balance, and a position sensor and a control system [13]. This technique allows measurements at pressures up to 200 MPa with an uncertainty in order of 0.01%.

1.1.2 Vibrating tube densimeter

The vibrating tube densimeter consists of a glass or metallic U-shaped capillary tube, with a volume of a few cm^3, isolated in a thermostated cell. The tube is filled with a sample of interest and vibrates perpendicular to its plane by means of a piezoelectric transducer. The period, τ, of the harmonic oscillation of the tube can be directly related to the density, ρ, of the fluid contained in the tube by:

$$\rho(T,p) = A(T,p)\tau^2(T,p) - B(T,p) \quad , \tag{1.2}$$

where A and B, both temperature and pressure dependent, are characteristic parameters of the instrument, defined as

$$A = \frac{K(T,p)}{4\pi^2 V(T,p)} \quad ; \quad B = \frac{M_0}{V(T,p)} \quad , \tag{1.3}$$

where K is the tube stiffness, V is the tube inner volume and M_0 is the evacuated tube mass. The instrument parameters are determined by measuring period in two reference fluids of well-known density. To simplify the calibration procedure, the period is usually measured in the evacuated tube and e.g. in water.
Even if vibrating tube densimeter has become the choice for routine and very accurate measurements, commercial instrument allows to measure density at pressures up to 140 MPa.

1.1.3 Pycnometry

Pycnometry can be an alternative method for density measurements, being usually less affected than vibrating tube by the physical properties of the examined fluid, i.e. viscosity and surface tension. Pycnometers are usually flasks of different shapes and materials (usually glass or metal for higher pressures) which volumes are known and filled with the liquid to be measured [14].

The measurement procedure consists of two steps: the determination of the pycnometer volume and the determination of the mass of fluid contained in the pycnometer.
The volume is obtained by measuring the mass of the empty pycnometer, M_0, and the mass of the pycnometer, M_{ref}, filled with a reference liquid of known density, ρ_{ref} at a fixed temperature T and pressure p:

$$V(T,p) = \frac{M_{\text{ref}} - M_0}{\rho_{\text{ref}}(T,p)} \quad . \tag{1.4}$$

Then, the pycnometer is filled with the fluid sample at a nominal temperature and compress by using a hand pressure pump. The pressure is adjusted to the nominal value after having reached the temperature equilibrium. Pressure and temperature are recorded for a long time before the pycnometer is closed by means of a valve. By weighing the pycnometer empty, M_0, and filled with the studied fluid, M, the mass of the sample, m, is determined. Finally, the unknown density is calculated by

$$\rho(T,p) = \frac{M - M_0}{M_{\text{ref}} - M_0}\rho_{\text{ref}}(T,p) = \frac{m}{V(T,p)} \quad . \tag{1.5}$$

To measure density over a wide (T,p) range, the volume of the pycnometer has to be corrected taking into account the deformation due to the effect of temperature and pressure.

1.1.4 Isochoric $p\rho T$ method

Among the methods used to measure density of fluids at very high pressure, the isochoric method is usually the best choice. This is because this approach allows relatively safe handling of hazardous fluids working in very critical operative conditions, since the samples are contained in a static pressure vessel during the entire experiment [15]; moreover, it allows to reach very high pressure. For that reason, isochoric method is one of the most used technique.

The isochoric apparatus usually consists of a high pressure cell placed into a thermostatic bath to control the temperature. The cell is filled with the fluid sample which can be compressed by a hand pump system to reach the desired pressure. After having changed the temperature, when the sample achieves the equilibrium, pressure and temperature are measured. The density is estimated from the volume of the cell and the mass of fluid inside it. Actually, the volume of a cell often cannot be considered constant, because of its dependence by temperature and pressure, the method is usually designated as pseudo-isochoric. The volume of the cell is measured at a reference temperature and pressure, usually by filling with a well known liquid and weighting the cell. Once the reference volume is known, the volume at different measuring conditions is determined from the knowledge of the thermal expansion and the mechanical deformations of the cell material. The various methods are distinguished by the different techniques used to determine the volume of the cell or the amount of fluid inside it. The isochoric method is widely used, because is the technique that permits to reach the higher pressures (up to 400 MPa).

1.2 Methods for subcooled water density measurement

Measure of density in stable and, especially, in metastable states of water is rather complicated because, in addition to the difficulties in achieving very high pressures, many problems occur in maintaining the temperature and avoiding crystallization. For these reasons, currently there are only a very few subcooled water density values determined experimentally.

Among the several methods, the technique more adaptable to the requested extreme conditions is a modified version of the before cited isochoric method. In fact, the high-pressure cell can be constructed to reach even pressures up to 400 MPa; the sample can be isolated in the cell without vibration and maintained in metastable states. Indeed, all the experiments performed up to date have been based on this technique.

1.2.1 State of the art

Focused in particular on pressure range of interest, between (140 and 400) MPa, currently there are just a few works reporting experimental values of subcooled water density. Table 1.1 summarizes the works concerning subcooled water measured in temperature and pressure ranges laying, at least in part, in the range under study, and the claimed uncertainty in density.

Firstly, Sotani *et al.* (2000) measured specific volume at pressures up to 200 MPa from (253 to 293) K along 11 isotherms. The measurements were carried out through the isochoric method, mainly consisting of a sample cell and a high-pressure burette. The volume change of the sample was determined by measuring the meniscus displacement of mercury in the burette used as a piston to compress the water sample of known mass. Specific volume was obtained taking into account also the correction for volume changes due to burette and cell deformation and mercury compression [16] with the following relation:

$$v = v_0 - \frac{\Delta V_{\text{app}} - \Delta V}{m} \quad ,$$

where v_0 is the specific volume at reference condition, m is the sample mass, V_{app} is apparent volume change calculated from the meniscus displacement and ΔV is the volume change correction.

The work was continued by Asada *et al.* (2002) [17], that measured water density, though the same experimental apparatus, at temperatures between (253 and 298) K and in the pressure range of (210 and 380) MPa, with an uncertainty of 0.1%. However, the experimental values are not given neither in the papers [16] [17] nor in supplemental materials; Holten *et al.* extracted their experimental values from the graphs [11].

The work of Guignon *et al.* (2010) [18] reports experimental data of water specific volume between (253 and 273) K and for pressures up to 350 MPa. A variable-volume piezometer with a solid-piston volumometer was used: it consisted of a stainless steel vessel containing the water sample and closed by a piston. A rod with a ferromagnetic core was screwed to the piston and placed into a capillary tube. Volume changes of the sample caused piston movements transferred to the ferromagnetic core and detected by the Linear Variable Differential Transformer (LVDT). The specific volume was determined as a function of pressure at constant temperature, along 10 isotherms, starting from the known reference value and measure the specific volume change owing to pressure increase. The uncertainty in density resulted in the order of 0.2%.

Finally, measurements reported by Mishima (2010) [19] were carried out at temperatures between (200 and 275) K and from (40 to 400) MPa.

An emulsion of water with a matrix of hydrocarbons (methylcyclohexane, methylcyclopentane and sorbitan tristerate) with a homogenizer was sealed in an indium container of fixed weight. The sample was compressed in a steel cylinder, keeping constant the temperature. During the pressure changes, at each temperature, the displacement of the piston, used to compress the emulsion sample, was measured. To determine the correction, compression of a sample composed just by the matrix substances (so without measuring water) and compression of just the indium containers were measured. By subtracting the values of the indium and matrix displacements, the specific volume of the matrix was obtained. Instead, the specific volume of water was obtained by subtracting the matrix volume in each emulsion measurement. The uncertainty in the matrix weight caused an uncertainty in the volume around 2%. For this reason, the measured specific volumes were shifted by the author to be in agreement with the density data of Kell and Whalley [20]. The final uncertainty of density was not explicitly reported in the paper.

Figure 1.1 shows the distribution of the measured thermodynamic states [11]. Focusing on the (T, p) region of interest, it is evident the need of more experimental data because just the Mishima's values were carried out below 253 K, so there are very few data in metastable states.

Table 1.1: Literature experimental density data of subcooled water at high pressure.

Authors	Year	Temperature/K	Pressure/MPa	Uncertainty
Sotani *et al.*	2000	253 - 298	0.1 - 200	0.01%
Asada *et al.*	2002	253 - 298	210 - 380	0.1%
Guignon *et al.*	2010	253 - 273	0.1 - 350	0.2%
Mishima	2010	200 - 275	40 - 400	undeclared

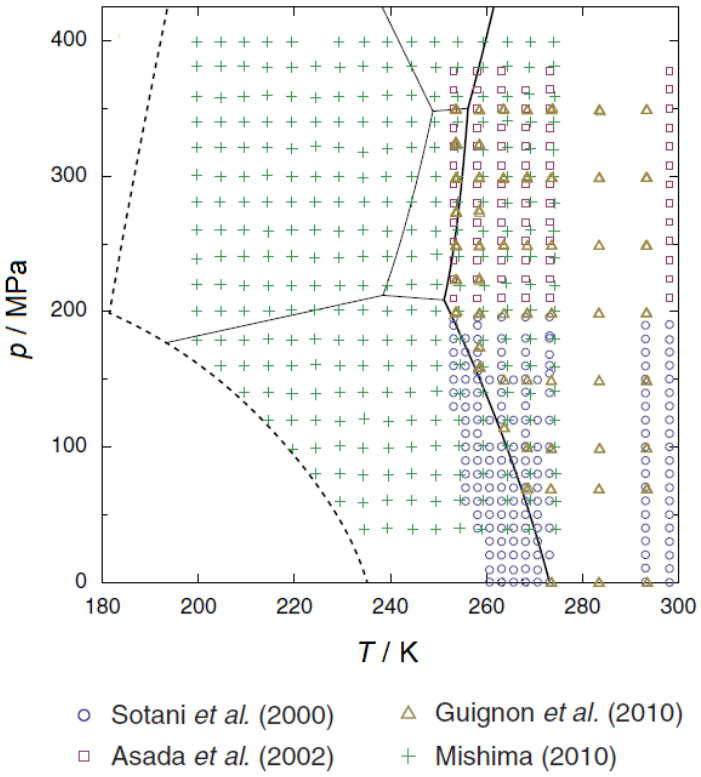

Figure 1.1: Location of experimental data of water density measured at high pressure.

1.2.2 Principle

In the work presented in this thesis, a pseudo-isochoric method was adopted for measuring subcooled water density up to 400 MPa and for temperatures down to 243 K. The technique consists in temperature and pressure measurements, using a high-pressure pseudo-isochoric cell connected by a valve to an expansion cell, employed to determine the mass of fluid. The measurement procedure requires to fill the main cell with the sample of water at a starting state of high pressure and at the desired temperature, while the expansion cell is isolated by the valve. Then, the temperature is decreased or increased of about 1 K in 3 hours and, when the new (T, p) state of equilibrium is reached, the pressure is measured. Therefore, each measuring curve is obtained at constant mass. According to the general definition, the density measurement consists of determining the mass and the bulk volume. This latter is independently determined firstly by measuring through the gravimetric method at reference condition (about 293 K and 80 MPa), and then by correcting this value taking into account also the thermal and the mechanical expansion of the high pressure measuring cell.

$$V(T,p) = V_0(T_0,p_0)\left[1 + \alpha(T - T_0) + \beta(p - p_0)\right] \quad , \tag{1.6}$$

where V_0 is the volume measured at the reference (T_0, p_0) condition, α is the thermal expansion coefficient and β the compressibility coefficient of the cell.

To determine the amount of water, at the end of each measuring cycle, the sample is expanded into the evacuated expansion cell linked to the main cell by opening the valve. In this way, the volume of the system increases and a new state of equilibrium at lower pressure (always below 10 MPa) and higher temperature (always above 273.15 K) can be reached, where density is known with an uncertainty of 0.001% [10]. Since the amount of water has been kept constant during the whole measuring cycle, its value is determined by the literature density, ρ' (at the final measured temperature and pressure) and the volume occupied by the sample, which, in this case, corresponds to the measuring cell and the expansion cell, at the final state of standard temperature and pressure:

$$m = \rho'\left(T', p'\right)\left[V'\left(T', p'\right) + v\left(T', p'\right)\right] \quad . \tag{1.7}$$

Afterwards, the density, ρ, was calculated by the ratio between the mass of water, m, and the volume of the measuring high pressure vessel, V, at each measured (T, p) thermodynamical point, according to the following relation

$$\rho\left(T,p\right) = \frac{m}{V(T,p)} = \frac{\rho'\left(T', p'\right)\left[V'\left(T', p'\right) + v\left(T', p'\right)\right]}{V(T,p)} \quad , \tag{1.8}$$

where ρ', and v are respectively the water sample density, the volume of the measuring cell and the volume of the expansion cell at the final equilibrium state, at temperature $T' > 273.15$ K and pressure $p' < 10$ MPa.

Chapter 2

Experimental apparatus

In this chapter, the experimental apparatus, based on the pseudo-isochoric method, used to carry out density measurements in subcooled water, is presented.

The apparatus, realized *ex novo* at INRiM, is schematically shown in Fig. 2.1 and pictured in Fig. 2.2. The measurement device can be divided in three main parts: the first one consisting of the main pseudo-isochoric cell and the expansion cell containing the fluid, the second one is dedicated to increase and adjust the pressure, and the third one to control the temperature.

2.1 Measurement cell

The core of the experimental apparatus consisted of a main temperature controlled high-pressure vessel and the expansion cell used to determine the mass of water in the further step. The material and dimensions of the measurement cell were chosen with the aim of reaching pressures up to 400 MPa.

Usually materials with low thermal expansion coefficients are desirable for vessel construction. The cell should have a high thermal conductivity and low heat capacity; in this way the temperature of the cell could change quickly from one temperature set point to another. For a better and faster temperature control, the thermal mass of the cell should be minimized by reducing the total mass of the cell [13]. Additionally, to achieve very high pressure, the vessel requires a material with high tensile strength. Since the determination of the cell volume was performed by an analytical balance, the internal volume should contain amount of fluid enough to minimize the ratio between the balance resolution and the sample weight. Taking into account these main requirements, stainless steel resulted the material with the better characteristics for the project purpose.

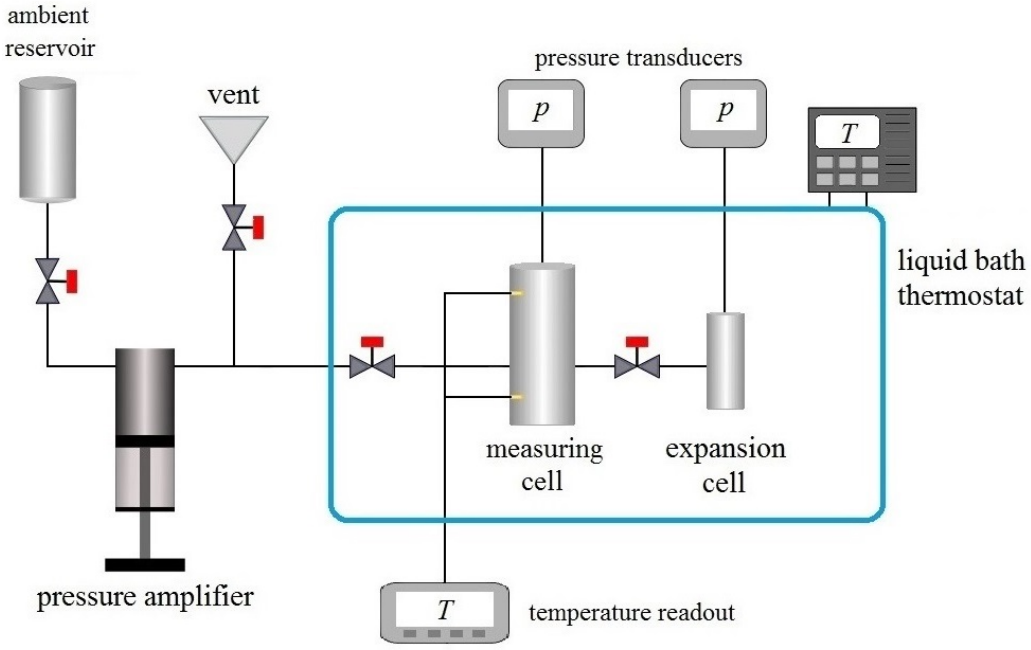

Figure 2.1: Schematic representation of the experimental apparatus.

Furthermore, considering the tensile strength of stainless steel ($\sim$ 515 MPa for AISI 304) and the maximum working pressure, the wall thickness that the vessel must have, was calculated with the following formula [21]

$$p_{\max} = 0.85Y \log\left(1 + \frac{D-d}{d}\right) \tag{2.1}$$

where $p_{\max}$ is the maximum pressure reached, Y is the tensile strength, D and d are respectively the external and internal diameter of the cell.

2.1.1 An aborted preliminary measurement cell

The first realized high-pressure vessel consisted of a cylindrical body, shown in Fig. 2.3(a), open on the both sides and closed by two flanges, such as the one shown in Fig. 2.3(b), made of AISI 304 stainless steel. The body had an internal diameter and height of 20 mm and 70 mm respectively, so the internal volume was about 22 cm^3. Moreover, the shape of two openings of the body and the two flanges were designed, as shown in the schematic representation of Fig. 2.4, to hold two copper gaskets with an external diameter of 38 mm, an internal diameter of 18 mm and a height of 3 mm. Figure 2.5 shows the cell assembled to be tested. This vessel was filled with

Figure 2.2: Experimental apparatus.

ethanol at room temperature and the pressure increased. The maximum pressure achieved was about 180 MPa.

To reach higher pressures, the cell was modified by adding a tooth on the indentation of the both sides of the body (see Fig. 2.6(a)) and on the two flanges (see Fig. 2.6(b) as an example) to incise and warp the gaskets for a better sealing. Nevertheless, with this configuration the cell was not able to reach a pressure higher than 200 MPa; the problem was due to the type of sealing that did not cause a sufficient deformation of the gasket. For that reason, a completely new cell had to be designed.

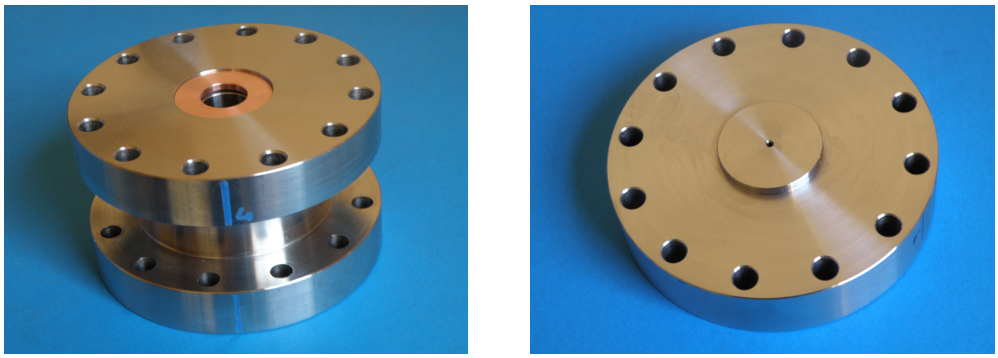

(a) (b)

Figure 2.3: Pictures of the body of the preliminary cell with the gasket (a) and one of the flange (b).

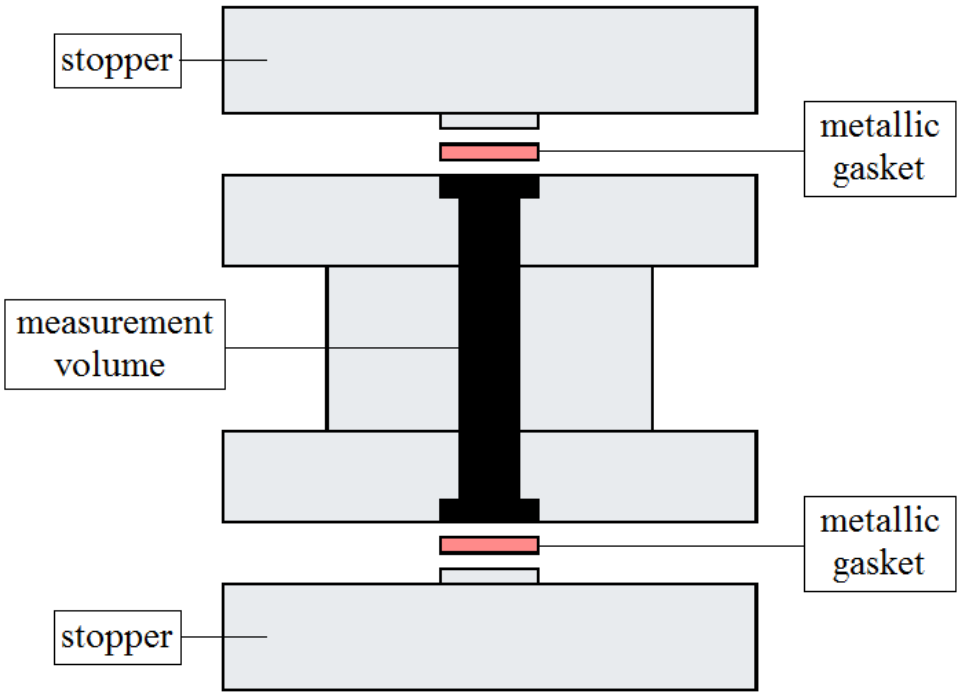

Figure 2.4: Schematic representation of the first version of the cell.

Figure 2.5: Photograph of the preliminary cell.

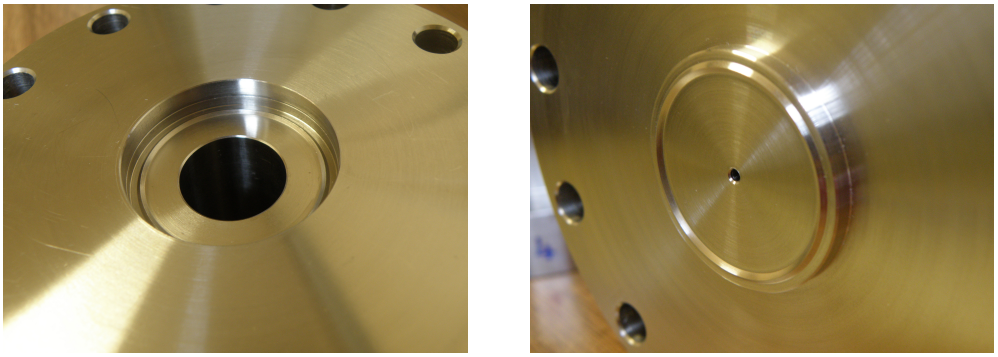

(a) (b)

Figure 2.6: Photographs of the body (a) and the flange (b) of the preliminary cell after the modifications.

2.1.2 Final version of the measuring cell

The new measuring cell was a high-pressure vessel with a cylindrical body machined of AISI 304 stainless steel, shown in Fig. 2.8(a). The body had an external diameter of 80 mm and the height was approximately 125 mm. At the center of the body, the internal volume containing the sample had a diameter of 20 mm and a height of approximately 60 mm: thus the volume is about 19 cm^3. The body had also a conical indent to hold a plug. The vessel was closed by an AISI 304 stainless steel gland, shown in Fig. 2.8(b), with squared thread and with a 40 mm diameter. Into the gland a titanium semi-conical plug (see Fig. 2.8(c)) was inserted: it had the maximum diameter of $\sim$ 30 mm and the height of $\sim$ 10 mm. The sealing was due to the peculiar shape of the titanium plug that was designed with an angle of 40° allowing to achieve the maximum pressure of 400 MPa. Figure 2.7 schematically shows the working components of the assembled pseudo-isochoric cell.

Finally, the cell was tested many times and the pressure stabilization was obtained up to 400 MPa.

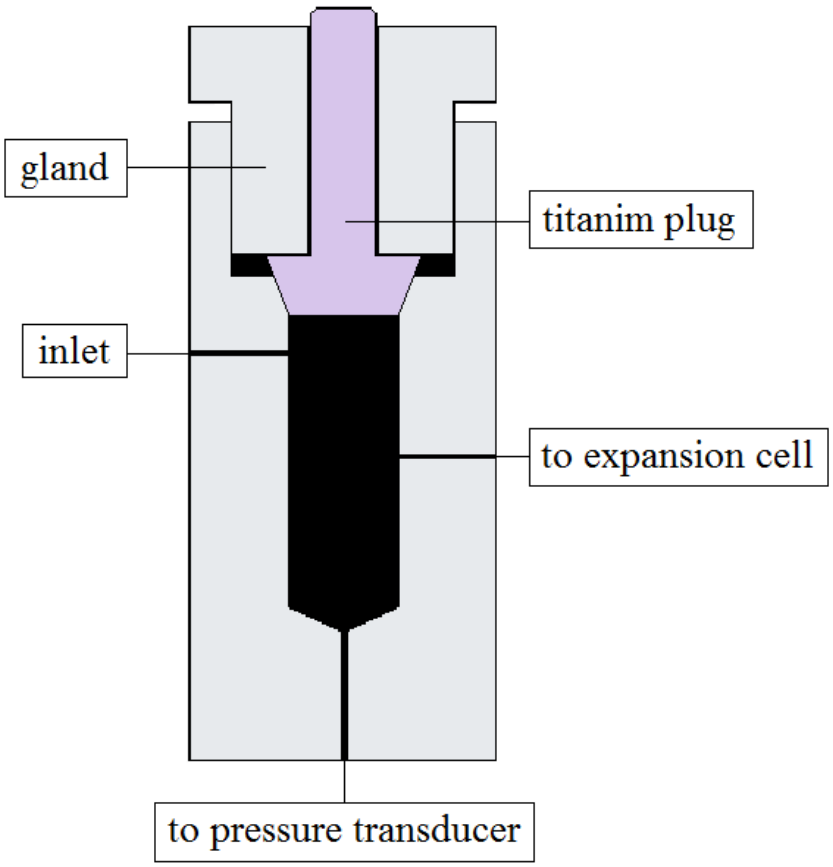

Figure 2.7: Schematic representation of the measuring cell.

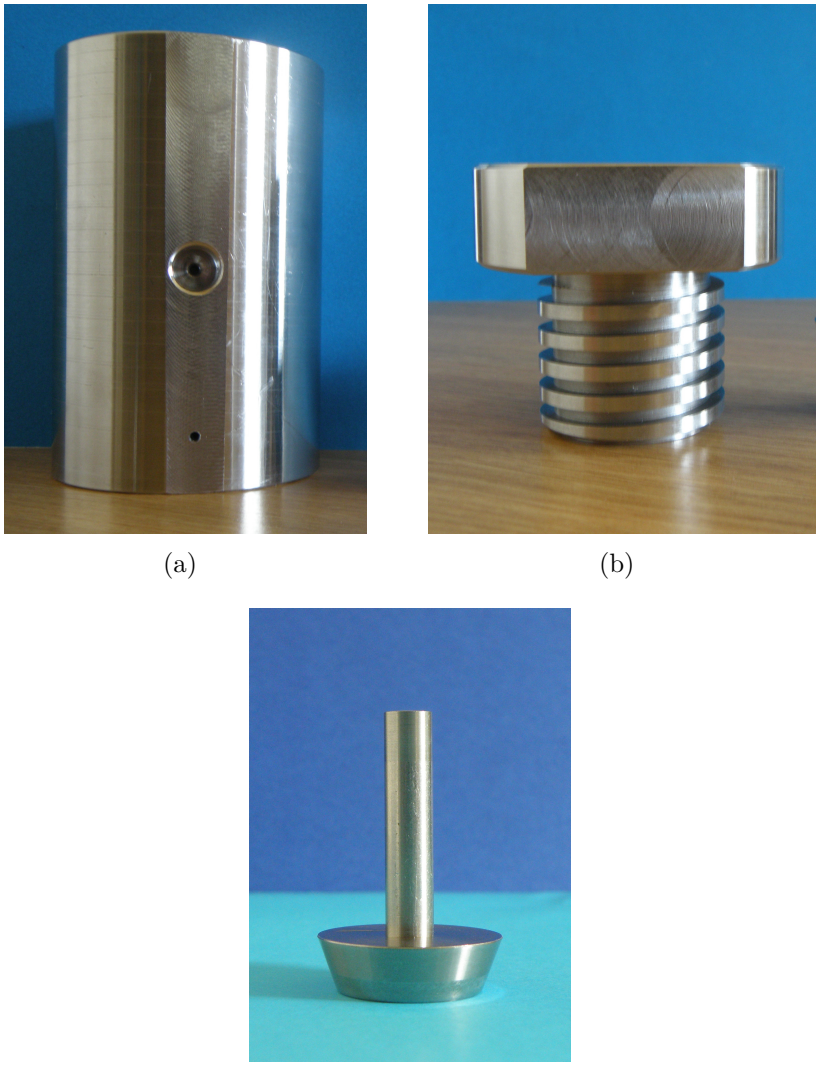

(a) (b)

(c)

Figure 2.8: Photographs of the stainless steel gland (a), the titanium plug (b) and the stainless steel body (c) of the final version of the cell.

2.2 Expansion cell

The expansion cell, shown in Fig. 2.9, was manufactured at INRiM. This cell was projected in order to have a volume that, added to the main volume, permitted the sample to reach a new equilibrium state at a pressure lower than 10 MPa above 273 K. In order to project the cell, the volume necessary was roughly calculated considering the volume of the main high-pressure vessel and the maximum and minimum densities expected to be achieved during the measurements. The minimum amount of water to be measured and contained in the main vessel (of known volume V_0) was

$$m_{\min} = \rho_{\min} \cdot V_0$$

where the minimum density value, $\rho_{\min}$, expected in the $T - p$ range to be measured was taken from the literature [10]. The volume at the end of the measuring cycle, V_{tot}, was given by the sum of the main vessel and the expansion cell, $v_{\min}$, and is equal to

$$V_{\text{tot}} = V_0 + v_{\min} = \frac{m_{\min}}{\rho} \quad ,$$

where ρ is the density given by the literature at 283 K and 5 MPa. The minimum volume for the expansion cell resulted from the following relation

$$v_{\min} = V_{\text{tot}} - V_0 \quad .$$

Similarly, the maximum value suitable for the expansion cell was calculated. It has to be noted that these were extremely rough calculations, performed just to qualitatively estimate the dimensions of the expansion cell.

Therefore, the expansion cell was a cylinder made of AISI 304 stainless steel with an internal diameter of approximately 12 mm, while the external diameter was 18 mm and the height was 26 mm. Hence, the volume of the chamber of the expansion cell was about 3 cm^3. The actual volume had to take into account also the volumes of the tube connecting the cell to the valve towards the main cell and the tube connecting the pressure transducer and its internal volume. The seal of the expansion cell was checked by pressurizing it, at ambient temperature, up to 20 MPa.

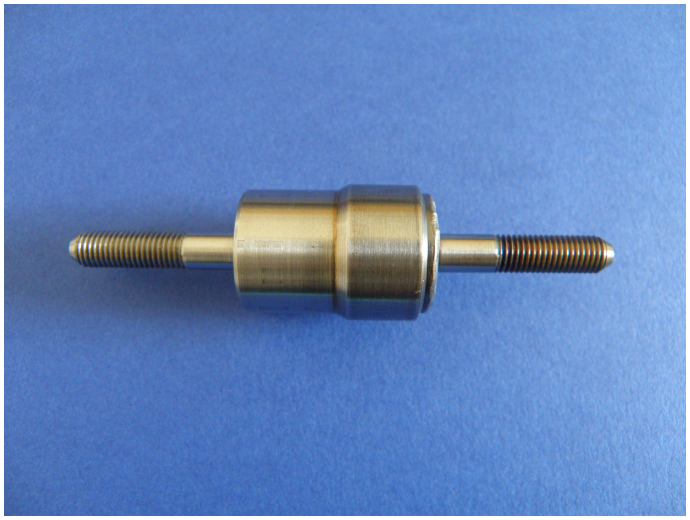

Figure 2.9: Picture of the expansion cell.

Figure 2.10 shows the final configuration of high-pressure vessel connected by the high pressure valve to the expansion cell, with the corresponding pressure transducers. The main vessel was also linked to another valve aimed to isolate the cell from the high-pressure circuit.

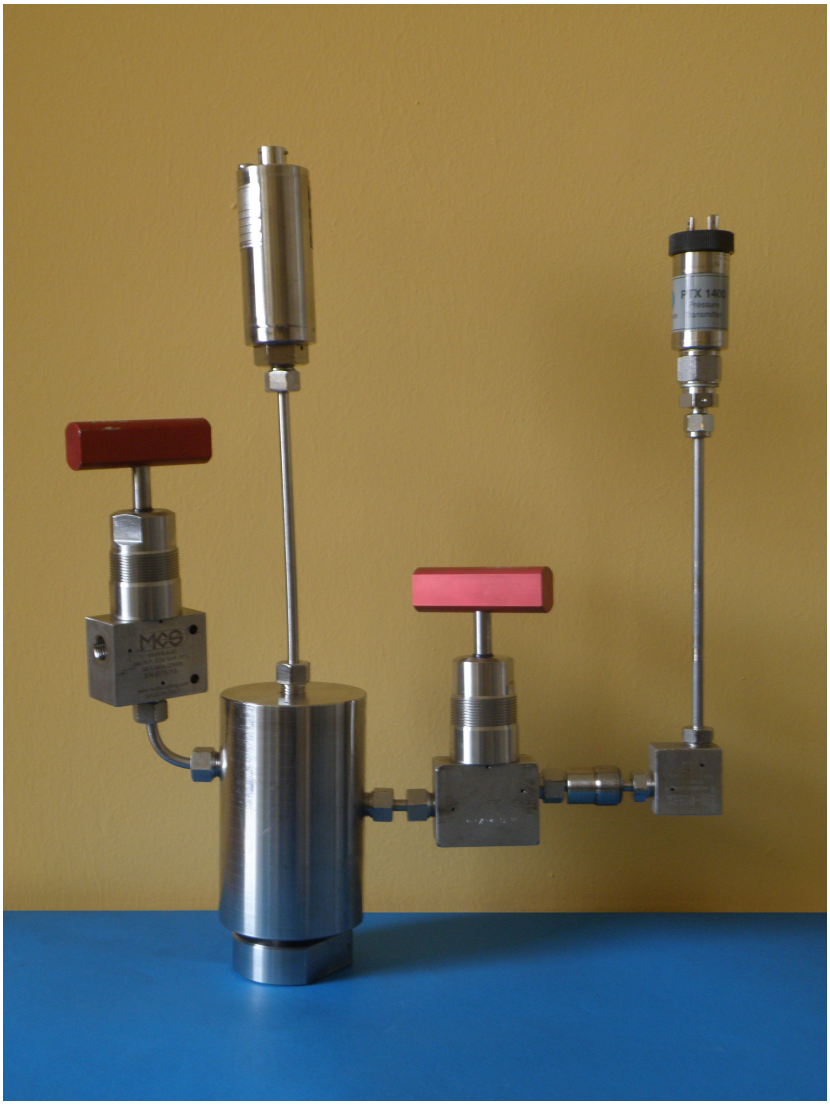

Figure 2.10: Picture of the high-pressure vessel and the expansion cell connected together by the valve and with the used pressure transducer.

2.3 High pressure system

In order to fill the vessel with the water sample and increase the pressure, the cell was linked to a high-pressure system consisting of a high-pressure circuit and a hand pump pressure amplifier, as shown in Fig. 2.11.

The high-pressure circuit was composed by stainless steel 1/4" tubes, high-pressure valves, used to isolate the different part of the system, and a manometer to firstly and approximately check its pressure. The pressure was generated and controlled by the manual hand-pump pressure amplifier, which was a cylinder-piston operating by mechanic screwing, connected by tubes and a valve to the reservoir containing the liquid sample at ambient pressure. The pressure amplifier was used to take the sample from the reservoir and fill the pseudo-isochoric cell. Moreover, another valve connects the high-pressure system to a mechanical vacuum pump to evacuate the circuit and the pseudo-isochoric and the expansion cells before starting the measurement cycle, and also to avoid air bubbles or any trace of the fluid, previously used to clean the circuit, in the liquid sample.

The pressure was measured by means of two different capacitance pressure transducers with two different full-scale ranges, chosen in order to minimize the pressure uncertainty, connected to the pseudo-isochoric cell and the expansion cell respectively (see Fig. 2.10). Inside the cell, the pressure was measured by a Honeywell TJF, with a full-scale range of 400 MPa (nominal accuracy ±0.1%), during the measuring cycle. The transducer connected to the expansion cell was a Druck PTX1400, with a full-scale range of 10 MPa (nominal accuracy ±0.15%) and it was employed for pressure measurements during the mass determination. The pressure transducers were supplied with an input voltage of approximately 18 V (by the Kepco Power Supply) and the output voltage was measured with a multimeter (Agilent 34410A). A program implemented in LabView, by means of the calibration curve that converts voltage into pressure, was used to record the pressure measurement.

2.4 Temperature control system

The other parameter to be accurately checked was the temperature. For this purpose, the cell and the expansion cell were placed into a liquid bath thermostat Lauda UD20 (with a stability of ±0.01 K), with a Proportional-Integral-Derivative controller (PID). The bath opening, where the cell was put into, has the width of 40.5 mm, the depth of 13.5 mm and the usable bath height is 26.5 mm, but totally the thermostat required approximately 20 l of thermostatic fluid. This thermostat was linked to another liquid bath thermostat, a Julabo FP50 with a stability of ±0.01 K, deployed as

chilling unit. It had to be filled with 8 l of thermostatic fluid. For both the thermostats, ethanol was used as thermostatic fluid. The thermostats, and the tube connecting them, were covered with flexible elastomeric foam to improve the thermal insulation. The temperature was measured by two platinum resistance PT100 thermometer placed at the top and at the bottom of the cell. In this way, the thermal gradient due to the stratification of the thermostatic fluid was considered. The thermometers were previously calibrated at INRiM in the temperature range from (223 to 353) K, by comparison with a standard PRT against ITS-90, causing an uncertainty within ±0.01 K. Before each measuring cycle they were again tested at the triple point of water. The thermometers were connected in four wire configuration to two channels of an available industrial thermometer bridge (Hart Scientific 1560 Black Stack with a resolution of 0.005 K), and the measurements were recorded by a program implemented in LabView.

The system used to control and measure the temperature, consisting of the two liquid bath thermostats and the temperature readout, is shown in Fig. 2.12.

Figure 2.11: Picture of the high-pressure circuit and the pressure amplifier.

Figure 2.12: Picture of the temperature control system.

Chapter 3

Volume and mass determination

In this chapter, the cell's volume measurement at reference conditions and the calibration procedure, to determine the correction for the effect of temperature and pressure, are explained. Moreover, the analysis of the uncertainty is reported. Finally, preliminary measurements in a temperature and pressure range of known density performed to verify the experimental method are presented.

3.1 Reference volume determination

The accurate determination of the volume is a fundamental step for the isochoric (or pseudo-isochoric) method, also to reduce the final uncertainty on the density measurement. During the measuring cycle at constant mass, the volume occupied by the fluid was the sum of the internal volume of the vessel, the volume of the tubes connecting the valves and the internal volume of the pressure transducer. Similarly, the volume of the fluid at the final stage (when the sample mass has to be determined) consisted of the previous one plus the internal volume of the expansion cell, its tubes and the internal volume of the corresponding pressure transducer. The total volume was estimated by using the gravimetric method.

3.1.1 Gravimetric method

The gravimetric method is the standard method used to calibrate instruments volume [22]. The general method consists of weighing the instrument both empty and filled with a reference fluid of known density, at a specific

temperature and pressure. For the determination of the measuring cell volume, water was chosen as a reference fluid, considering the density values given by the IAPWS-95 formulation [10].

For the volume determination a commercial analytical balance (Mettler XP10003) was used as a comparator, with stainless steel standards masses (Mettler Toledo 470). The technique used for each weighing (the empty and filled cell) was the double substitution weighing. It is generally used to perform high accuracy measurements by comparing the weight of the object to be studied with standard masses of similar nominal value. Sometimes it is necessary to use as standard several calibrated weights, or additional masses in the object weighing to make a closer value [23]. When a weight A (the standard masses) is compared with a weight B (the object), there is a difference ΔR between the two readings with each of the weights on the pan, expressed as:

$$A = B + \Delta R \quad . \tag{3.1}$$

For each weighing, the $ABBA$ calibration scheme was used. It consisted in applying in the pan of the balance the weights and recording the values in the following order: standard masses (reading A_1), object (reading B_1), object (reading B_2) and standard masses (reading A_2). The mass difference in this case was given by

$$\Delta R = \frac{A_1 + A_2}{2} - \frac{B_1 + B_2}{2} \quad . \tag{3.2}$$

Thus, considering the weighing for the empty cell, firstly the standard masses were placed on the balance pan and the reading A_1 recorded. The empty cell was weighted, as shown in Fig. 3.1(a), placing twice on the pan, to have two independent readings B_1 and B_2, as shown in Fig. 3.1(b). Then, the standard masses were weighted recording the reading A_2. This procedure was repeated 10 times.

The mass of the empty cell, M_0, was given by the value of the standard masses provided by the calibration and the difference between the readings:

$$M_0 = M_{\mathrm{eq}} + \Delta R \quad . \tag{3.3}$$

Finally, the value of Eq. 3.3 had to be corrected by adding the term for the buoyancy:

$$M_0 \left(1 - \frac{\rho_{\mathrm{a}}}{\rho_{\mathrm{s}}}\right) \quad , \tag{3.4}$$

where ρ_{a} is the air density during the weighing, and $\rho_{\mathrm{s}} = 8\ \mathrm{g \cdot cm^{-3}}$ is the standard weights density.

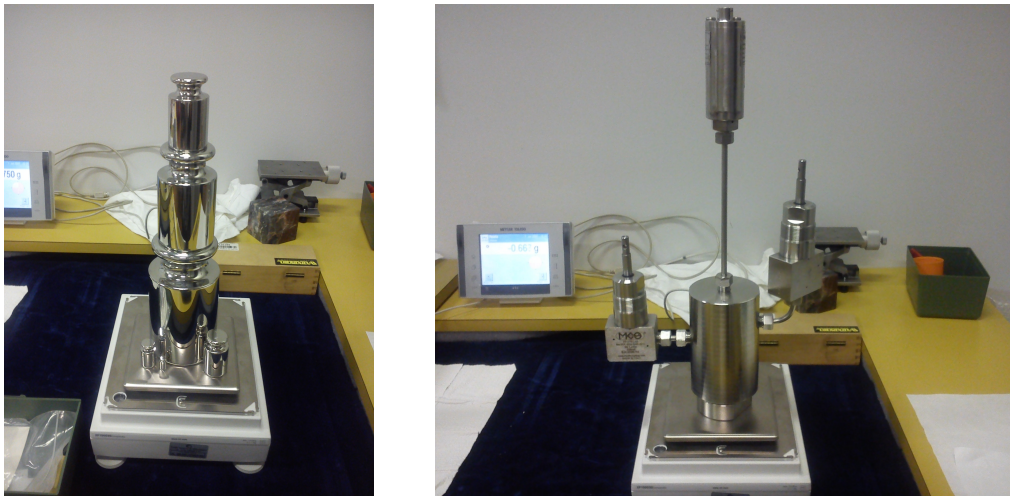

(a) (b)

Figure 3.1: Photographs of the analytical balance during the sample masses weighing (a) and the cell weighing.

Then, the cell was filled with water (the reference fluid) at (293.16 ± 0.01) K and (80.0±0.4) MPa and, after the stabilization, the $ABBA$ weighing procedure repeated. According to Eq. 3.4 the mass of the filled cell was given by:

$$M_{\mathrm{w}} \left(1 - \frac{\rho_{\mathrm{a}}}{\rho_{\mathrm{s}}}\right) \quad . \tag{3.5}$$

The weighing for the empty cell was again performed. During each weighing the air density was measured.

The volume was estimated by the difference between the empty and filled cell and by the reference water density [10]. The equation for the volume determination was thus $V = \frac{M}{\rho}$ or

$$V_0(T_0, p_0) = \frac{M_{\mathrm{w}} - M_0}{\rho_{\mathrm{w}}(T_0, p_0) - \rho_{\mathrm{a}}} \left(1 - \frac{\rho_{\mathrm{a}}}{\rho_{\mathrm{s}}}\right) \quad , \tag{3.6}$$

where ρ_{w} is the water density at the filling temperature T_0 and pressure p_0.

The volume of the measuring cell was determined, at the temperature of 293.16 K and the pressure of 80.0 MPa, as

$$V_0 = (21.915 \pm 0.002)\ \mathrm{cm}^3 \ . \tag{3.7}$$

The volume of the expansion cell (considering also the volume of the tubes, valve and pressure transducer) was similarly determined by the gravimetric

method, following the procedure described. The expansion cell volume was measured at (294.93 ± 0.01) K and (9.7 ± 0.1) MPa, and its value was

$$v_0 = (3.664 \pm 0.001)\ \mathrm{cm}^3\ . \tag{3.8}$$

3.1.2 Uncertainty analysis of the reference volume and the expansion cell

The uncertainty of the reference volume, V_0, of the pseudo-isochoric cell was determined by applying the error propagation formula to Eq. 3.7, considering the contributions of the mass of the fluid ($\Delta M = M_\mathrm{w} - M_0$), the density of water, air and standard weights, and the filling temperature and pressure:

$$V_0 = V_0(\Delta M, \rho_\mathrm{w}, \rho_\mathrm{a}, \rho_s, T_0, p_0)\ \ .$$

By applying the error propagation to V_0, the relative uncertainty, $u(V_0)/V_0$, is expressed by

$$\frac{u(V_0)}{V_0} = \frac{1}{V_0}\left[\left(\frac{\partial V_0}{\partial \Delta M}\right)^2 u^2\left(\Delta M\right) + \left(\frac{\partial V_0}{\partial \rho_\mathrm{w}}\right)^2 u^2\left(\rho_\mathrm{w}\right) + \left(\frac{\partial V_0}{\partial \rho_\mathrm{a}}\right)^2 u^2\left(\rho_\mathrm{a}\right) + \left(\frac{\partial V_0}{\partial \rho_\mathrm{s}}\right)^2 u^2\left(\rho_\mathrm{s}\right) + \left(\frac{\partial V_0}{\partial T_0}\right)^2 u^2(T_0) + \left(\frac{\partial V_0}{\partial p_0}\right)^2 u^2(p_0)\right]^{\frac{1}{2}}\ . \tag{3.9}$$

The mass uncertainty, $u(\Delta M) = 0.002$ g, takes into account the standard deviation of the difference of the readings $\sigma(\Delta R)$, the digital resolution d of the scale, as a triangular distribution [24], and the sum of each standard weights used uncertainty $u(M_\mathrm{eq})$ provided by the calibration certificate, as follows

$$u(\Delta M) = \sqrt{u(M_\mathrm{eq})^2 + \sigma^2(\Delta R) + \left(\frac{d}{\sqrt{6}}\right)^2} \tag{3.10}$$

The contributions of the uncertainties of the standard weights density, $u(\rho_\mathrm{s})$, and the air density, $u(\rho_\mathrm{a})$, resulted negligible in the final value estimation. According to IAPWS-95 [10], water density at 293.16 K and 80.0 MPa has an uncertainty equal to 0.003%. The uncertainty $u(T_0)$, affecting the temperature measurement, is due to the fit calibration, the resolution of the instrument and the reading repeatability, and its value is within 0.01 K. The value of the pressure uncertainty $u(p_0)$ due to the used pressure transducer is 0.4 MPa.

All considered contributions in the evaluation of the final uncertainty associated to relative magnitude are summarized in Table 3.3 and the relative uncertainty in the reference volume of the measuring cell, V_0, is 0.01%.

Table 3.1: Uncertainty budget of the measuring cell reference volume.

Uncertainty source	Relative magnitude %
Mass of the reference fluid	0.010
Reference water density	0.003
Air density	negligible
Standard weights density	negligible
Temperature	0.001
Pressure	0.002
Estimated overall uncertainty	**0.011**

3.2 Correction to the reference volume

The gravimetric method allowed only to determine the volume of the measuring cell V_0, at the reference temperature T_0 and pressure p_0. In order to determine the volume of the measuring cell V, at any temperature T and pressure p, the reference volume had to be corrected for the effect of temperature and pressure, resulting in the following expression

$$V(T,p) = V_0(T_0,p_0)[1 + \alpha(T - T_0) + \beta(p - p_0)] , \tag{3.11}$$

where α and β are, respectively, the thermal expansion coefficient and the isothermal compressibility coefficient of the measuring cell. Because of the non-homogeneous shape and the different materials (stainless steel and titanium) composing the measuring cell, the values of the coefficients had to be determined experimentally [14].

The elastic properties of the measuring cell were estimated by using three different experimental approaches, obtained by temperature and pressure measurements and the literature values for the properties of water, used as reference fluid. In order to estimate the α and β coefficients, measurements for two samples of water were carried out in the temperature range of (278 and 343) K and at pressures between (50 and 100) MPa. In Fig. 3.2, the plot of pressure measurements versus temperature is shown.

3.2.1 First method

The first method is based on a function derived from the definition of density and considering the relation for the volume change with temperature and pressure, as expressed by Eq. 3.11

$$\rho(T,p) \cong \rho_0(T_0,p_0)[1 - \alpha(T - T_0) - \beta(p - p_0)] . \tag{3.12}$$

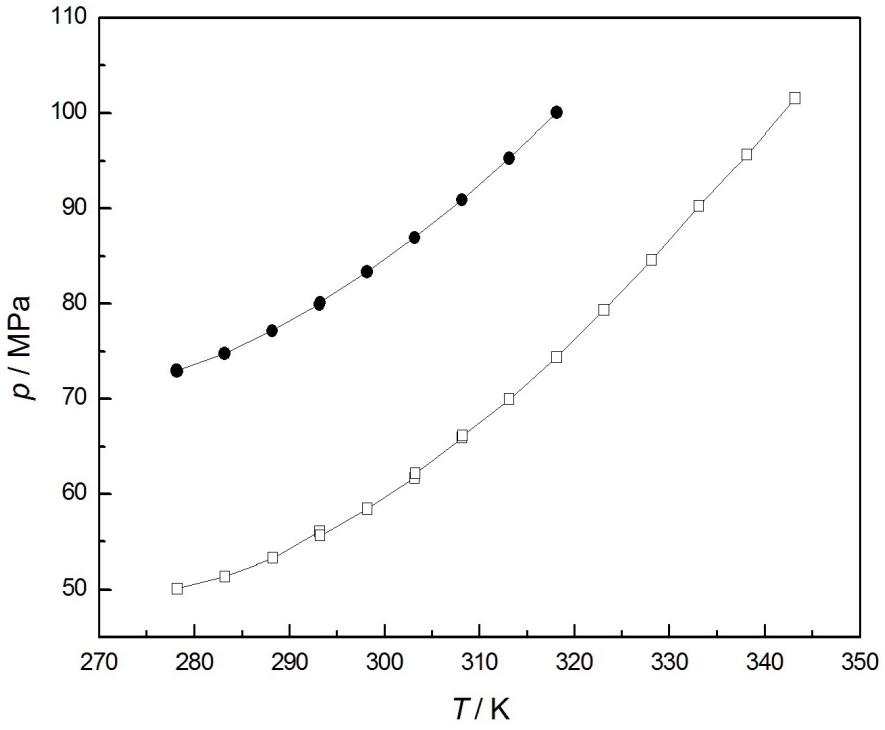

Figure 3.2: Pressure measurements as a function of temperature for the volume calibration: •, $m = 22.30$ g; □, $m = 22.07$ g.

By the temperature, T, and pressure, p, measurements and the corresponding density values, ρ, given by the IAPWS-95 formulation, a system of equations was built for each measuring curve, with α and β as unknown parameters:

$$\begin{cases} \rho_1(T_1, p_1) &= \rho_0(T_0, p_0)\left[1 - \alpha(T_1 - T_0) - \beta(p_1 - p_0)\right] \\ \rho_2(T_2, p_2) &= \rho_1(T_1, p_1)\left[1 - \alpha(T_2 - T_1) - \beta(p_2 - p_1)\right] \\ \vdots & \\ \rho_n(T_n, p_n) &= \rho_{n-1}(T_{n-1}, p_{n-1})\left[1 - \alpha(T_n - T_{n-1}) - \beta(p_n - p_{n-1})\right] \end{cases}$$

where the different indeces refer to consecutive measurements.

Through the least square analysis it was possible to evaluate the values for α and β from two systems of equations associated to the two fillings of different masses.

3.2.2 Second method

In the second approach, the ratio between the mass of the sample used for the calibration curve, m, and the mass of water weighted to determine the

reference volume, m_0, was considered:

$$\frac{m}{m_0} = \frac{\rho\,(T,p)\,V\,(T,p)}{\rho_0\,(T_0,p_0)\,V_0\,(T_0,p_0)}\ , \tag{3.13}$$

where V is the volume during the calibration cycles and V_0 is the volume of Eq. 3.6 at the reference conditions. The density ρ of the sample of mass m, at the measured temperatures T and pressures p, and the density ρ_0, at the reference temperature T_0 and pressure p_0, are given by the literature.

By substituting Eq. 3.11 for the volume V into Eq. 3.13, the following function is obtained:

$$\frac{m}{m_0} = \frac{\rho\,(T,p)}{\rho_0\,(T_0,p_0)}[1+\alpha\,(T-T_0)+\beta\,(p-p_0)]\ . \tag{3.14}$$

An equation is associated to each measured point (T, p) of the calibration curve at constant mass. Thereby, the two calibration curves, shown in Fig. 3.2, provided two different systems of equations, such as

$$\begin{cases} \frac{m}{m_0} &= \frac{\rho_1(T_1,p_1)}{\rho_0(T_0,p_0)}\,[1+\alpha\,(T_1-T_0)+\beta\,(p_1-p_0)] \\ \frac{m}{m_0} &= \frac{\rho_2(T_2,p_2)}{\rho_0(T_0,p_0)}\,[1+\alpha\,(T_2-T_0)+\beta\,(p_2-p_0)] \\ \vdots & \\ \frac{m}{m_0} &= \frac{\rho_n(T_n,p_n)}{\rho_0(T_0,p_0)}\,[1+\alpha\,(T_n-T_0)+\beta\,(p_n-p_0)]\ . \end{cases}$$

The unknowns of the system of equations were the mass m, and the α and β coefficients, which values were estimated by means of the least squares method.

3.2.3 Third method

A further function, used for the calibration, was obtained starting from the differential of the mass that can be expressed as follows:

$$\begin{aligned} \mathrm{d}m = V\mathrm{d}\rho + \rho\mathrm{d}V = \\ V\left[\left(\frac{\partial\rho}{\partial T}\right)_p \mathrm{d}T + \left(\frac{\partial\rho}{\partial p}\right)_T \mathrm{d}p\right] + \rho\left[\left(\frac{\partial V}{\partial T}\right)_p \mathrm{d}T + \left(\frac{\partial V}{\partial p}\right)_T \mathrm{d}p\right] = \\ = \rho V\,[-\alpha_\mathrm{w}\mathrm{d}T + \beta_\mathrm{w}\mathrm{d}p] + \rho\,V\,[\alpha\mathrm{d}T + \beta\mathrm{d}p]\ , \end{aligned} \tag{3.15}$$

where α_w and β_w are the thermal expansion and the isothermal compressibility coefficients of the water sample.

Since the calibration curves are at constant mass $\mathrm{d}m = 0$, Eq. 3.15 can be rewritten as

$$(\alpha-\alpha_\mathrm{w})\mathrm{d}T + (\beta+\beta_\mathrm{w})\mathrm{d}p = 0\ . \tag{3.16}$$

By integrating, the result is a function of pressure versus temperature

$$p\,(T) = p_0 + \frac{\alpha_{\mathrm{w}}(T_0, p_0) - \alpha}{\beta_{\mathrm{w}}(T_0, p_0) + \beta}(T - T_0)\ . \tag{3.17}$$

Each measuring constant-mass curve allowed building a system of equations (each equation corresponding to a thermodynamic state) which has α and β as unknowns:

$$\begin{cases} p_1\,(T_1) & = p_0 + \frac{\alpha_{\mathrm{w}}-\alpha}{\beta_{\mathrm{w}}+\beta}(T_1 - T_0) \\ p_2\,(T_2) & = p_1 + \frac{\alpha_{\mathrm{w}}-\alpha}{\beta_{\mathrm{w}}+\beta}(T_2 - T_1) \\ \vdots & \\ p_n\,(T_n) & = p_{n-1} + \frac{\alpha_{\mathrm{w}}-\alpha}{\beta_{\mathrm{w}}+\beta}(T_n - T_{n-1})\ . \end{cases}$$

Water thermal expansion and compressibility are actually dependent by temperature and pressure. Accordingly, the values of water thermal expansion and compressibility at each temperature and pressure measured were provided by the IAPWS-95 equation [10]. The least squares method was used to estimate the α and β coefficients of the measuring cell from each system of equation obtained from the calibration curves.

In Table 3.2 the experimental thermal expansion and the isothermal compressibility values are reported. Lastly, the averages of the six values, calculated by the two calibration curves and by using the three different methods presented, have been assumed as final thermal expansion and isothermal compressibility, and are:

$$\alpha = (3.9 \pm 0.2) \cdot 10^{-5}\ \mathrm{K}^{-1} \tag{3.18}$$

$$\beta = (5.6 \pm 0.2) \cdot 10^{-5}\ \mathrm{MPa}^{-1}\ . \tag{3.19}$$

For the studied temperature and pressure range, variations of the elastic properties with temperature and pressure were within the declared uncertainty; for this reason they were considered constant over the whole examined (T, p) range.

Regarding to the expansion cell, the volume determined had also to be corrected in the same way as 3.11, or rather

$$v\,(T, p) = v_0(T_0, p_0)[1 + \alpha_{\mathrm{e}}\,(T - T_0) + \beta_{\mathrm{e}}\,(p - p_0)]\ , \tag{3.20}$$

where α_{e} and β_{e} are, respectively, the thermal expansion coefficient and the isothermal compressibility coefficient of the expansion cell, which values were considered as the standard used for stainless steel AISI 304. However, because the expansion cell was used in a tiny (T, p) range, the variation of the volume from the reference value of 3.8 were smaller than its uncertainty and consequently considered negligible.

Table 3.2: Thermal expansion and compressibility coefficients calculated from the two curves at constant mass through the three function of Eqs. 3.12, 3.14, 3.17.

	Filling 1		Filling 2	
	α/K^{-1}	β/MPa^{-1}	α/K^{-1}	β/MPa^{-1}
First method	$3.8{\cdot}10^{-5}$	$5.3{\cdot}10^{-5}$	$3.8{\cdot}10^{-5}$	$5.8{\cdot}10^{-5}$
Second method	$3.9{\cdot}10^{-5}$	$5.9{\cdot}10^{-5}$	$3.7{\cdot}10^{-5}$	$5.8{\cdot}10^{-5}$
Third method	$4.1{\cdot}10^{-5}$	$5.3{\cdot}10^{-5}$	$4.0{\cdot}10^{-5}$	$5.9{\cdot}10^{-5}$

3.3 Volume uncertainty analysis

According to Eq. 3.11, the uncertainty of the pressure vessel volume determination was determined considering the volume V as a function of the reference volume V_0, the thermal expansion coefficient α, the isothermal compressibility coefficient β, the temperature T and the pressure p:

$$V = V(V_0, \alpha, \beta, T, p) \ .$$

The relative uncertainty, $u(V)/V$, was evaluated by using the standard formulation for the error propagation, as follows

$$\frac{u(V)}{V} = \frac{1}{V}\left[\left(\frac{\partial V}{\partial V_0}\right)^2 u^2(V_0) + \left(\frac{\partial V}{\partial \alpha}\right)^2 u^2(\alpha) + \left(\frac{\partial V}{\partial \beta}\right)^2 u^2(\beta) + \right.$$
$$\left. + \left(\frac{\partial V}{\partial T}\right)^2 u^2(T) + \left(\frac{\partial V}{\partial p}\right)^2 u^2(p)\right]^{\frac{1}{2}} \quad (3.21)$$

and resulting in the following equation:

$$\frac{u(V)}{V} = \frac{1}{V}\left[(1 + \alpha\Delta T + \beta\Delta p)^2\, u^2(V_0) + (V_0\Delta T)^2\, u^2(\alpha) + \right.$$
$$\left. + (V_0\Delta p)^2\, u^2(\beta) + (V_0\alpha)^2\, u^2(T) + (V_0\beta)^2\, u^2(p)\right]^{\frac{1}{2}} \quad (3.22)$$

where $\Delta T = T - T_0$, $\Delta p = p - p_0$ and $u(V_0)$ is 0.002 cm^3. The uncertainties of the α and β coefficients, $u(\alpha)$ and $u(\beta)$, are due to the fitting process for their estimations; other sources of uncertainty are negligible.

The combined uncertainty of temperature, $u(T) = 0.02$ K, was estimated by the uncertainty on the fit calibration, the resolution of the instrument and the reading repeatability.

The uncertainty of the pressure transducer $u(p)$ is 0.4 MPa; this value is given by the declared uncertainty of the instrument at the full scale.

In Table 3.3, all contributions to the relative uncertainty of the measuring volume, both at low pressure (during the mass determination) and at high pressure (during the measuring cycle at high pressure) along with their relative values are reported. The major source of uncertainty is due to the correction for the pressure effect, given by the isothermal compressibility coefficient estimation.

Table 3.3: Volume uncertainty budget.

Uncertainty source	Relative magnitude %	
	$p < 10$ MPa	$p > 10$ MPa
Reference volume	0.011	0.011
Thermal expansion coefficient	negligible	0.010
Compressibility coefficient	0.016	0.060
Temperature	0.001	0.001
Pressure	0.002	0.002
Estimated overall uncertainty	**0.02**	**0.06**

3.4 Mass uncertainty analysis

For the determination of the water sample mass, at the end of each cycle, the expansion cell was used. Consequently, the volume occupied by the sample of water was the volume of the measuring cell and the expansion cell connected together. The amount of water was determined by the density $\rho'(T', p')$ and the volume of the system $(V'(T', p') + v(T', p'))$. The following model can be considered

$$m = m(\rho', V', v) \ .$$

The relative uncertainty in the water mass estimation, $u(m)/m$, was calculated with the error propagation, expressed as:

$$\frac{u(m)}{m} = \frac{1}{m}\left[\left(\frac{\partial m}{\partial \rho_0}\right)^2 u^2(\rho_0) + \left(\frac{\partial m}{\partial V_0}\right)^2 u^2(V_0) + \left(\frac{\partial m}{\partial v_0}\right)^2 u^2(v_0)\right]^{\frac{1}{2}} \tag{3.23}$$

that becomes as follows

$$\frac{u(m)}{m} = \frac{1}{m}\left[(V' + v)^2\, u^2(\rho') + \rho^2 u^2(V') + \rho^2 u^2(v)\right]^{\frac{1}{2}} \ . \tag{3.24}$$

The uncertainty of the density, $u(\rho_0)$, is given by the literature [10] and equal to 0.001%, that is the uncertainty on the dedicated equation of state by IAPWS-95 above 273.15 K and for pressures below 10 MPa. Since ρ_0 is a function of the measured temperature and pressure, their uncertainties were considered, but were negligible with respect to the nominal uncertainty of density. The uncertainty of the measuring cell volume $u(V')$ and of the expansion cell volume $u(v)$ were calculated according to relation 3.21 at the temperature T' and pressure p'.

In Table 3.4, the sources of uncertainty affecting the mass determination along with their relative magnitudes are considered. The final relative uncertainty value of the water mass is about 0.03%.

Table 3.4: Mass of the water sample uncertainty budget.

Uncertainty source	Relative magnitude %
Reference density	0.001
Volume of the measuring cell	0.030
Volume of the expansion cell	0.005
Estimated overall uncertainty	**0.03**

3.5 Density uncertainty analysis

The experimental density of the water sample can be expressed as a function of the mass m, determined at the end of each measurement cycle, and the volume V corrected at each measuring state (T, p), as follows

$$\rho = \rho(m, V) \ .$$

Consequently, the error propagation formula was applied in order to estimate the relative uncertainty of water density, given by

$$\frac{u(\rho)}{\rho} = \frac{1}{\rho}\left[\left(\frac{\partial \rho}{\partial m}\right)^2 u^2\left(m\right) + \left(\frac{\partial \rho}{\partial V}\right)^2 u^2(V)\right]^{\frac{1}{2}} \tag{3.25}$$

that finally becomes:

$$\frac{u(\rho)}{\rho} = \frac{1}{\rho}\left[\frac{1}{V^2}u^2\left(m\right) + \frac{m^2}{V^4}u^2(V)\right]^{\frac{1}{2}} \ , \tag{3.26}$$

where $u(m)$ is the mass uncertainty equal to 0.008 g, while $u(V)$ is the uncertainty of the corrected volume of the vessel at the measured temperature and pressure during the measuring cycle, which value is 0.01 cm^3. As reported in Table 3.5, the density uncertainty budget is dominated by the volume determination, as expected considering the complexity of the measuring cell. The relative uncertainty of subcooled water density, considering the worst scenario (therefore at high pressure), was estimated to be 0.07%.

Table 3.5: Density uncertainty budget.

Uncertainty source	Relative magnitude %
Mass	0.03
Volume	0.06
Estimated overall uncertainty	**0.07**

3.6 Method validation

The experimental method was validated by performing experimental density measurements of two different fillings of freshly double-distilled water, at temperatures between (278 and 353) K and at pressures between (50 and 150) MPa, to compare the results with the corresponding IAPWS-95 values, which have, in this (T, p) range an uncertainty of 0.003% [10]. In Fig. 3.3, the experimental densities as a function of the temperature at constant mass are reported, along with the densities given by IAPWS-95 formulation at the measured temperature and pressure.

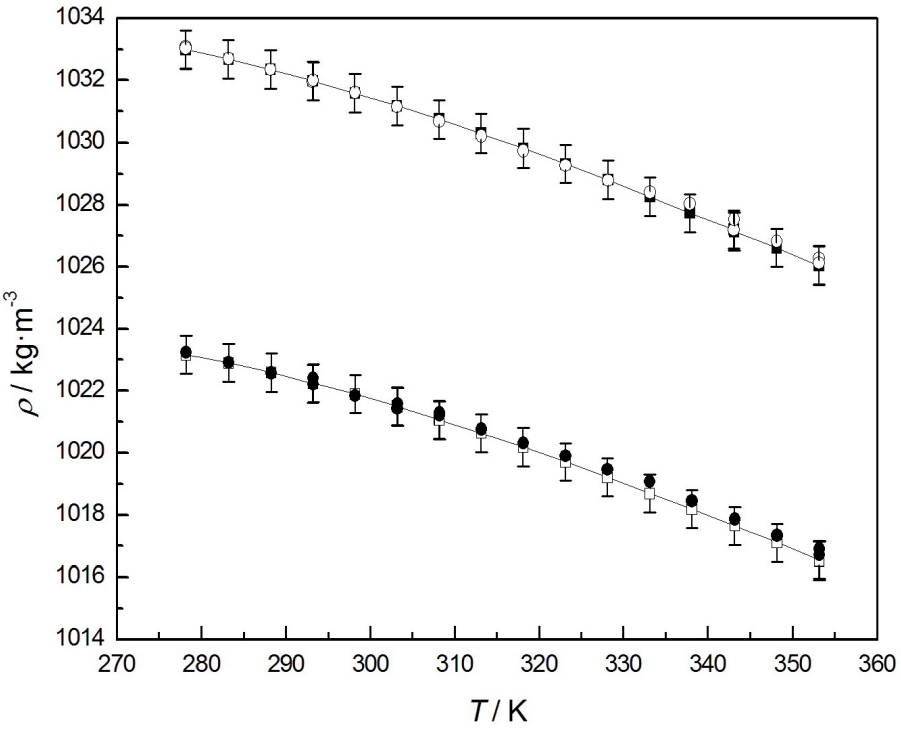

Figure 3.3: Density as a function of temperature, with the uncertainty bars: ■, experimental values of this work at $m = 22.62$ g; ○, IAPWS-95 values at $m = 22.62$ g; □, experimental values of this work at $m = 22.37$ g ●, IAPWS-95 values at $m = 22.37$ g.

Figure 3.4 shows the deviation of the experimental measurements from the literature values. For both the studied samples, the values deviate from the IAPWS-95 equation no more than 0.04%. The uncertainty of density measured for the validation of the method was estimated according to Eq. 3.26. Considering that the relative uncertainty of densities is 0.07% at temperatures between (278 and 353) K and at pressures from (50 to 150) MPa,

all the experimental values resulted in agreement with the literature values [10].

For a further proof of the procedure validity, the experimental densities were compared with the corresponding IAPWS-95 densities by means of the normalized error, defined as follows:

$$E_{\mathrm{n}} = \frac{\rho_{\mathrm{exp}} - \rho_{\mathrm{IAPWS}}}{\sqrt{U^2(\rho_{\mathrm{exp}}) + U^2(\rho_{\mathrm{IAPWS}})}} \quad , \tag{3.27}$$

where $U(\rho_{\mathrm{IAPWS}})$ and $U(\rho_{\mathrm{exp}})$ are the uncertainties respectively of the IAPWS and the experimental densities, at the confidence level of 95% ($k = 2$). As can be observed in Table 3.6, the values of the E_{n}-number are reported. All the E values lie in the interval ± 1, thus, this confirms the experimental compatibility of the results obtained and the validity of the method presented.

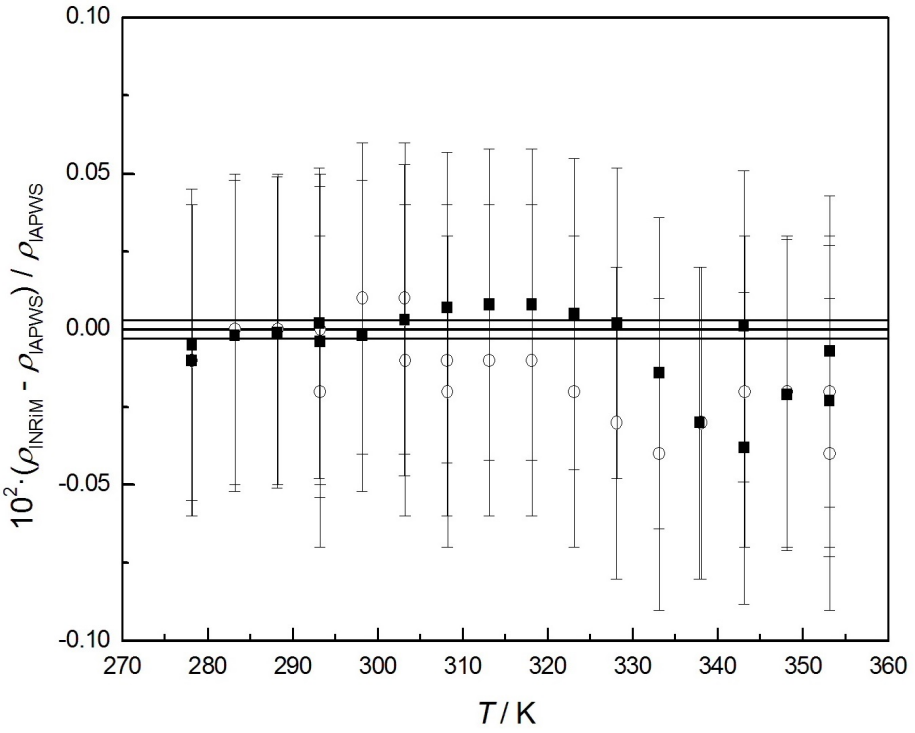

Figure 3.4: Deviations of experimental density values, with the uncertainty bars, from IAPWS-95 equation of state (zero line) as a function of temperature: ○, $m = 22.62$ g; ■, $m = 22.37$ g; the solid lines reveal the uncertainty band of IAPWS-95.

Table 3.6: IAPWS-95 and experimental water density ρ at temperature T and pressure p and the corresponding normalized errors.

T/K	p/MPa	ρ_{IAPWS}/kg·m^{-3}	ρ_{exp}/kg·m^{-3}	E_{n}
		$m = 22.37$ g		
278.23	50.1	1023.24	1023.17	-0.09
283.21	51.4	1022.91	1022.89	-0.02
288.28	53.3	1022.58	1022.58	0.01
293.20	56.1	1022.41	1022.23	-0.22
293.25	55.6	1022.21	1022.25	0.05
298.21	58.5	1021.84	1021.89	0.07
303.20	61.7	1021.43	1021.51	0.10
303.26	62.2	1021.59	1021.48	-0.14
308.18	65.9	1021.21	1021.07	-0.17
308.23	66.1	1021.28	1021.05	-0.28
313.17	70.0	1020.76	1020.64	-0.15
318.15	74.4	1020.31	1020.19	-0.16
323.15	79.4	1019.90	1019.70	-0.24
328.14	84.6	1019.46	1019.21	-0.31
333.15	90.3	1019.07	1018.68	-0.48
338.14	95.7	1018.45	1018.18	-0.33
343.21	101.5	1017.86	1017.65	-0.26
348.15	107.7	1017.33	1017.10	-0.28
353.16	113.8	1016.71	1016.55	-0.19
353.18	114.54	1016.89	1016.52	-0.46
		$m = 22.62$ g		
278.18	73.0	1033.08	1032.98	-0.12
278.20	72.9	1033.04	1032.99	-0.06
283.18	74.8	1032.70	1032.68	-0.03
288.17	77.2	1032.35	1032.34	-0.01
293.16	80.0	1031.96	1031.98	0.02
293.23	80.1	1032.00	1031.96	-0.05
298.19	83.4	1031.60	1031.58	-0.02
303.18	86.9	1031.14	1031.17	0.04
308.16	90.9	1030.67	1030.74	0.08
313.15	95.3	1030.20	1030.29	0.10
318.16	100.1	1029.74	1029.82	0.09
323.15	105.2	1029.27	1029.32	0.06
328.19	110.6	1028.78	1028.81	0.03
333.16	116.6	1028.41	1028.26	-0.17
337.90	122.6	1028.03	1027.73	-0.37
343.12	128.2	1027.19	1027.20	0.02
343.16	129.2	1027.53	1027.14	-0.47
348.11	135.1	1026.83	1026.61	-0.26
353.13	141.7	1026.27	1026.03	-0.28
353.14	141.3	1026.13	1026.05	-0.09

Chapter 4

Results

In this chapter, the procedure followed for the density measurements of cooled and supercooled water performed at pressures up to 400 MPa and the results are reported. Furthermore, the comparison with two different equations of state and the experimental values given in the literature is presented.

4.1 Measurement procedure

In order to maintain the water in liquid metastable states, it is necessary to use high purity samples. For this study, the water was purified by double-distillation, after having removed dissolved inorganic solids by means of an ion-exchange resin system. The samples were prepared just before being used.

The measurement procedure consisted of the following main steps:

- Placing the pseudo-isochoric system into the thermostatic bath connected to the high pressure circuit;
- Evacuating the filling circuit, the measuring cell and the expansion cell with the mechanical vacuum pump;
- Isolating the expansion cell from the measuring cell by the valve;
- Filling the measuring cell at the desired pressure by using the pressure amplifier and the high pressure circuit;
- Isolating the measuring cell from the rest of the apparatus at ambient temperature by the valve;

- Decreasing the temperature very slowly in order to avoid crystallization (usually it required between 1 and 3 hours for a change of 1 K at the lower temperatures);
- Measuring through the LabView software the temperature and the pressure at the equilibrium, after the temperature stabilization within 0.01 K (see Fig. 4.1), the pressure required about 1 hour to equilibrate (see Fig. 4.2).
- Increasing the temperature up to 273.15 K, remeasuring the density at some (T, p) points to control the hysteresis of the measuring curve.

At the end of each cycle, the thermostat temperature was slowly increased to values higher than 273.15 K up to about 293 K and the valve, connecting the measuring and the expansion cell, was lightly opened causing the slow pressure drop to less than 10 MPa. After the stabilization, the temperature and the pressure were again recorded. Finally, the sample was removed from the high pressure vessel and the expansion cell that were cleaned with ethanol and put through vacuum into the oven at $\sim$ 40 °C for at least 48 hours to be dried. Afterward the procedure was repeated by filling with a fresh sample of water.

During the measuring cycle, if crystallization occurred, it caused a sudden change in pressure (a rapid increase or decrease depending on the studied region of the phase diagram) the plot of the pressure showed a peak, as shown as an example in Fig. 4.3. In this case, the temperature was set to the ambient value and the measuring cycle rejected.

Figure 4.1: Picture of the LabView software used to measure the temperature when stabilized.

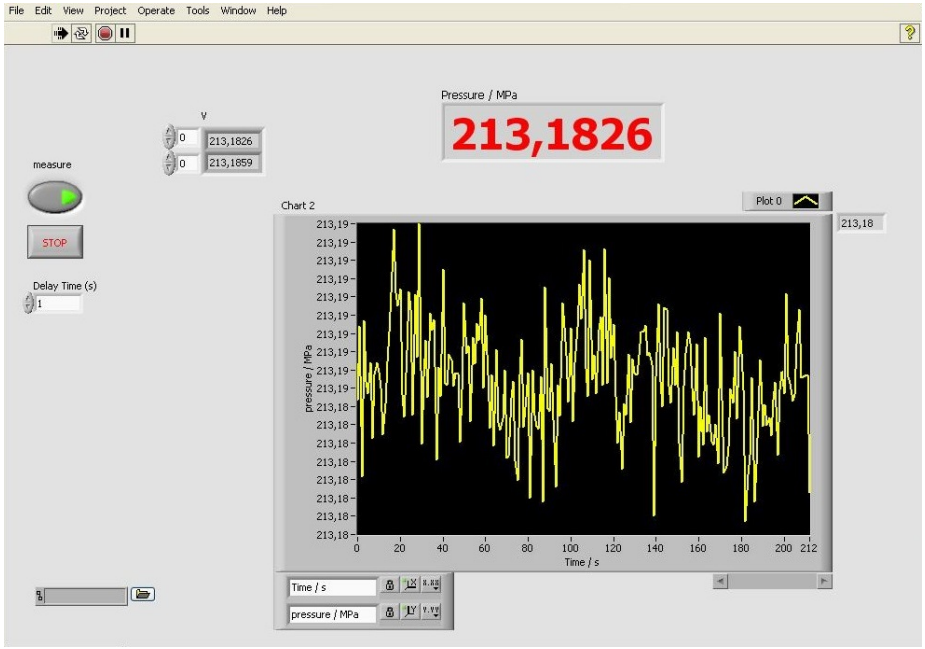

Figure 4.2: Picture of the LabView software used to measure the pressure when stabilized.

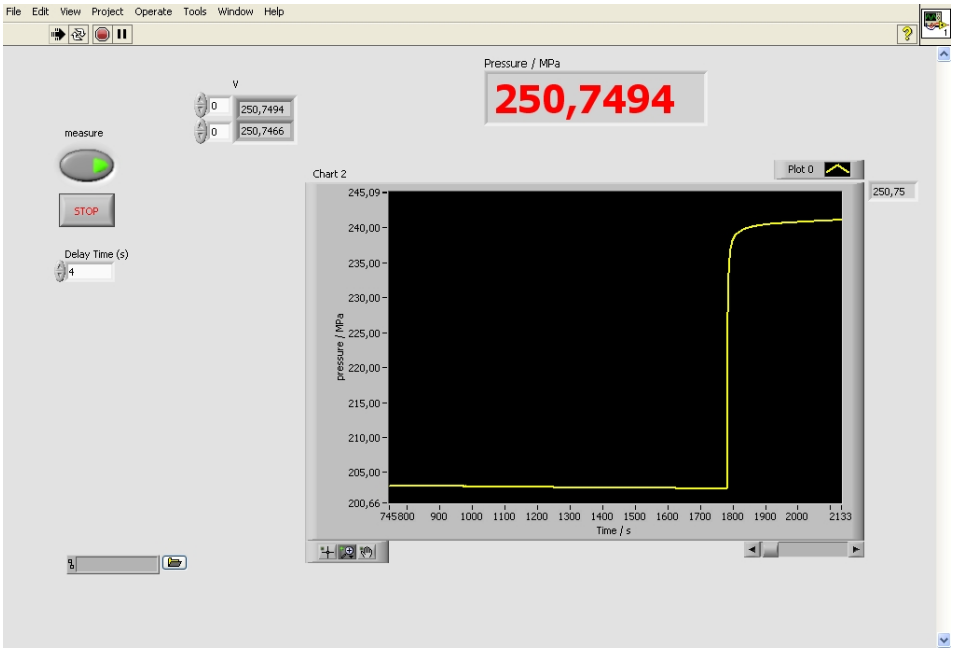

Figure 4.3: Pressure measurement with the LAbView software, when crystallization occurred: freezing is revealed by the suddenly change in pressure.

4.2 Experimental densities

The density of subcooled water was measured along eight constant-mass curves at temperatures down to 243 K and for pressures between (140 and 400) MPa. Whereas Fig. 4.4 shows pressure measurements as a function of temperature, Fig. 4.5 shows the density values of the eight different water samples versus temperature. As the plots show, both stable and metastable states of water were studied. Every curve has a smooth trend and none of the reported curves present discontinues; therefore, freezing did not occurred during the whole measuring process. All density measurements along the constant-mass curves are reported in Table 4.1, where the values related to metastable states are expressed in italic.

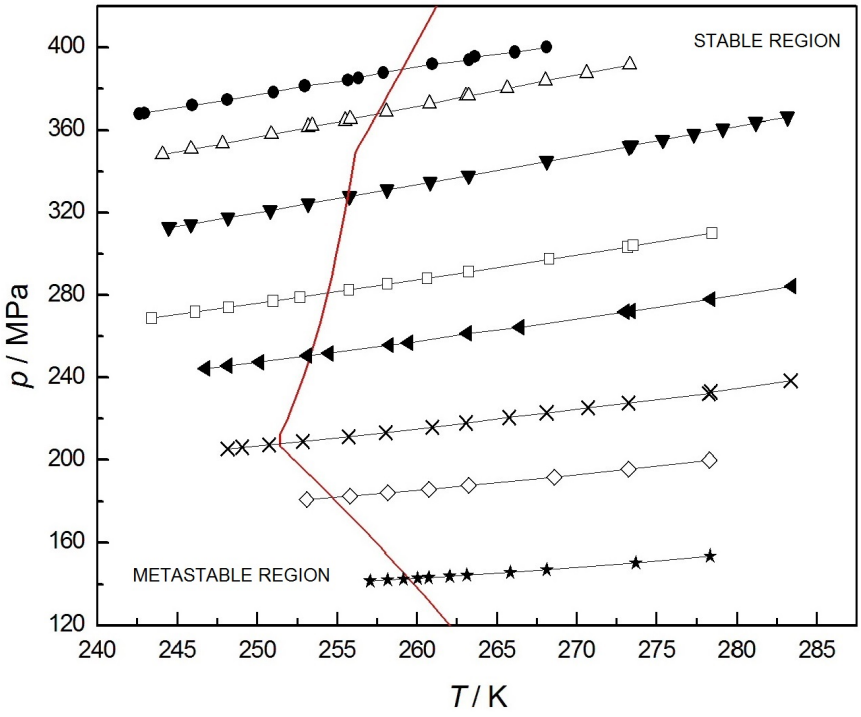

Figure 4.4: Pressure as a function of temperature at constant mass of different water fillings: •, $m = 25.45$ g; △, $m = 25.32$ g; ▼, $m = 25.05$ g; □, $m = 24.69$ g; ◀, $m = 24.45$ g; ×, $m = 24.09$ g; ◊, $m = 23.81$ g; ★, $m = 23.40$ g; —, melting curve.

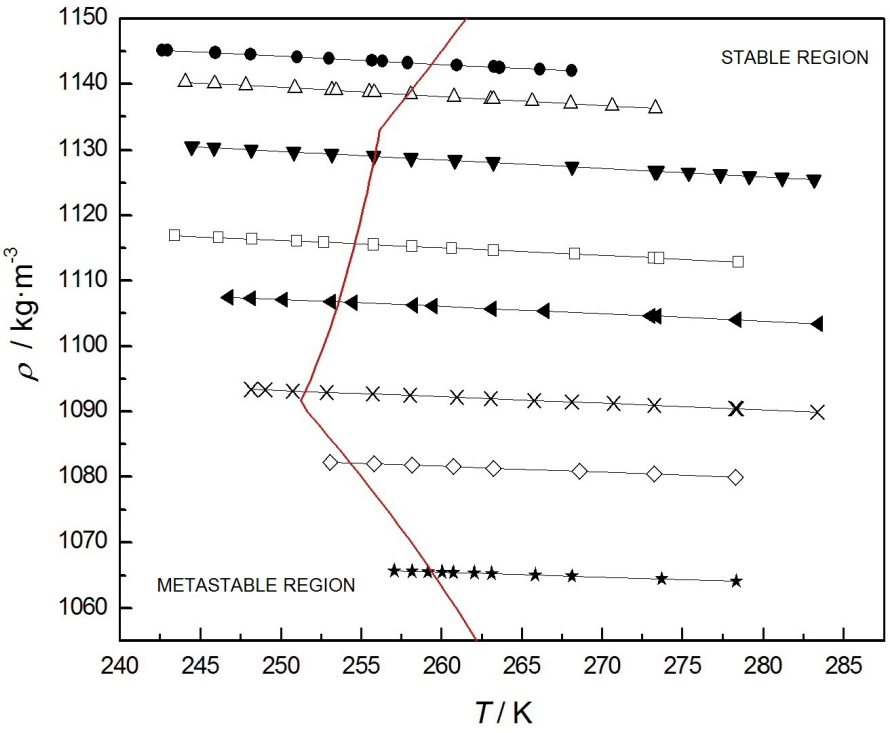

Figure 4.5: Subcooled water density as a function of temperature at constant mass: •, $m = 25.45$ g; △, $m = 25.32$ g; ▼, $m = 25.05$ g; □, $m = 24.69$ g; ◀, $m = 24.45$ g; ×, $m = 24.09$ g; ◊, $m = 23.81$ g; ★, $m = 23.40$ g; —, melting curve.

Table 4.1: Experimental water density ρ at temperature T and pressure p. Entries in italics refer to measurements in metastable states of liquid water.

T/K	p/MPa	ρ/kg·m^{-3}	T/K	p/MPa	ρ /kg·m^{-3}	T/K	p/MPa	ρ/kg·m^{-3}
				m = 23.40 g				
257.06	*141.6*	*1065.72*	260.74	143.1	1065.47	268.12	147.0	1064.94
258.17	*142.0*	*1065.64*	262.05	143.8	1065.38	273.71	150.3	1064.51
259.15	*142.5*	*1065.58*	263.13	144.3	1065.30	278.36	153.6	1064.12
260.04	142.9	1065.52	265.83	145.7	1065.11			
				m = 23.81 g				
253.08	*180.8*	*1082.19*	260.75	185.8	1081.56	273.24	195.5	1080.45
255.82	182.5	1081.97	263.24	187.6	1081.35	278.31	199.9	1079.97
258.16	184.0	1081.78	268.61	191.7	1080.87			
				m = 24.09 g				
248.14	*205.3*	*1093.37*	258.05	213.2	1092.48	270.71	225.3	1091.21
249.03	*206.2*	*1093.29*	260.96	215.8	1092.20	273.25	227.8	1090.95
250.73	*207.4*	*1093.14*	263.07	217.9	1091.98	278.29	232.1	1090.5
252.85	209.1	1092.95	265.78	220.6	1091.70	278.39	233.0	1090.4
255.71	211.3	1092.69	268.12	222.8	1091.47	283.37	238.4	1089.9
				m = 24.45 g				
246.78	*244.4*	*1107.5*	258.28	255.8	1106.3	273.42	272.2	1104.6
248.16	*245.7*	*1107.3*	259.48	256.9	1106.1	278.40	278.1	1104.0
250.15	*247.5*	*1107.1*	263.15	261.5	1105.7	283.44	284.4	1103.4
253.15	*250.6*	*1106.8*	266.45	264.4	1105.4			
254.49	251.7	1106.7	273.04	272.0	1104.6			
				m = 24.69 g				
243.42	*268.8*	*1116.9*	255.76	282.6	1115.5	273.21	303.3	1113.5
246.11	*271.8*	*1116.6*	258.16	285.3	1115.3	273.55	304.1	1113.4
248.20	*274.1*	*1116.4*	260.65	288.2	1115.0	278.49	310.1	1112.9
250.98	*277.1*	*1116.1*	263.24	291.2	1114.7			
252.67	*279.0*	*1115.9*	268.30	297.5	1114.1			
				m = 25.05 g				
244.50	*312.9*	*1130.5*	258.12	331.3	1128.7	275.40	355.3	1126.5
245.84	*314.4*	*1130.3*	260.85	334.9	1128.4	277.36	358.2	1126.2
248.17	*317.7*	*1130.0*	263.22	337.9	1128.1	279.17	360.7	1126.0
250.81	*321.0*	*1129.7*	268.14	345.1	1127.4	281.17	363.6	1125.7
253.18	*324.4*	*1129.4*	273.30	352.2	1126.8	283.16	366.4	1125.5
255.78	*327.9*	*1129.1*	273.44	352.7	1126.7			
				m = 25.32 g				
244.09	*348.3*	*1140.4*	*255.50*	*364.5*	*1138.9*	265.65	380.0	1137.5
245.86	*350.8*	*1140.2*	*255.82*	*365.2*	*1138.8*	268.05	383.8	1137.1
247.83	*353.6*	*1139.9*	258.09	368.6	1138.5	270.63	387.4	1136.8
250.88	*358.0*	*1139.5*	260.79	372.5	1138.1	273.33	391.5	1136.4
253.18	*361.4*	*1139.2*	263.08	376.4	1137.8			
253.44	*362.0*	*1139.1*	263.23	376.4	1137.8			
				m = 25.45 g				
242.65	*367.6*	*1145.1*	*252.98*	*381.2*	*1143.8*	263.25	393.9	1142.5
242.97	*368.1*	*1145.0*	*255.68*	*384.0*	*1143.5*	263.62	395.4	1142.4
245.92	*371.8*	*1144.7*	*256.33*	*385.1*	*1143.4*	266.13	397.6	1142.2
248.12	*374.5*	*1144.4*	*257.90*	*387.7*	*1143.2*	268.12	400.0	1141.9
251.01	*378.2*	*1144.1*	260.96	391.9	1142.8			

4.3 Comparison with equations of state

Firstly, the experimental values of water density obtained in this work were compared with the values provided by two equations of state of water [10, 11].

The first equation considered was the current international reference equation of state, the "IAPWS Formulation 1995 for the Thermodynamic Properties of Ordinary Water Substance for general and Scientific Use", the IAPWS-95 formulation [10]. The IAPWS-95 equation of state was based on experimental data available by 1995 [9]. However, until 2000, there were a very few works on experimental thermodynamic properties of water and in particular for the density down 273 K. Since the lowest temperature in the IAPWS-95 range of validity corresponds to the melting curve, supercooled states are outside the range of validity. For pressures higher than 100 MPa, the IAPWS-95 uncertainty of stable water density is 0.05% above 273.15 K, while it is 0.2% for temperatures below 273.15 K.

Figures 4.6 and 4.7 show the deviations of experimental water density of the present data, in stable and metastable states respectively, from the IAPWS-95 equation of state. In particular, Fig. 4.6 focused on the stable region, while Fig. 4.7 shows the deviations in the metastable region, outside the range of validity of the IAPWS-95 formulation. Considering the declared IAPWS-95 uncertainty in the stable region, all the experimental measurements are in agreement with the equation of state, but the deviations systematically increase (up to nearly 0.2% for stable states and 0.5% for metastable states) as the temperature decreases. The general trend observed in Fig. 4.7 is a consequence of the extrapolation of the IAPWS equation outside the range of validity. Actually, this trend starts at the lower temperatures of the stable region, as can be observed in Fig. 4.6. This may be due probably to the shortage of experimental data available for implementing the equation of state, and attests that new measurements could be useful even at the lower temperatures of the stable states.

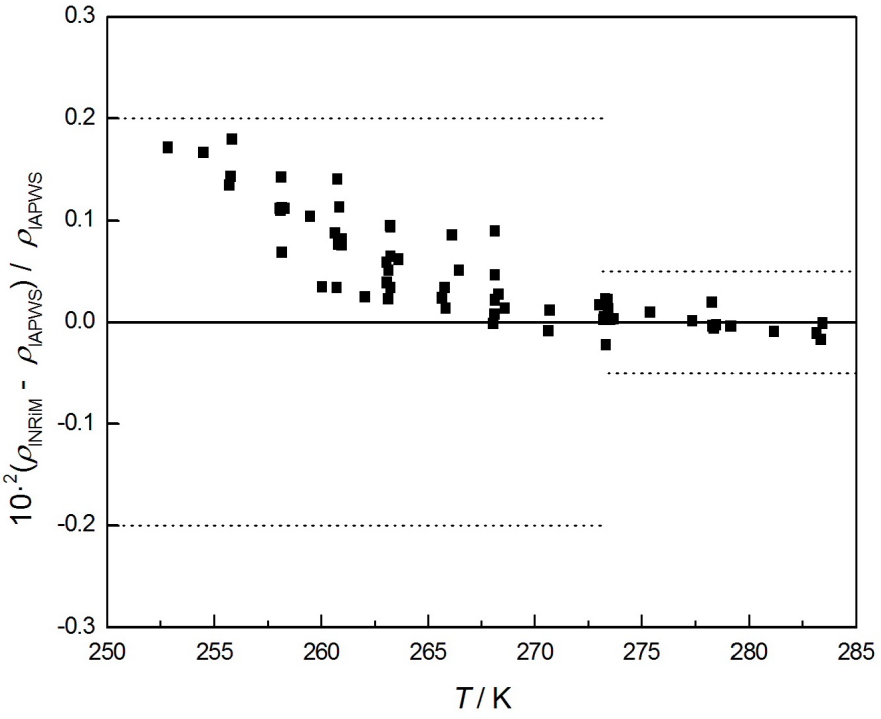

Figure 4.6: Deviations of experimental density of liquid water in stable states from the values of IAPWS-95 equation of state (zero line) as a function of temperature: the dot lines show the uncertainty band of IAPWS-95 for stable states of water at pressures higher than 100 MPa, which is 0.05% above 273.15 K and 0.2% below 273.15 K.

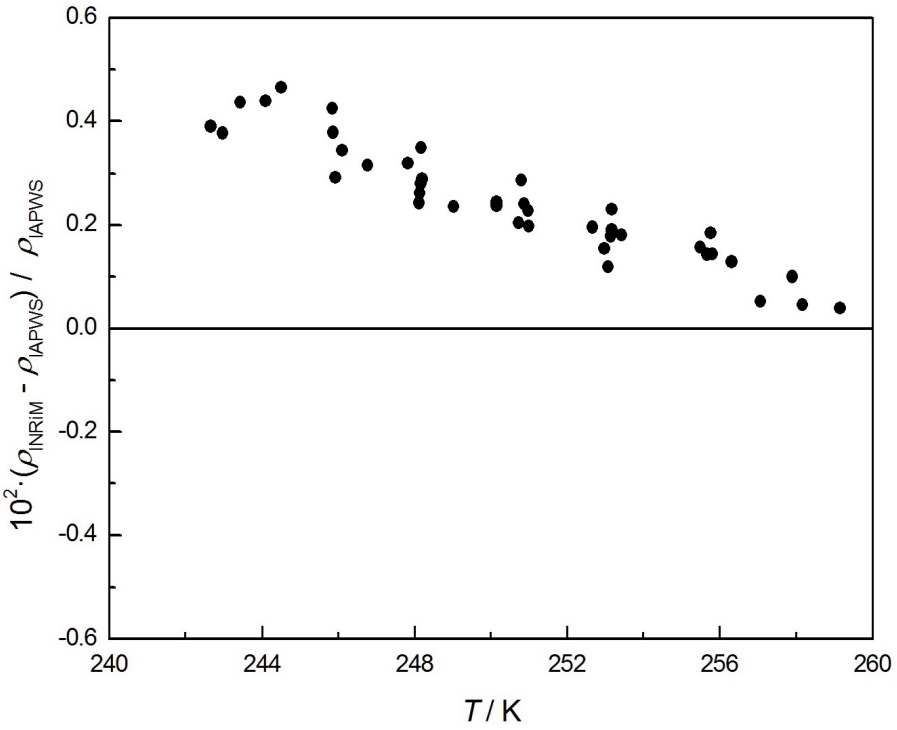

Figure 4.7: Deviations of experimental density of metastable liquid water from values of IAPWS-95 equation of state (zero line), outside its range of validity, as a function of temperature.

The second equation considered for the comparison was developed by Holten *et al.* in 2012 [25]. The equation was chosen for the comparison since it focuses on the cooled and subcooled region, so outside the range of validity of the IAPWS-95 equation, and is able to represent the recent experimental values available after IAPWS formulation. In its final form of 2014 [11], this equation is valid from the homogeneous ice nucleation temperature up to 300 K and at pressures up to 400 MPa. In the studied (T, p) range, the uncertainty of Holten's densities in stable states varies from 0.04% to 0.1%, while in metastable states it is 0.5%. Figures 4.8 and 4.9 show the deviations of the results here presented from density calculated, at the same (T, p) points, with Holten's equation in stable and metastable states respectively. In particular, stable densities deviate from the equation within 0.07%. In the metastable region shown in Fig. 4.9, most of the measurements have deviations lower than 0.07%; the measurements corresponding to the highest densities deviate from the equation within 0.2%. So that, all the data are in agreement with Holten's equation of state, within the declared uncertainty.

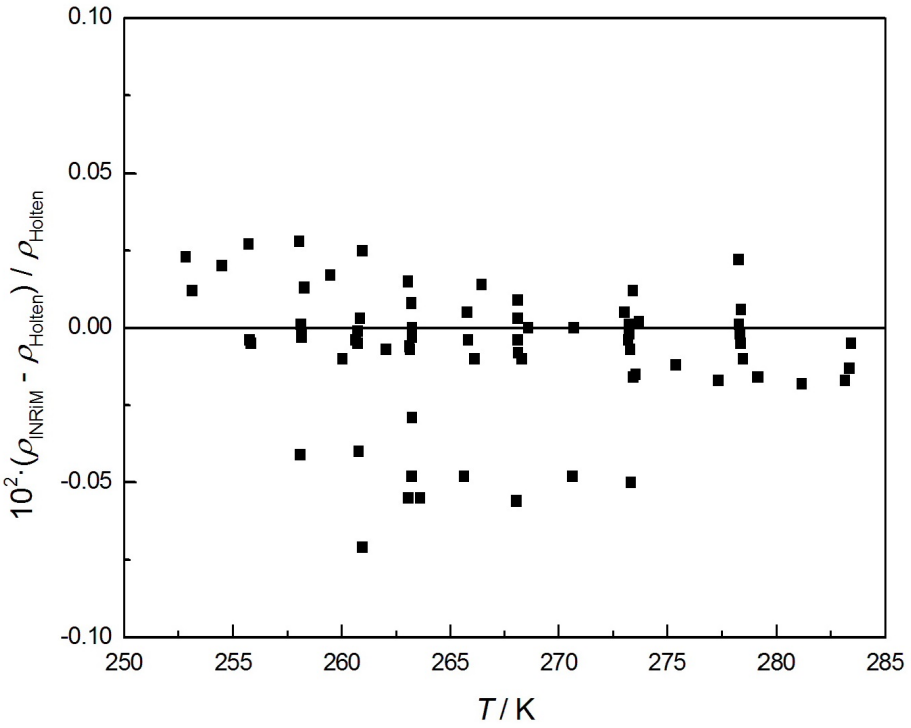

Figure 4.8: Deviations of experimental density of stable liquid water from Holten *et al.* equation of state (zero line) as a function of temperature: the dotted lines reveal Holten equation's uncertainty band for stable states of liquid water.

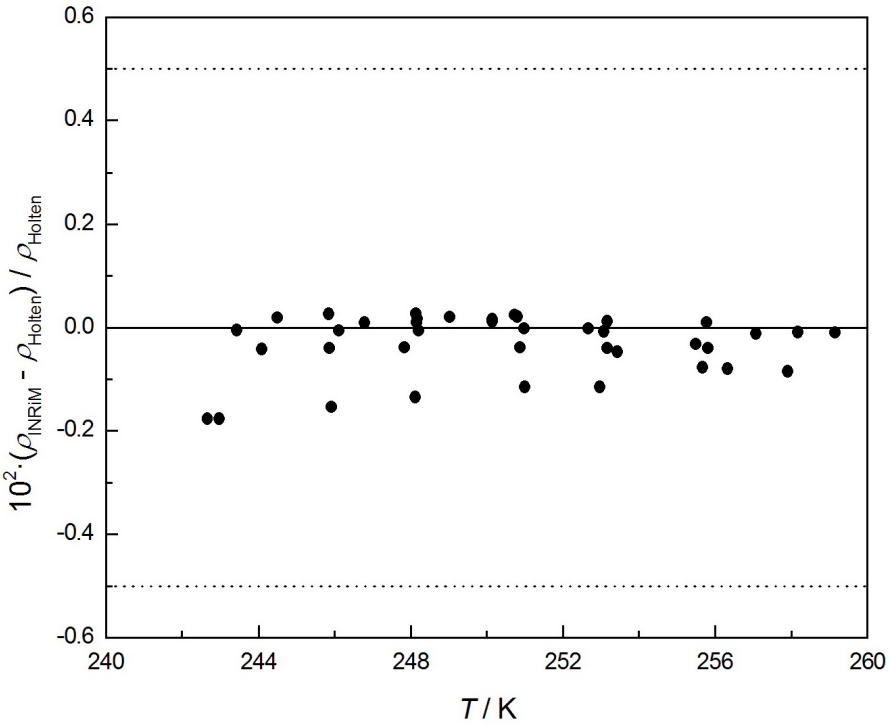

Figure 4.9: Deviations of experimental density of metastable liquid water from Holten *et al.* equation of state (zero line) as a function of temperature: the dot lines show the uncertainty band for metastable states of liquid water of the Holten equation.

Even if all the values of the experimental density and the values given by the two equations of state are in good agreement, by observing the plot of density as a function of temperature, shown in Fig. 4.10, it is possible to notice that experimental and IAPWS-95 curves have opposite behaviors. On the other hand, the behavior of the experimental curves is the same as Holten's equation. At constant mass, the experimental densities as well as those calculated by the Holten equation increase as temperature decreases in the whole measuring range. In contrast at temperatures lower than 260 K, thus in the metastable region, where IAPWS-95 equation is outside the range of validity, the densities, decrease as temperature decreases. This confirms that the extrapolated equation of state of the IAPWS-95 formulation could be reviewed in the metastable region.

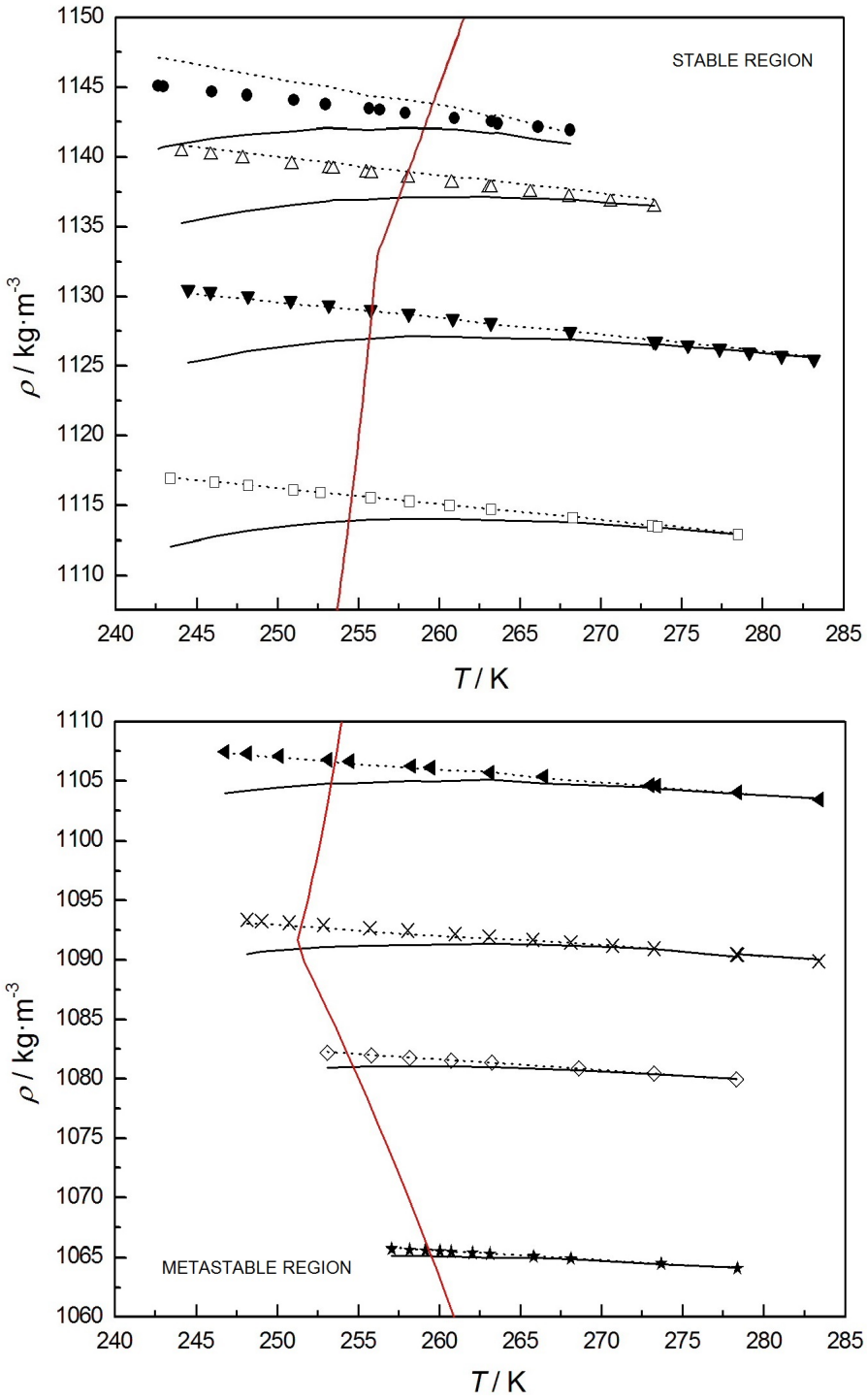

Figure 4.10: Density of water as a function of temperature, measured in this work (identified by the symbols), calculated by IAPWS-95 equation of state (solid lines) and Holten *et al.* equation of state (dotted lines) at the measurement temperatures and pressures: •, $m = 25.45$ g; △, $m = 25.32$ g; ▼, $m = 25.05$ g; □, $m = 24.69$ g; ◀, $m = 24.45$ g; ×, $m = 24.09$ g; ◇, $m = 23.81$ g; ★, $m = 23.40$ g; —, melting curve. The plots at the top and at the bottom refer to the four sample with the higher mass values and to the four samples with the lower mass values respectively.

4.4 Comparison with the literature measurements

The measurements of density were also compared with the experimental values of subcooled water available in the literature: Sotani *et al.* [16], Asada *et al.* [17], Guignon *et al.* [18] and Mishima [19]. Figure 4.11 reports the distribution of the thermodynamic states investigated by this work and cited literature works.

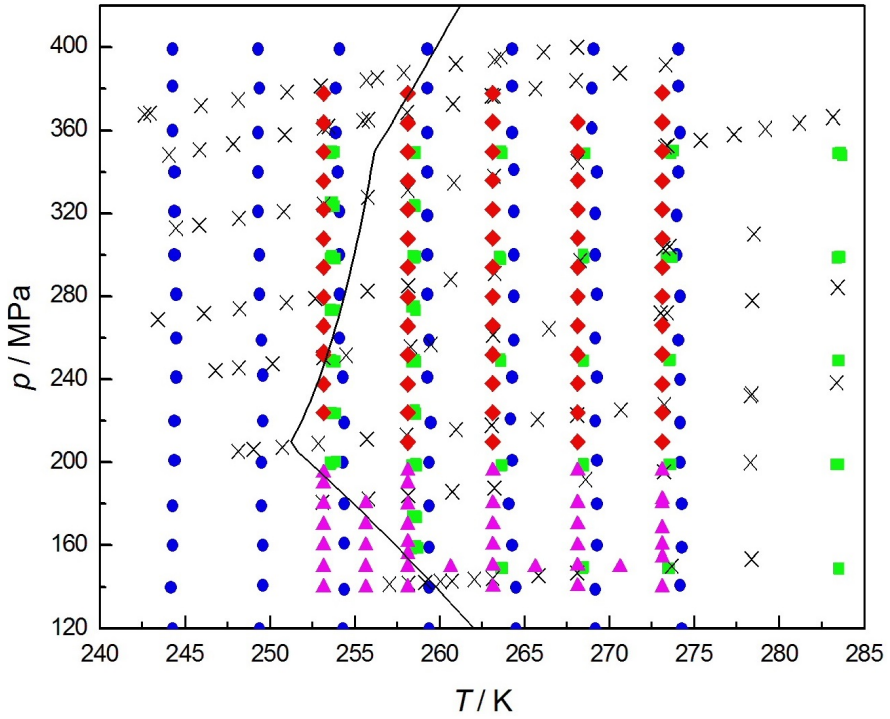

Figure 4.11: Location of investigated states of subcooled water: ▲, Sotani *et al.*; ♦, Asada *et al.*; ■, Guignon *et al.*; ●, Mishima; ×, this work; —, melting curve.

As can be clearly observed in Fig. 4.11, the measurements from the different works are not located exactly at the same values of temperature and pressure. For that reason, in order to compare the experimental densities with the literature measurements carried out at different thermodynamic states, density was expressed by a polynomial function of temperature and pressure in a boundary of the arbitrary point (T_0, p_0).

Table 4.2: Coefficients for the interpolation function of density 4.1 determined from the experimental densities, temperatures and pressures by means of the least square method.

i	j	ρ_{ij}/kg·m^{-3}·K^{-i}·MPa^{-j}
0	0	1113.62
0	1	0.30
0	2	-3.11·10^{-4}
1	0	-0.47
1	1	-6.91·10^{-4}
1	2	6.67·10^{-6}
2	0	2.40·10^{-4}
2	1	-4.85·10^{-6}
2	2	-1.26·10^{-7}

Thus, the measurements here obtained were regressed by the following expression:

$$\rho\,(T,p) = \sum_{i=0}^{2}\sum_{j=0}^{2} \rho_{ij}(T-T_0)^i(p-p_0)^j \quad , \tag{4.1}$$

where $T_0 = 259$ K, $p_0 = 280.3$ MPa.

The values of the ρ_{ij} coefficients, calculated through the least squares analysis, are reported in Table 4.2.

The interpolation function of Eq. 4.1, obtained from the experimental values of this thesis, allowed to determine the density exactly at the same thermodynamic states measured by Sotani *et al.*, Asada *et al.*, Guignon *et al.* and Mishima. Hence, such calculated values and the literature measurements could be compared.

Figure 4.12 reports the percentage deviation of the literature values from densities here obtained.

All the deviations of Sotani *et al.* are less than 0.025%, so the data are in agreement with the the values here obtained. The densities of Asada *et al.* are within the uncertainty here calculated (0.07%) except the highest value, which is within 0.1%. Most of Guignon *et al.* density values are lower than those obtained in this work. The density uncertainty of Guignon *et al.* is 0.2% below 273 K, therefore all the values result in agreement with the data presented in this work. On the other hand, the deviations of the Mishima data from this work's density systematically increase with density up to 0.5%: thus the higher deviations between this work and Mishima's values correspond to the measurements performed at lower temperatures and higher pressures. In the paper of Mishima, the uncertainty is not reported, however, Holten *et al.* [11] assigned to Mishima's measurements an uncertainty of

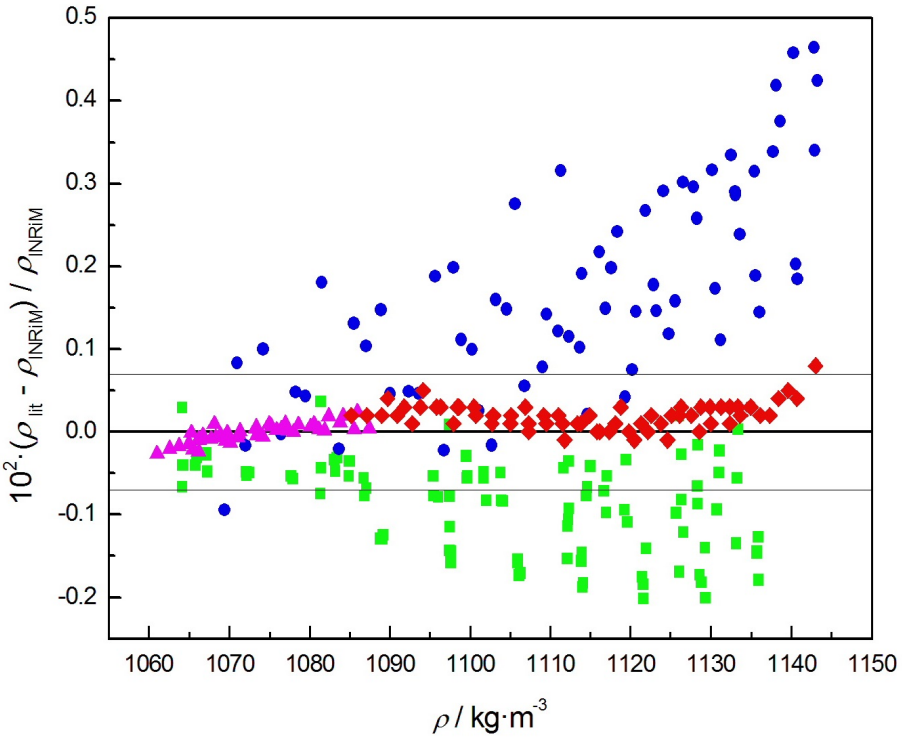

Figure 4.12: Deviations of the literature density of water from the experimental values of this work (zero line) as a function of density: ▲, Sotani *et al.*; ♦, Asada *et al.*; ■, Guignon *et al.*; ●, Mishima; the solid lines represent the experimental uncertainty of this work (0.07%).

0.5% for temperatures above 253 K and all the experimental data result still in agreement with the densities of this work.

Chapter 5

Development of a fundamental equation of state

Accurate experimental measurements of thermodynamic properties are necessary for the development of the equation of state of any fluid. Therefore, the measurements presented in this work may be used to improve the equation of state for water.

This last part of the thesis reports briefly the theory and the procedure to develop a fundamental equation of state. The research work presented in this chapter was carried out within the four months period as visiting student at the *National Institute of Standards and Technology* (NIST) in Colorado, USA.

However, water is a very complex fluid and developing its equation of state presents a lot of difficulties because of its many complexities and anomalies. For that reason water was obviously not studied, since it was the first approach to the implementation of an equation of state.

Nevertheless, in this chapter two practical examples are given: the fundamental equations of state for *n*-hexadecane and *n*-docosane. These fluids were chosen because they are common alkanes, with behavior typical of most of the fluids, so the implementation of their equations of state do not bump into particular drawbacks and they resulted suitable fluids to be studied by a beginner. Furthermore, the equations of state for *n*-hexadecane and *n*-docosane have not been developed yet, even if there is a considerable interest in their knowledge for industrial applications.

5.1 *n*-hexadecane and *n*-docosane

n-hexadecane ($C_{16}H_{34}$) and *n*-docosane ($C_{22}H_{46}$) are normal alkanes of interest in the petroleum industry for multiple applications. They can be combined in mixtures and are mainly used as fuel, especially for aviation. In this work, fundamental equations of state, in terms of the Helmholtz energy, for *n*-hexadecane and *n*-docosane are presented. Fundamental equations of state are valid over the whole fluid region, and through them all thermodynamic properties can be calculated. Measurements of vapor pressure, density, speed of sound, and heat capacity are available in the literature for both *n*-hexadecane and *n*-docosane. Although the amount of data available for *n*-hexadecane is quite large, *n*-docosane is less studied, as for other high weight alkanes. The experimental data available in the literature for *n*-hexadecane and for *n*-docosane were used to develop the equations of state.

5.1.1 Critical and fixed values

The critical values are among the most important parameters in the development of equations of state, such as the reduced parameters and in ancillary equations. In the work of Lemmon and Goodwin [26], equations for the critical temperatures and pressures of normal alkanes, as functions of the carbon number, were determined. In the present work, the critical temperature values calculated by Lemmon and Goodwin were adopted for *n*-hexadecane and *n*-docosane. The critical densities, ρ_c, of *n*-hexadecane and *n*-docosane were determined during the fitting process of their equations of state. The critical pressures, p_c, were calculated from the final equations of state as a fixed point at the critical temperature and density.

The values of the *n*-hexadecane critical point are

$$T_c = 722.1 \text{ K}$$
$$p_c = 1.4799 \text{ MPa}$$
$$\rho_c = 1.000 \text{ mol} \cdot \text{dm}^{-3}$$

The triple point temperature of *n*-hexadecane is 291.329 K and its molar mass is 226.441 g·mol^{-1} [27].

The critical values of *n*-docosane are

$$T_c = 792.2 \text{ K}$$
$$p_c = 1.1740 \text{ MPa}$$
$$\rho_c = 0.723 \text{ mol} \cdot \text{dm}^{-3}$$

The triple point temperature of *n*-docosane is 587.6 K and its molar mass is 310.601 g·mol^{-1} [27].

5.2 Equation of state in terms of Helmholtz energy

The common form of the equation of state is based on the Helmholtz energy as a function of density and temperature $a(\rho, T)$, which is used for the calculation of thermodynamic properties of pure fluids and mixtures with low uncertainties. Indeed, expressing equations in terms of the Helmholtz energy has the advantage that thermodynamic properties are simple derivatives of the equation of state, and thus only one equation is necessary to obtain any properties, which are estimated as derivatives of the Helmholtz energy.

An example is given by pressure p, calculated as

$$p = \rho^2 \left(\frac{\partial a}{\partial \rho} \right)_T \tag{5.1}$$

otherwise the entropy s is

$$s = - \left(\frac{\partial a}{\partial T} \right)_\rho \quad . \tag{5.2}$$

The derivatives of the Helmholtz energy, required to calculate other thermodynamic properties not reported here, can be seen in several works, e.g. [28]. Nevertheless, the functional form is the reduced Helmholtz energy α, as a function of the dimensionless density and temperature.

$$\frac{a(\rho, T)}{RT} = \alpha(\delta, \tau) = \alpha^0(\delta, \tau) + \alpha^{\mathrm{r}}(\delta, \tau) \quad , \tag{5.3}$$

where $\delta = \rho/\rho_{\mathrm{c}}$, $\tau = T_{\mathrm{c}}/T$, and R is the molar gas constant equal to 8.3144621 J mol^{-1} K^{-1} [29]. The reduced Helmholtz energy, α, is expressed from the ideal gas contribution, α^0, which represents the ideal gas properties, and the residual or real Helmholtz energy α^{r} due to interactions between molecules.

5.2.1 Properties of the ideal gas

The dimensionless Helmholtz energy of the ideal gas is defined as

$$\alpha^0(\delta, \tau) = \frac{h_0^0 \tau}{RT_{\mathrm{c}}} - \frac{s_0^0}{R} - 1 + \ln \frac{\delta \tau_0}{\delta_0 \tau} - \frac{\tau}{R} \int_{\tau_0}^{\tau} \frac{c_p^0}{\tau^2} \mathrm{d}\tau + \frac{1}{R} \int_{\tau_0}^{\tau} \frac{c_p^0}{\tau} \mathrm{d}\tau \tag{5.4}$$

where c_p^0 is the ideal gas isobaric heat capacity, $\delta_0 = \frac{\rho_0}{\rho_{\mathrm{c}}}$, $\tau_0 = \frac{T_{\mathrm{c}}}{T_0}$, h_0^0 and s_0^0 are respectively the ideal enthalpy and the ideal entropy at the arbitrary reference state (T_0, p_0).

The ideal gas Helmholtz energy is generally considered in the following simplified form [30]:

$$\alpha^0(\delta,\tau) = \ln\delta + (v_1 - 1)\ln\tau + \sum_{k=1}^{2} a_k \tau^{i_k} + \sum_{k=2}^{3} v_k \ln\left(1 - e^{-u_k\tau/T_c}\right) \quad . \tag{5.5}$$

In order to calculate thermodynamics properties, a model for the ideal gas isobaric heat capacity is necessary. The expression for the ideal gas isobaric heat capacity c_p^0, used in this work, required to derive the ideal gas Helmholtz energy is

$$\frac{c_p^0}{R} = v_1 + \sum_{k=2}^{3} v_k \left(\frac{u_k}{T}\right)^2 \frac{e^{u_k/T}}{\left(e^{u_k/T} - 1\right)^2} \quad . \tag{5.6}$$

The u_k coefficients contained in the Einstein functions used in this equation give the proper shape of the ideal gas heat capacity similar to that derived from statistical mechanical model. The values of a_k, i_k, v_k and u_k, used in Eq.s 5.4 and 5.5, are given in Table 5.1 for n-hexadecane and in Table 5.2 for n-docosane.

Table 5.1: Coefficients and exponents of Eqs. 5.5 and 5.6 for n-hexadecane.

k	a_k	i_k	v_k	u_k/K
1	45.96	0	23.0	
2	-26.19	1	18.9	420
3			76.2	1860

Table 5.2: Coefficients and exponents of Eqs. 5.5 and 5.6 for n-docosane.

k	a_k	i_k	v_k	u_k/K
1	66.73	0	33.9	
2	-44.17	1	61.6	1000
3			77.7	2400

5.2.2 Properties of the real fluid

The functional form used to about the year 2000 for the residual (or real) Helmholtz energy equation was

$$\alpha^{\mathrm{r}}(\delta,\tau) = \sum N_k \delta^{d_k} \tau^{t_k} + \sum N_k \delta^{d_k} \tau^{t_k} e^{-\delta^{l_k}} \quad . \tag{5.7}$$

where the density exponents d_k and l_k have to be positive integers to ensure that α^{r} and its derivatives vanish in the limit of zero density [30].

However, a form using only simple polynomial and exponential terms is not able to describe the critical point. Thus, a form for Helmholtz energy containing additional Gaussian bell-shaped terms is now preferred. These Gaussian terms are useful since they are able to represent the fluid properties in the critical region.

For the studied alkanes, α^{r} is expressed as

$$\alpha^{\mathrm{r}}(\delta,\tau) = \sum_{k=1}^{5} N_k \delta^{d_k} \tau^{t_k} + \sum_{k=6}^{10} N_k \delta^{d_k} \tau^{t_k} \exp\left(-\delta^{l_k}\right) + \\ + \sum_{k=11}^{15} N_k \delta^{d_k} \tau^{t_k} \exp\left[-\eta_k(\delta-\epsilon_k)^2 - \beta_k(\tau-\gamma_k)^2\right] \quad , \tag{5.8}$$

where the coefficients and exponents are reported in Table 5.3 for n-hexadecane and in Table 5.4 for n-docosane.

The equation of state is developed by correlating selected experimental data through least squares fitting methods. Firstly, all experimental data available in the literature have to be collected. The fitting procedure to get the equation of state required setting the fitting programs that use REFPROP Fortran routines [31], entering the experimental data into the files read by the fitter program, running iterative the fit routines. The sum of squares decreased as the fitting program minimized the deviations of the equation to the experimental data by adjusting the parameters of the equation through the nonlinear algorithm. The residual sum of squares, S is represented by [28]

$$S = \sum W_\rho F_\rho^2 + \sum W_p F_p^2 + \sum W_{c_v} F_{c_v}^2 + \ldots \tag{5.9}$$

where W is the weight assigned to each data point and F is the function used to minimize the deviations, such as

$$F_p = \frac{p_{\mathrm{data}} - p_{\mathrm{calc}}}{p_{\mathrm{data}}} \tag{5.10}$$

The weight of the data point were chosen according to type, region or uncertainty. Thus, the program calculate the thermodynamic properties

by the experimental values fitted and the equation was evaluated at the end of each iterative running by comparing it with all the other collected experimental data. Then, the experimental data was added (or removed) to the fit, with different weight, in order to minimize the sum of squares.

Besides changing the experimental data to be fitted, the equation was repetitively improved by imposing constraints on the properties behavior, as better explained in following sections.

Table 5.3: Coefficients of Eq. 5.8 for n-hexadecane.

k	N_k	t_k	d_k	l_k	η_k	β_k	γ_k	ϵ_k
1	0.03965879	1.000	4					
2	1.945813	0.224	1					
3	-3.738575	0.910	1					
4	-0.3428167	0.950	2					
5	0.3427022	0.555	3					
6	-2.519592	2.360	1	2				
7	-0.8948857	3.580	3	2				
8	0.10760773	0.500	2	1				
9	-1.297826	1.72	2	2				
10	-0.04832312	1.078	7	1				
11	4.245522	1.14	1		-0.641	-0.516	1.335	0.75
12	-0.31527585	2.43	1		-1.008	-0.669	1.187	1.616
13	-0.7212941	1.75	3		-1.026	-0.25	1.39	0.47
14	-0.2680657	1.1	2		-1.21	-1.33	1.23	1.306
15	-0.7859567	1.08	2		-0.93	-2.1	0.763	0.46

Table 5.4: Coefficients of Eq. 5.8 for n-docosane.

k	N_k	t_k	d_k	l_k	η_k	β_k	γ_k	ϵ_k
1	0.0423455	1.000	4					
2	2.370432	0.224	1					
3	-4.30263	0.910	1					
4	-0.4039603	0.950	2					
5	0.4005704	0.555	3					
6	-2.643419	2.360	1	2				
7	-0.9199641	3.580	3	2				
8	0.1394402	0.500	2	1				
9	-1.448862	1.72	2	2				
10	-0.0547678	1.078	7	1				
11	4.579069	1.14	1		-0.641	-0.516	1.335	0.75
12	-0.3534636	2.43	1		-1.008	-0.669	1.187	1.616
13	-0.8217892	1.75	3		-1.026	-0.25	1.39	0.47
14	-0.2604273	1.1	2		-1.21	-1.33	1.23	1.306
15	-0.7618884	1.08	2		-0.93	-2.1	0.763	0.46

5.3 Ancillary equations

The boundaries between the liquid and vapor phases are defined by saturation states that can be estimated through the use of ancillary equations. These give close estimates for the pressures and densities required, as initial estimates, in the iterative process to find the saturation states, but are not required to calculate properties from the equation of state. The ancillary equations were developed by fitting calculated values of saturation states, determined with the application of the Maxwell criteria applied to the equation of states.

5.3.1 Ancillary equations for *n*-hexadecane

The ancillary form for the **vapor pressure** p_σ is

$$\ln \frac{p_\sigma}{p_c} = \frac{T_c}{T}\left[N_1\Theta + N_2\Theta^{1.5} + N_3\Theta^{2.8} + N_4\Theta^{6.7} + N_5\Theta^{8.9} + N_6\Theta^{15.5}\right] \quad (5.11)$$

where $\theta = 1 - \frac{T}{T_c}$, and where $N_1 = -10.4856$, $N_2 = 3.8226$, $N_3 = -8.6727$, $N_4 = -4.1440$, $N_5 = 0.8801$ and $N_6 = -5.7224$.

The **saturated liquid density** ρ' is determined by the following ancillary equation

$$\frac{\rho'}{\rho_c} = 1 + N_1\Theta^{0.39} + N_2\Theta^{0.84} + N_3\Theta^{1.27} + N_4\Theta^{1.72} + N_5\Theta^{2.26} \quad (5.12)$$

where $N_1 = 3.4300$, $N_2 = -4.0080$, $N_3 = 8.4779$, $N_4 = -7.8940$, and $N_5 = 3.4824$.

The ancillary equation that represents the **saturated vapor density** ρ'' is

$$\ln \frac{\rho''}{\rho_c} = N_1\Theta^{0.44} + N_2\Theta^{2.32} + N_3\Theta^{1.75} + N_4\Theta^{4.40} + N_5\Theta^{9.97} + N_6\Theta^{20.90} \quad (5.13)$$

where $N_1 = -5.0096$, $N_2 = 0.9061$, $N_3 = -61.4138$, $N_4 = -143.5222$, and $N_5 = -369.0229$.

5.3.2 Ancillary equations for *n*-docosane

The ancillary form representing the **vapor pressure** p_σ is

$$\ln \frac{p_\sigma}{p_c} = \frac{T_c}{T}\left[N_1\Theta + N_2\Theta^{1.5} + N_3\Theta^{2.7} + N_4\Theta^{5.5} + N_5\Theta^{14.1} + N_6\Theta^{52.1}\right] \quad (5.14)$$

where $N_1 = -12.3834$, $N_2 = 2.8818$, $N_3 = -11.6292$, $N_4 = -2.7357$, $N_5 = -7.3103$, and $N_6 = 1188.9117$.

The **saturated liquid density** ρ' is determined by

$$\frac{\rho'}{\rho_c} = 1 + N_1\Theta^{0.5} + N_2\Theta^{0.8} + N_3\Theta^{1.2} + N_4\Theta^{1.8} + N_5\Theta^{2.5} \tag{5.15}$$

where $N_1 = 6.6254$, $N_2 = -11.0123$, $N_3 = 13.6452$, $N_4 = -8.8244$, and $N_5 = 3.1241$.

The ancillary equation that represents the **saturated vapor density** ρ'' is

$$\ln\frac{\rho''}{\rho_c} = N_1\Theta^{0.5} + N_2\Theta^{24.0} + N_3\Theta^{1.7} + N_4\Theta^{4.2} + N_5\Theta^{10.3} + N_6\Theta^{10.6} \tag{5.16}$$

where $N_1 = -5.9790$, $N_2 = -586.6421$, $N_3 = -14.3725$, $N_4 = -71.0676$, $N_5 = -213.3123$, $N_6 = 15.7901$.

5.4 Fitting constraints

In order to develop the equations of state, several constraints were used to control the shape of fluid properties. Most of the constraints for *n*-hexadecane were used as constraints for *n*-docosane, adapting the working range for this fluid. Because the constraints for *n*-docosane are mostly the same, they are not reported here. In Table 5.5, a list of the main constraints for *n*-hexadecane is given. The table shows the properties for which a constraint was needed, the kind of constraint imposed, and the range over which it was applied.

For example, the rectilinear diameter, defined as [32]

$$\rho^d = \frac{1}{2}(\rho' + \rho'') \quad , \tag{5.17}$$

was constrained to be linear by imposing zero curvature from 650 K to the critical temperature; it results in the behavior shown in Fig. 5.1. In preliminary fits the fourth virial coefficient was negative around (1500 to 2500) K, thus it was forced to give positive values in the temperature range between (1300 and 3000) K.

The phase identification parameter (PIP) is a very useful and sensitive instrument for the equation evaluation [33]. For that reason, putting constraints on this parameter can considerably improve the behavior of the equation of state. For both *n*-hexadecane and *n*-docosane, the PIP either as function of temperature or density required many constraints. An example is the constraint acting on the isobar at 1 MPa in the temperature

range from (200 to 420) K that imposed the slope, curvature, and third and fourth derivatives to all be positive. A further constraint was used to obtain negative curvature of the isotherm at 1000 K between 1.08 mol·dm^{-3} and 1.85 mol·dm^{-3} (the plot of the PIP as a function of density is shown in Fig. 5.2).

More details about the phase identification parameter are reported in a following section.

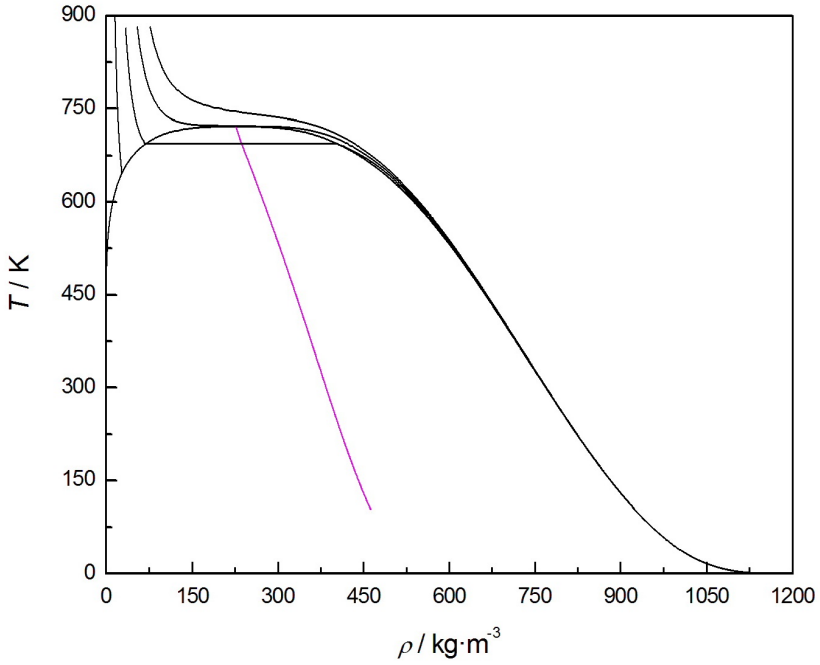

Figure 5.1: Temperature as a function of density for n-hexadecane: the pink curve is the rectilinear diameter.

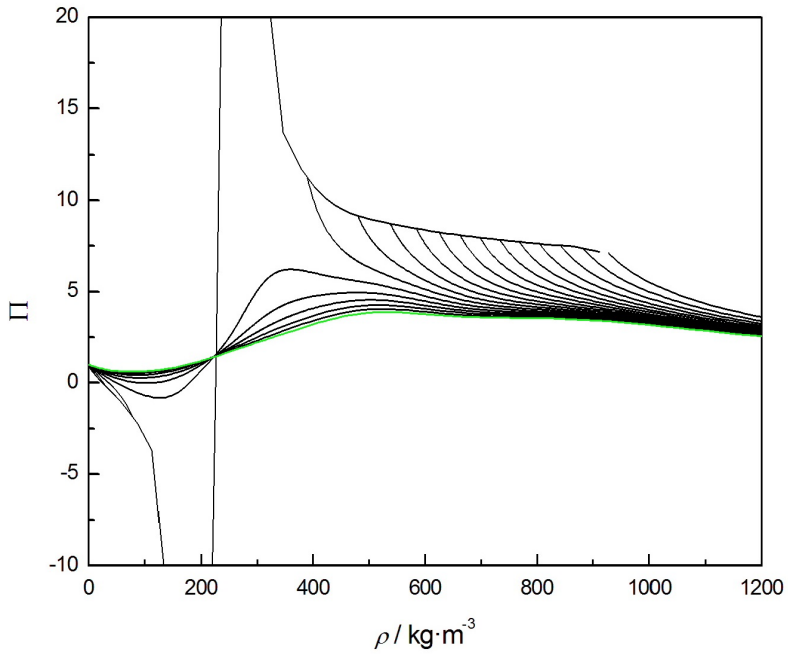

Figure 5.2: Phase identification parameter (PIP) as a function of density for n-hexadecane along isotherms: the green curve is the isotherm at 1000 K.

Table 5.5: Main constraints used for *n*-hexadecane.

Property	Constraint	Range
speed of sound	negative slope and 3^{rd} derivative	1 MPa, (35 - 115) K
speed of sound	positive curvature and 4^{th} derivative	1 MPa, (35 - 115) K
isochoric heat capacity	negative slope and 3^{rd} derivative	3 MPa, (430 - 625) K
rectilinear diameter	zero curvature	liquid saturation line, from 650 K to T_c
isochoric heat capacity	positive curvature and 4^{th} derivative	3 MPa, (430 - 625) K
phase identification parameter	negative curvature	1000 K, (1.08 - 1.85) mol·dm^{-3}
phase identification parameter	zero curvature	725 K, (0.80 - 0.95) mol·dm^{-3}
phase identification parameter	positive derivatives	1 MPa, (200 - 420) K
phase identification parameter	positive derivatives	liquid saturation line, (580 - 650) K
4^{th} virial coefficient	positive line	(1300 - 3000) K
4^{th} virial coefficient	negative slope	(1000 - 1200) K
ideal curve	zero curvature	(0.02 - 2.00) mol·dm^{-3}
Joule inversion curve	positive curvature	(0.05 - 2.50) mol·dm^{-3}
Joule-Thomson curve	positive curvature	(0.1 - 2.0) mol·dm^{-3}

5.5 Comparison to experimental data

The experimental data collected by the literature and used for this work are summarized in Tables 5.6 and 5.7 for *n*-hexadecane and in Table 5.8 for *n*-docosane. The experimental data were converted to kelvins (ITS-90) for temperatures, megapascals for pressures, and moles per cubic decimeter for densities. In order to estimate the uncertainties of the equations of state, all available experimental data are considered, even those not fitted in the development of the equations. The uncertainties are considered as estimates of combined expanded uncertainties with a coverage factor of 2. The accuracy of the equations of state were determined by statistical comparison between the properties calculated from the equations of state and the experimental values by the average absolute deviations (AAD) for any generic property X, defined as follows

$$\mathrm{AAD} = \frac{1}{n}\sum_{i=1}^{n}|\Delta X_i| \tag{5.18}$$

where n is the number of data and ΔX is defines as:

$$\Delta X = 100 \cdot \left(\frac{X_{\mathrm{data}} - X_{\mathrm{calc}}}{X_{\mathrm{data}}}\right) \tag{5.19}$$

The AAD values between experimental data and the equations of state are reported in Tables 5.6 and 5.7 for *n*-hexadecane and in Table 5.8 for *n*-docosane.

The following sections focus on the the comparison between the implemented equations of state here presented and the experimental data available in the literature. For reason of clarity, the plots of the experimental deviations from the equations do not show all the experimental data collected (the data less represented by the equations are only excluded from the plots) and only the main sets of data are analyzed.

Table 5.6: Experimental data for *n*-hexadecane.

author	year		AAD %
speed of sound			
Aminabhavi and Bindu	1994	[34]	0.69
Ball and Trusler	2001	[35]	0.42
Boelhouwer	1967	[36]	0.26
Bolotnikow *et al.*	2005	[37]	0.13
Khasanshin and Shchemelev	2001	[38]	0.11
Nascimento *et al.*	2015	[39]	0.12
Neruchev *et al.*	2005	[40]	3.21
Outcalt *et al.*	2010	[41]	0.03
Paredes *et al.*	2011	[42]	0.04
Plantier *et al.*	2005	[43]	0.64
Prak *et al.*	2013	[44]	0.03
density			
Amorim *et al.*	2007	[45]	0.13
Banipal *et al.*	1991	[46]	0.02
Boelhouwer	1960	[47]	0.16
Chang *et al.*	1998	[48]	0.13
Doolittle	1964	[49]	0.76
Dymond *et al.*	1979	[50]	0.06
Dymond *et al.*	1992	[51]	0.06
Glaser *et al.*	1985	[52]	0.22
Gouel	1978	[53]	0.07
Matthews *et al.*	1987	[54]	0.31
Outcalt *et al.*	2010	[41]	0.11
Snyder and Winnick	1970	[55]	0.09
Tanaka *et al.*	1991	[56]	0.06
Wu *et al.*	2011	[57]	0.15
Wuerflinger *et al.*	2001	[58]	0.08
Zolghadr *et al.*	2013	[59]	0.35
heat capacity			
Baba *et al.*	1992	[60]	3.71
Banipal *et al.*	1991	[46]	0.12
Benson *et al.*	1971	[61]	0.32
Gollis *et al.*	1962	[62]	3.64

Table 5.7: Experimental data for *n*-hexadecane.

author	year		AAD %
saturated liquid density			
Aminabhavi and Bindu	1994	[34]	0.08
Asfour *et al.*	1990	[63]	0.06
Aucejo *et al.*	1995	[64]	0.05
Baños *et al.*	1992	[65]	0.02
Boelhouwer	1960	[47]	0.02
Bolotnikov *et al.*	2005	[37]	0.03
Calingaert *et al.*	1941	[66]	0.04
Camin *et al.*	1954	[67]	0.03
Doolittle	1964	[49]	0.52
Dymond *et al.*	1979	[50]	0.07
Dymond and Young	1980	[68]	0.08
El-Banna and El-Batouti	1998	[69]	0.06
Espeau and Ceolin	2006	[70]	1.61
Findenegg	1970	[71]	0.02
Gomez-Ibanez and Liu	1963	[72]	0.01
Graaf *et al.*	1992	[73]	0.31
Krafft	1882	[74]	0.10
Lauer and King	1956	[75]	0.04
Mansker *et al.*	1987	[76]	0.24
Paredes *et al.*	2011	[42]	0.03
Plebanski *et al.*	1986	[77]	0.07
Prak *et al.*	2013	[44]	0.03
Queimada *et al.*	2003	[78]	0.02
Vogel	1946	[79]	0.17
Wu *et al.*	1998	[80]	0.07
vapor pressure			
Abdi and Meisen	1998	[81]	7.36
Camin *et al.*	1954	[67]	0.07
Eggertsen *et al.*	1969	[82]	3.38
Lee *et al.*	1992	[83]	1.76
Mills and Fenton	1987	[84]	0.84
Morgan and Kobayashi	1994	[85]	0.22
Myers and Fenske	1955	[86]	3.25
Parks and Moore	1949	[87]	10.10
Siitsman *et al.*	2014	[88]	0.86
Viton *et al.*	1996	[89]	2.92

Table 5.8: Experimental data for *n*-docosane.

author	year		AAD %
vapor pressure			
Chickos and Hanshaw	2004	[90]	7.18
Francis and Wood	1926	[91]	21.3
Grenier *et al.*	1981	[92]	3.16
Morgan and Kobayashi	1994	[85]	0.46
Piacente *et al.*	1994	[93]	26.4
Sasse	1988	[94]	3.00
Young	1928	[95]	5.44
saturated liquid density			
Dutour *et al.*	2001	[96]	0.05
Neruchev *et al.*	1967	[97]	0.06
Queimada *et al.*	2003	[78]	0.06
density			
Peters *et al.*	1988	[98]	0.95
speed of sound			
Dutour *et al.*	2001	[96]	0.56
Neruchev *et al.*	1967	[97]	0.06
heat capacity			
Durupt *et al.*	1996	[99]	5.23
Atkinson *et al.*	1969	[100]	0.26

5.5.1 Comparison to *n*-hexadecane experimental data

In Fig. 5.3 the deviations of experimental **vapor pressures** from the equation are shown. The measurements cover a range of temperatures between 298 K and 600 K. Most of the experimental data show scatter within 2%. The data of Morgan and Kobayashi [85], Viton *et al.* [89], and Camin *et al.* [67] are best represented by the equation of state. The three data sets overlap between 460 K to 470 K, and the data show deviations on average within 0.1%. Above 470 K, only the Morgan and Camin data are available, and they are in agreement with the equation within 0.2%. The data of Morgan *et al.* were carried out for temperatures up to 583 K, and the equation maintains deviations below 0.2%. For temperatures lower than 460 K, the data of Morgan and Viton *et al.* show deviations from the equation of 1%.

The deviations of *n*-hexadecane **saturated liquid densities** from the fundamental equation of state are shown in Fig. 5.4. Most of the data have a deviations lower than 0.1% between 273 K and 373 K. In the temperature range between 303 K and 373 K, the data of Bolotnikov *et al.*, Prak *et al.* 2013 [44], and Prak *et al.* 2014 show a deviation lower than 0.05%. The measurements of Plebanski *et al.* [77] were performed over the widest range of temperature (from about 300 K to 490 K), with a maximum deviation of 0.07% from the equation and better than 0.02% between (340 and 420) K.

All of the **density** data available are represented by the equation here implemented with deviations up to 1% and most of them within 0.3%, as can be observed in Fig. 5.5. The data of Banipal *et al.* [46] are represented by the equation within 0.1% for temperatures between (318 and 373) K, and at pressures up to 10 MPa. At ambient pressure the deviation is reduced to 0.05%. The deviations of the data of Snyder *et al.* are below 0.1% at 298 K. In the pressure range of (0.6 and 28) MPa the data are within 0.05%. The measurements performed by Outcalt *et al.* [41] are in agreement with the equation of state within 0.2%, but the deviations are consistently negative.

The deviation in **speed of sound** data from the equation are shown in Fig. 5.6. The only available measurements at temperatures higher than 473 K are those in the work of Neruchev *et al.* [40]. The data show good agreement with the equation and are less than 0.5% for temperatures up to 693 K. At pressures between 10 MPa and 50 MPa, the data of Ball and Trusler [35], Nascimento *et al.* [39], Khasanshin and Shchemelev [38], and Boelhouwer [36] are in agreement and fitted to within 0.25%. Above 50 MPa, the measurements of Boelhouwer, which were carried out up to 120 MPa, spread no more than 0.3%. On the other hand, for the other available data above 50 MPa (Ball and Trusler), the deviations increase at higher pressures. The deviations become increasingly negative down to -3.2% at 100 MPa. The speed of sound data at ambient pressure between 290 K and 373 K are represented by the equation within 0.2%.

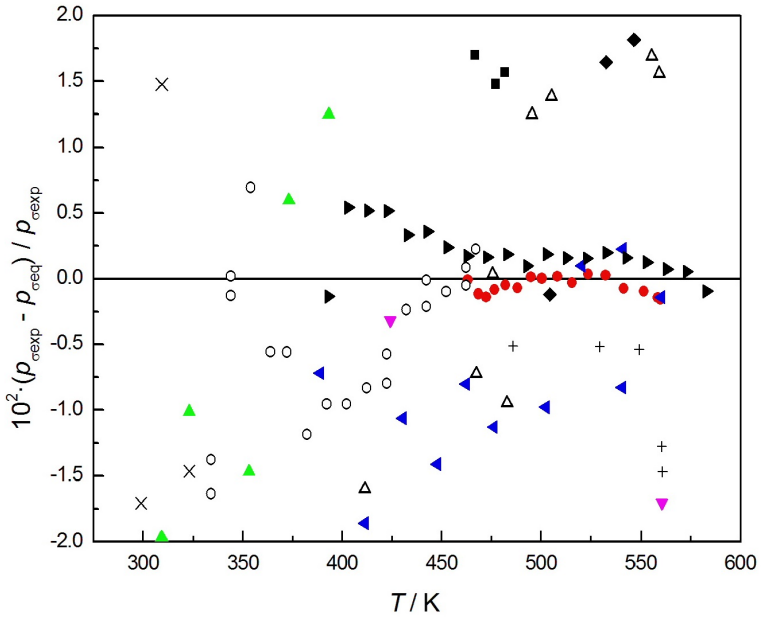

Figure 5.3: Comparison between the experimental vapor pressure and the equation of state (zero line) for *n*-hexadecane: ■, Abdi and Meisen; ●, Camin *et al.*; ▲, Eggertsen *et al.*; ▼, Kraaft; ♦, Lee *et al.*; ◀, Mills and Fenton; ▶, Morgan and Kobayashi; △, Myers and Fenske; ×, Parks and Moore; +, Siitsman *et al.*

For the **isobaric heat capacity**, there are less experimental data than those of the properties previously discussed. The measurements, shown in Fig. 5.7, are within 6% from the equation. The work with the largest number of measurements is that of Banipal *et al.* [46]. They are well represented by the equation of state; the deviations are not higher than 0.3% in the temperature range from 318 K and 373 K. At 298 K, the measurements of Benson *et al.* [61] deviate from the equation by less than 0.02%. The deviations of their isobaric heat capacities increase to 0.5% for higher temperatures (up to 358 K), and all of them are negative.

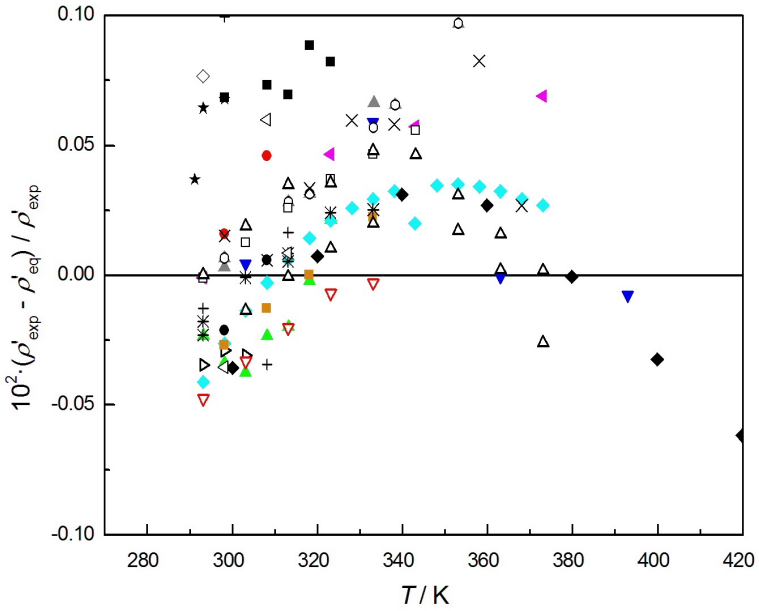

Figure 5.4: Comparison between the experimental saturated liquid densities and the equation of state (zero line) for *n*-hexadecane: ■, Aminabhavi and Bindu; ●, Asfour *et al.*; ▲, Boelhouwer; ▼, Bolotnikov *et al.*; ♦, Calingaert *et al.*; ◀, Camin *et al.*; ▷, Doolittle; ■, Dymond *et al.*; ▲, El-Banna and El-Batouti; ○, Espeau and Ceolin; +, Findenegg; ∗, Graaf *et al.*; ●, Krafft; ★, Mansker *et al.*; ×, Paredes *et al.*; □, Prak *et al.*; ♦, Queimada *et al.*; △, Vogel; ▽, Wu *et al.*

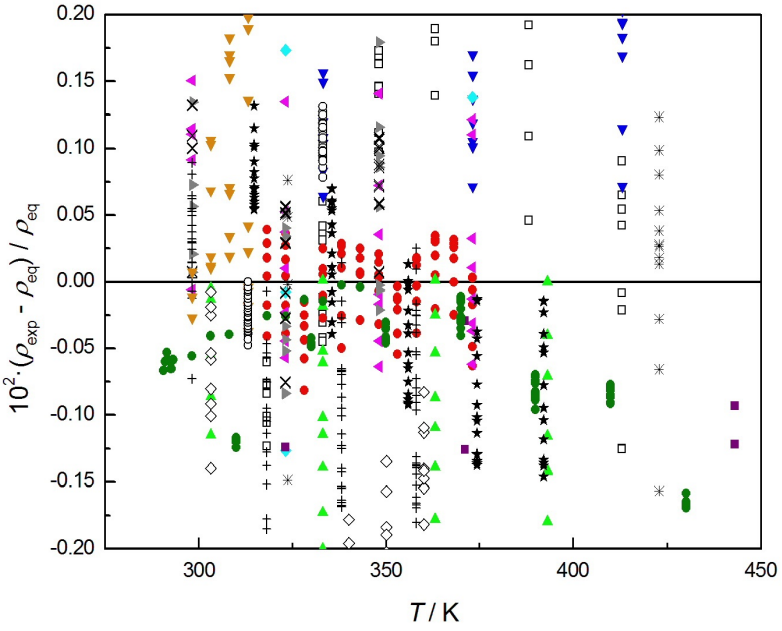

Figure 5.5: Comparison between the experimental density and the equation of state (zero line) for *n*-hexadecane: □, Amorim *et al.*; ●, Banipal *et al.*; ▲, Boelhouwer; ▼, Chang *et al.*; ♦; ▲, Doolittle *et al.* (1980); ◀, Dymond *et al.* (1992); ◊, Glaser *et al.*; ★, Gouel; ■, Matthews *et al.*; ●, Outcalt *et al.*; +, Snyder *et al.*; ×, Tanaka *et al.*; ∗, Wu *et al.*; ▼, Wuerflinger *et al.*; ○, Zolghadr *et al.*

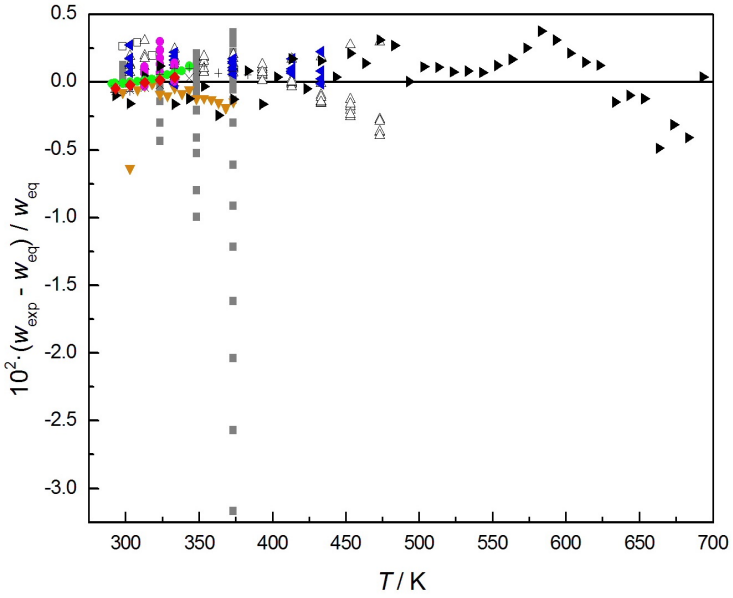

Figure 5.6: Comparison between the experimental speed of sound and the equation of state (zero line) for *n*-hexadecane: □, Aminabhavi and Bindu; ■, Ball and Trusler; ▽, Boelhouwer; ▼, Bolotnikov *et al.*; ◀, Khasanshin and Shchemelev; ●, Nascimento *et al.*; ▶, Neruchev *et al.*; ●, Outcalt *et al.*; ∗ Paredes *et al.*; +, Plantier; ♦, Prak *et al.* .

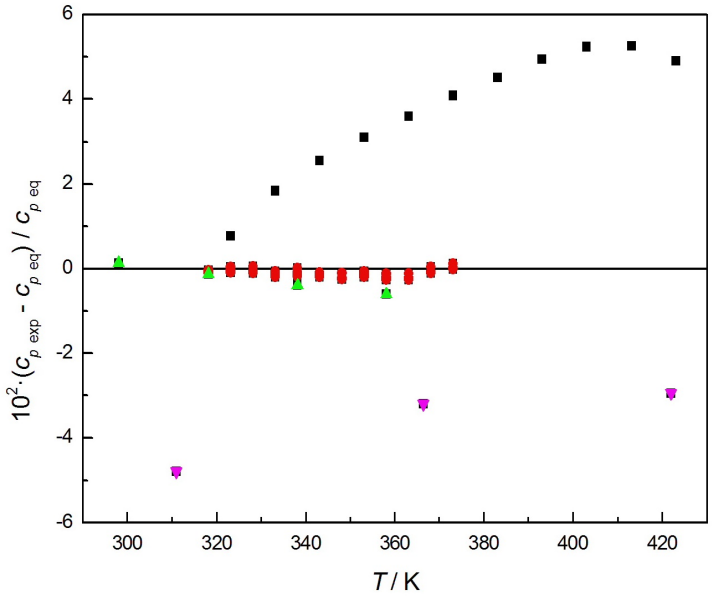

Figure 5.7: Comparison between the experimental speed of sound and the equation of state (zero line) for *n*-hexadecane: ■, Baba *et al.*; ●, Banipal *et al.*; ▲, Benson *et al.*; ▼, Gollis *et al.*

5.5.2 Comparison to *n*-docosane experimental data

For *n*-docosane, there are not as many data points as for *n*-hexadecane. The **vapor pressure** is the most studied property, covering a wide range of temperature (see Fig. 5.8). The data set of Morgan and Koabayashi [85] is best represented by the equation at high temperatures, between 453 K and 573 K, with an average deviation of 2.5%. The data given in Sasse *et al.* [94] present different behavior with respect to temperature. Between (393 and 423) K the data spread with respect to the equation is 2%. Below 393 K, they all show negative deviations between -4% and -8%. Above 423 K the data differ with the equation constantly around 2%.

All the experimental **saturated liquid densities** deviate from the equation of state within 0.2%, as shown in Fig. 5.9. The measurements of Dutour *et al.* [96] deviate more from equation as the temperature increases, starting from -0.001% at 323.15 K to -0.12% at 393.15 K. Queimada *et al.* [78] measured three points of saturated liquid density which deviate from the calculated values around 0.57%. The measurements of Neruchev *et al.* cover a wider range of temperature from (333 to 473) K. All of them are in agreement with the presented equation of state within ±0.15%.

Peters *et al.* [98] published the only **density** data reported for *n*-docosane with pressures up to 16 MPa. The data show a systematic average deviation of -1% from the equation of state (see Fig. 5.10). These data at pressures near ambient differ from the saturated liquid density data by this amount. The data are consistently offset from the equation here proposed at all pressures.

The measurements presented in Neruchev *et al.* [97] and Dutour *et al.* [96] are the only available data for *n*-docosane **speed of sound** as shown in Fig. 5.8. Between (353 and 373) K the two sets overlap, and the deviations from the equation and both sets are lower than 0.2% at ambient pressure. Over their whole temperature range from (333 to 473) K the Neruchev data are accurately represented by the equation of state, with a maximum deviation of 0.44%. The data presented by Dutour *et al.* deviate from the equation of state within 1.7%, but for the measurements performed at ambient pressure, the maximum deviation is less than 0.3%.

For the **isobaric heat capacity**, just two sets of data are available: Atkinson *et al.* [100] and Durupt *et al.* [99]. The plot of the deviations of the data with respect to the equation of state shows opposite trends as shown in Fig. 5.12, and the deviations increase at higher temperatures. The deviations of the Atkinson *et al.* data vary from of +0.6% at 320 K to -2.6% at 450 K, while the deviations of Durupt data are 2.2% at 273 K and increase to 5.4% at 473 K.

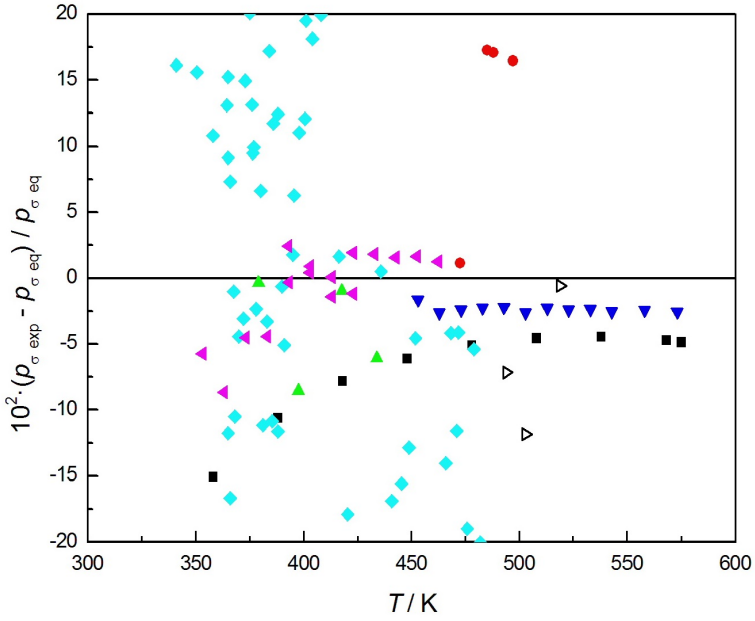

Figure 5.8: Deviation of the experimental vapor pressures from the equation of state (zero line) for *n*-docosane: ■, Chickos and Hanshaw; ●, Francis and Wood; △, Grenier *et al.*; ▼, Morgan and Kobayashi; ♦, Piacente *et al.*; ◀, Sasse *et al.*; ▷, Young.

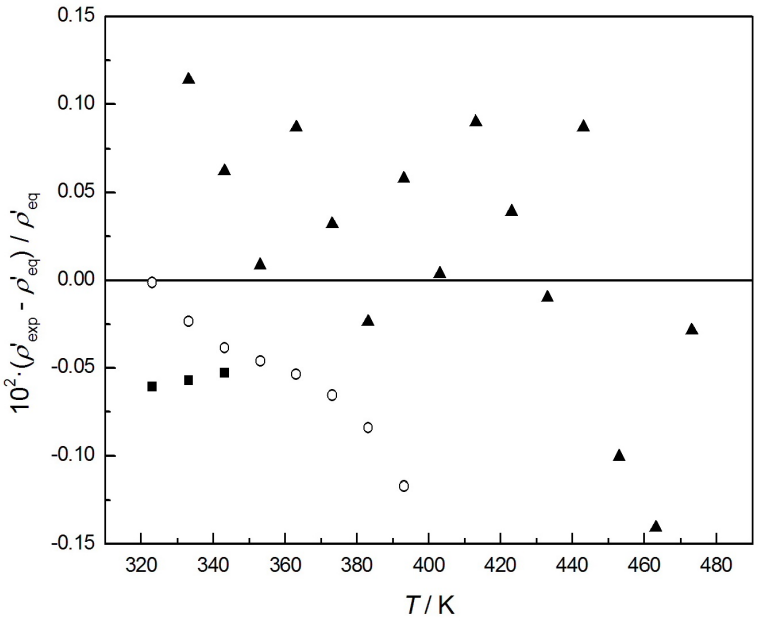

Figure 5.9: Deviation of the experimental saturated liquid densities from the equation of state (zero line) for *n*-docosane: ■, Queimada *et al.*; ○, Dutour *et al.*; ▲, Neruchev *et al.*

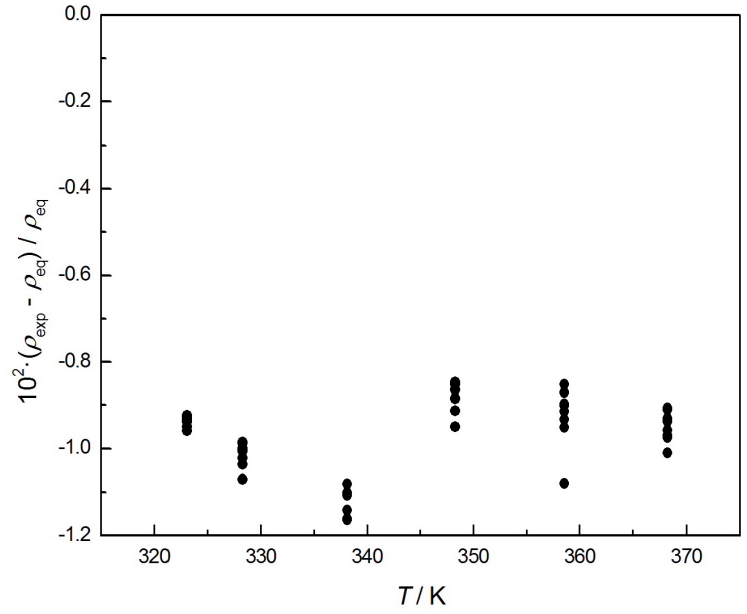

Figure 5.10: Deviation of the experimental densities from the equation of state (zero line) for *n*-docosane: •, Peters *et al.*

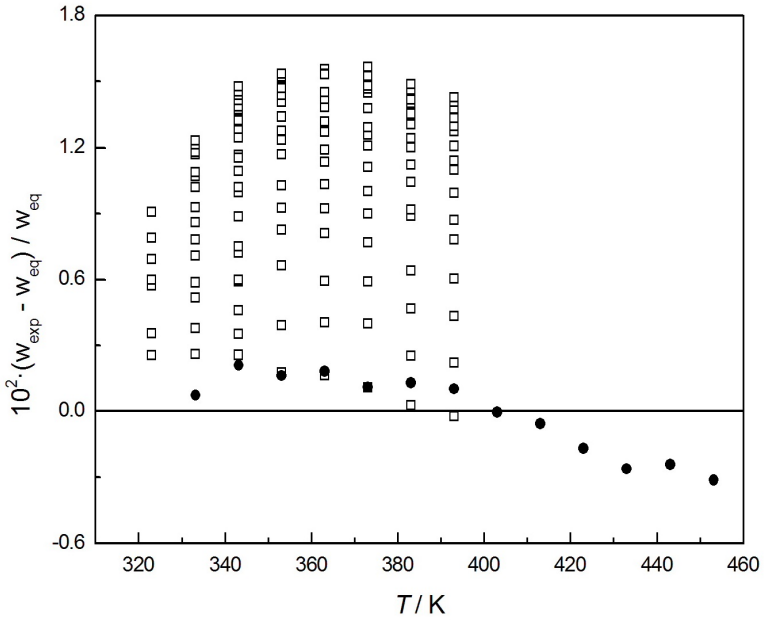

Figure 5.11: Deviation of the experimental speed of sound from the equation of state for *n*-docosane: □, Dutour *et al.*; •, Neruchev *et al.*

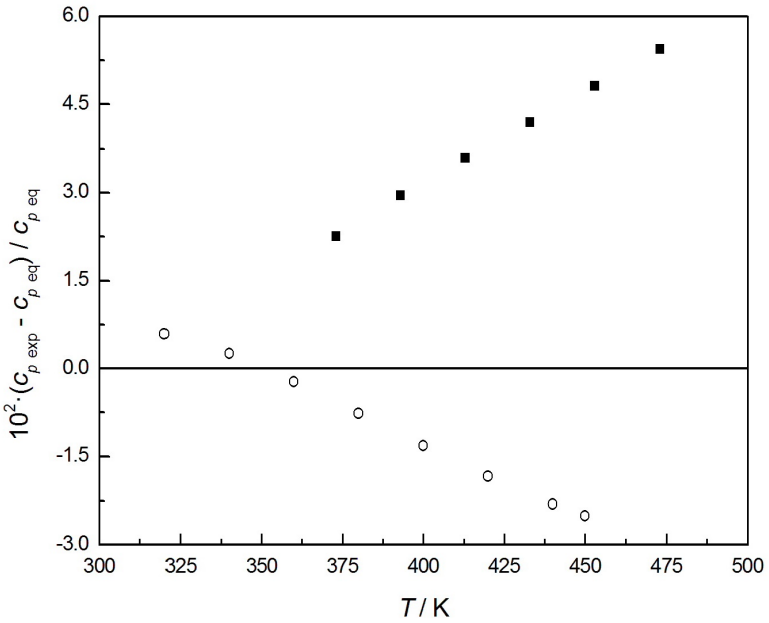

Figure 5.12: Deviation of the experimental isobaric heat capacity from the equation of state (zero line) for *n*-docosane: ■, Durupt *et al*; ○, Atkinson *et al.*

5.6 Extrapolation behavior

The REFPROP software (NIST Reference Fluid Thermodynamic and a Transport Properties Database) [31] was used to generate diagrams for inspection of the extrapolation behavior of the equation for both analyzed fluids. One of the most important parameters used to verify the correct behavior of the equations is the phase identification parameter (PIP) defined in the work of Venkatarathnam and Oellrich [33], as follows

$$\Pi = 2 - \rho \left[\frac{\dfrac{\partial^2 p}{\partial \rho \partial T}}{\left(\dfrac{\partial p}{\partial T}\right)_\rho} - \frac{\left(\dfrac{\partial^2 p}{\partial \rho^2}\right)_T}{\left(\dfrac{\partial p}{\partial \rho}\right)_T} \right] \quad . \tag{5.20}$$

This is a very sensitive property from which small inconsistencies can be seen that are not visible with other properties. The PIP is now used heavily during fitting to determine the quality of the fit.

This parameter identifies the pseudo-phase of a state above the critical temperature. If the value is greater than one it indicates either a liquid state or a liquid-like vapor state, while if Π is less than one, it indicates a vapor state.

In Fig. 5.13 the PIP for *n*-hexadecane as a function of temperature is shown, along isobars and at saturation states. The plot shows positive curvature in most of the liquid region, except for the region between 150 K and about 200 K. At very low temperature (below 20 K) the curvature is still negative. This behavior of the PIP is also present in the plots for R-1234z(E) reported in the work of Thol and Lemmon [101] and for R-245ca reported in Zhou end Lemmon [102]. Similar behavior could be observed in the plot of the PIP versus temperature for *n*-docosane, shown in Fig. 5.14. The curvature is almost positive over the liquid region, although it becomes slightly negative between 175 K and 205 K. The PIP for *n*-docosane, even at temperature lower than 15 K, has positive curvature. The validation of the equations can also be done by checking the behavior of some other properties such as density, speed of sound, heat capacity, and ideal curves. All these properties show the expected trends as explained in other recent publication on equation of state, such as the work for the equation of state of propane [28] or R-125 [103]. Since the behavior of these parameters is similar to that of some other fluids, the plots are not reported here.

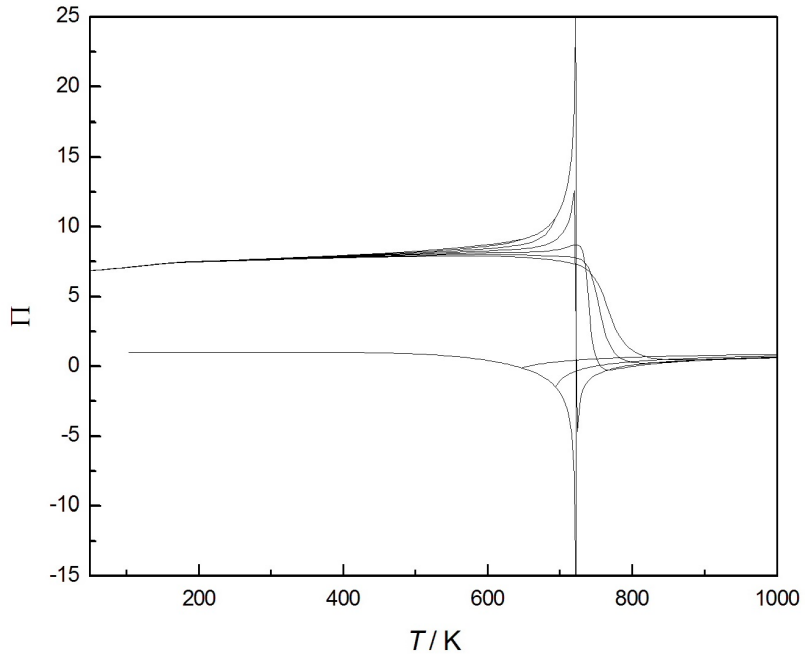

Figure 5.13: Phase identification parameter (PIP) as a function of temperature for n-hexadecane along isobars.

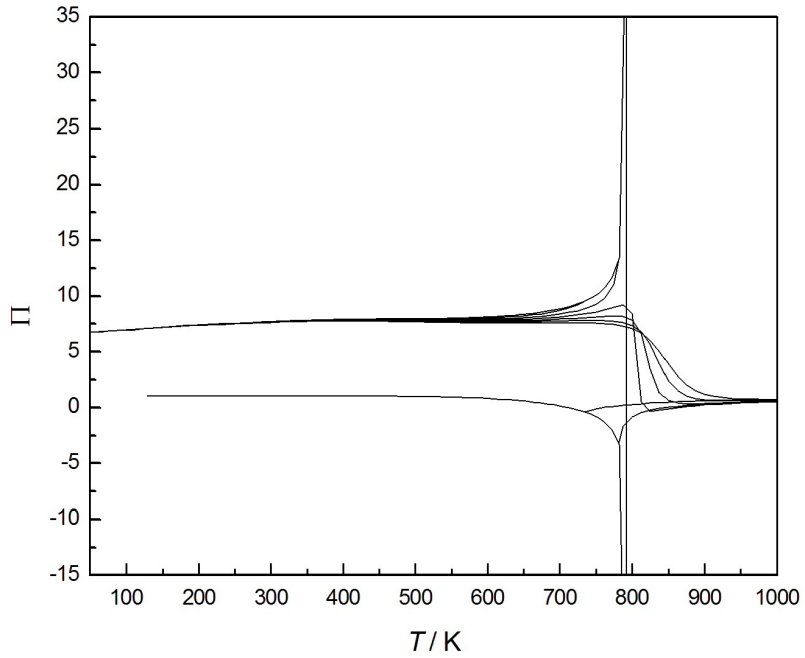

Figure 5.14: Phase identification parameter (PIP) as a function of temperature for n-docosane along isobars.

5.6.1 Representation of the ideal curves

The ideal curves are curves along which one property of a real fluid is equal to the hypothetical ideal gas considering the same temperature and density. Even if this definition can refer to any properties, usually the ideal curves of the compressibility factor and the derivatives are considered, defined in terms of the compression factor, $Z(T,\rho)$, and of the residual Helmholtz energy, $\alpha(T,\rho)$ as follows [30]

Ideal curve:

$$Z = 1 \qquad \left(\frac{\partial \alpha^{\mathrm{r}}}{\partial \delta}\right)_{\tau} = 0$$

Boyle curve:

$$\left(\frac{\partial Z}{\partial \rho}\right)_{T} = 0 \qquad \left(\frac{\partial \alpha^{\mathrm{r}}}{\partial \delta}\right)_{\tau} + \delta \left(\frac{\partial^2 \alpha^{\mathrm{r}}}{\partial \delta^2}\right)_{\tau} = 0$$

Joule-Thomson curve:

$$\left(\frac{\partial Z}{\partial T}\right)_{p} = 0 \qquad \left(\frac{\partial \alpha^{\mathrm{r}}}{\partial \delta}\right)_{\tau} + \left(\frac{\partial^2 \alpha^{\mathrm{r}}}{\partial \delta^2}\right)_{\tau} + \tau \left(\frac{\partial^2 \alpha^{\mathrm{r}}}{\partial \delta \partial \tau}\right) = 0$$

Joule inversion curve:

$$\left(\frac{\partial Z}{\partial T}\right)_{\rho} = 0 \qquad \tau \left(\frac{\partial^2 \alpha^{\mathrm{r}}}{\partial \delta \partial \tau}\right) = 0$$

The ideal curves are used to judge the behavior of the equation of state. Even if the curves do not provide numerical information, reasonable shapes of the curves, such as the plots for propane [28], indicate a qualitatively correct extrapolation behavior of the equation of state extending to high pressures and temperatures far in excess of the likely thermal stability of the fluid. Consequently, the behavior of the ideal curves should always be analyzed and checked during the equation development process. Figures 5.15 and 5.16 show the plots of the ideal curves obtained for *n*-hexadecane and *n*-docosane, which have the shape expected, so the extrapolations can be considered correct.

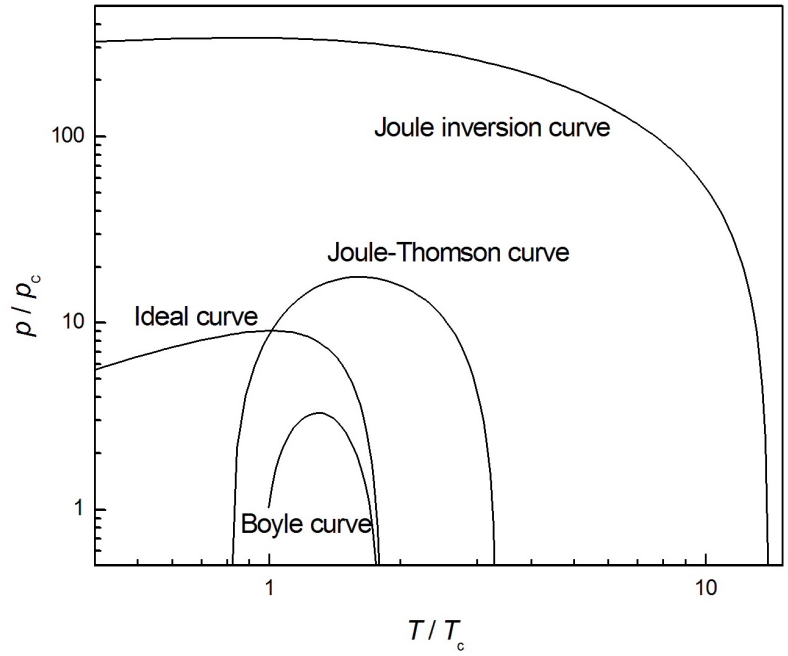

Figure 5.15: Ideal curves for n-hexadecane.

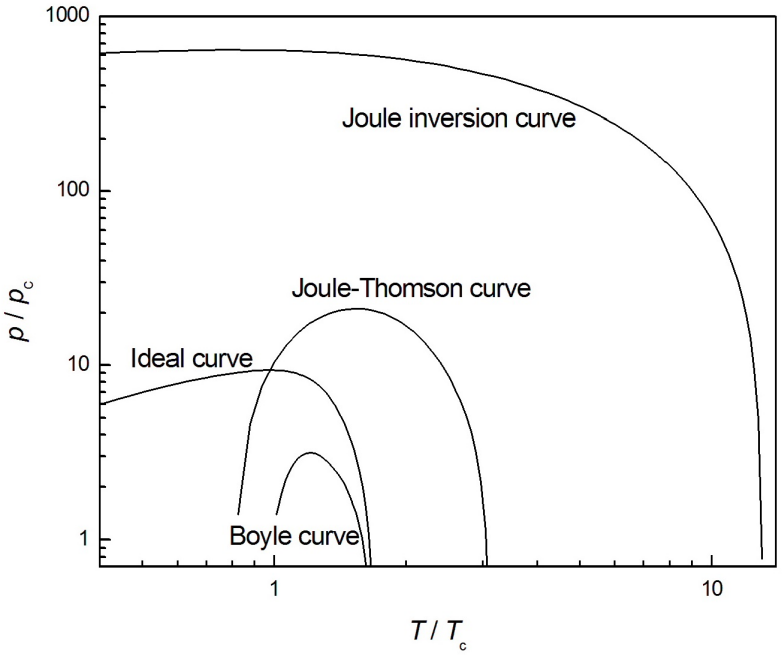

Figure 5.16: Ideal curves for n-docosane.

Conclusions

Water has always been studied since it is involved in various fields of science, in industrial applications, and also commonly used as reference fluid. However, water presents many anomalies causing several gaps in the knowledge of its properties. The need of water investigation grows even further if extreme regions of the phase diagram, or its metastable states, are considered. Particularly, experimental measurements of the thermophysical properties of metastable liquid water that are paramount for developing the equation of state, are absent or lacking of the needed accuracy. The aim of this thesis was indeed to perform measurements of liquid water density in cooled and supercooled regions at very high pressures.

A new experimental apparatus to measure density was realized at the *Istituto Nazionale di Ricerca Metrologica* (INRiM) laboratories. Because of the extreme working conditions of temperature and pressure, and the necessity to maintain water in metastable states, measurements were carried out by using a pseudo-isochoric method, consisting of a measuring high pressure vessel of known volume, connected to an expansion cell to determine the mass of the sample under study. The density of liquid water both in stable and metastable states was measured at temperatures between (243 and 283) K and at pressures from (140 to 400) MPa.

Because of the wide range of temperature and pressure investigated, an accurate calibration of the measuring volume was necessary to estimate experimentally the elastic properties of the apparatus. Before performing the measurements in the subcooled states, the method was validated at temperatures between (278 and 353) K and pressures from (50 to 150) MPa corresponding to accurate values of density given in the literature (uncertainty in the order of 0.003%). All the experimental values resulted in good agreement with densities provided by the IAPWS equation of state [10]. Subcooled water density was then measured along eight constant-mass curves with an overall relative uncertainty of 0.07%. Experimental results were compared with the two most advanced equations of state (IAPWS-95 [10] and Holten *et al.* [11] formulations), with all measured points within the combined uncertainty. In particular, very good agreement between the results of this work and Holten's equation was observed, although the deviations increased systematically for the highest densities. However, in

the supercooled region, which is outside the range of validity, IAPWS equation shows an opposite trend with respect to the experimental curves and Holten's equation. The measurements of this work were also compared with the experimental values available in the literature, i.e. Sotani *et al.* [16], Asada *et al.* [17], Guignon *et al.* [18] and Mishima [19]. The experimental data that overlap the temperature and pressure range here investigated were considered. An interpolation function, developed by the experimental values through the least square analysis, and valid over the measured pressure and temperature range, was used to evaluate and compare the densities at the same thermodynamic states measured by the cited authors. Considering the declared uncertainties, the comparison showed a good agreement among the experimental works.

The good experimental density results of this work, which confirm the previous experimental data, may allow the improvement of the current equation of state close to the melting curve and the development of a more accurate water equation of state in the supercooled region. Further developments will regard the increase in the pressure and temperature range of investigation, in particular measuring density at lower temperatures, by improving the experimental apparatus. Moreover, the next step will be to start up the experiment for the measurements of speed of sound in the supercooled region up to 400 MPa, which are almost absent in the literature (as reported in Holten *et al.* [11]).

The importance of having experimental measurements of density, along with heat capacity, speed of sound and vapor pressure, is relevant because these data are the basis for developing a fundamental equation of state, which allows to obtain all the thermodynamic properties over the whole fluid range. Nowadays, fundamental equations of state are commonly developed in terms of Helmholtz energy. This functional form was also used in this work to implement the equations of state of two alkanes. Indeed, the last part of the thesis, carried out at the National Institute of Standards and Technology (NIST), gives an overview of how an equation of state is developed, how experimental measurements are used in the process and the practical example of equations implementation. The fluids under study were *n*-hexadecane ($C_{16}H_{34}$) and *n*-docosane ($C_{22}H_{46}$), two alkanes mainly applied in aviation as fuel. Firstly, the experimental data of density, speed of sound, vapor pressure and heat capacity were collected. Then, by means of an iterative nonlinear least squares fitting process, the coefficients and exponents of the polynomial equation of the Helmholtz energy as a function of temperature and density were calculated. The equations were validated by comparing them with the experimental measurements as well as by evaluating qualitatively the extrapolation behavior of its properties. The final equations of state for *n*-hexadecane and *n*-docosane have been presented.

Bibliography

[1] P. G. Debenedetti, "Supercooled and glassy water," *Journal of Physics: Condensed Matter*, vol. 15, no. 45, p. R1669, 2003.

[2] J. Kalová, *Thermodynamic modeling of supercooled water*. PhD thesis, University of West Bohemia, Faculty of Mechanical Engineering, Pilsen, 2012.

[3] A. J. Heymsfield and L. M. Miloshevich, "Homogeneous ice nucleation and supercooled liquid water in orographic wave clouds," *Journal of the Atmospheric Sciences*, vol. 50, no. 15, pp. 2335–2353, 1993.

[4] D. Rosenfeld and W. L. Woodley, "Deep convective clouds with sustained supercooled liquid water down to -37.5 °C," *Nature*, vol. 405, no. 6785, pp. 440–442, 2000.

[5] L. Otero and P. D. Sanz, "High-pressure shift freezing. part 1. amount of ice instantaneously formed in the process," *Biotechnology Progress*, vol. 16, no. 6, pp. 1030–1036, 2000.

[6] T. A. Berendsen, B. G. Bruinsma, C. F. Puts, N. Saeidi, O. B. Usta, B. E. Uygun, M.-L. Izamis, M. Toner, M. L. Yarmush, and K. Uygun, "Supercooling enables long-term transplantation survival following 4 days of liver preservation," *Nature medicine*, vol. 20, no. 7, pp. 790–793, 2014.

[7] O. Schlüter, G. U. Benet, V. Heinz, and D. Knorr, "Metastable states of water and ice during pressure-supported freezing of potato tissue," *Biotechnology progress*, vol. 20, no. 3, pp. 799–810, 2004.

[8] T. Norton and D.-W. Sun, "Recent advances in the use of high pressure as an effective processing technique in the food industry," *Food and Bioprocess Technology*, vol. 1, no. 1, pp. 2–34, 2008.

[9] W. Wagner and M. Thol, "The behavior of IAPWS-95 from 250 to 300 K and pressures up to 400 MPa: Evaluation based on recently derived property data," *Journal of Physical and Chemical Reference Data*, vol. 44, no. 4, p. 043102, 2015.

[10] W. Wagner and A. Pruß, "The IAPWS formulation 1995 for the thermodynamic properties of ordinary water substance for general and scientific use," *Journal of Physical and Chemical Reference Data*, vol. 31, no. 2, pp. 387–535, 2002.

[11] V. Holten, J. V. Sengers, and M. A. Anisimov, "Equation of state for supercooled water at pressures up to 400 MPa," *Journal of Physical and Chemical Reference Data*, vol. 43, no. 4, p. 043101, 2014.

[12] M. O. McLinden and C. Lösch-Will, "Apparatus for wide-ranging, high-accuracy fluid (p, ρ, t) measurements based on a compact two-sinker densimeter," *The Journal of Chemical Thermodynamics*, vol. 39, no. 4, pp. 507–530, 2007.

[13] J. Zhou, *Automatic isochoric apparatus for PVT and phase equilibrium studies of natural gas mixtures*. PhD thesis, Texas A&M University, 2005.

[14] S. Lorefice, R. Romeo, M. Santiano, and A. Capelli, "Original pycnometers for volatile liquid density over wide ranges of temperature and pressure: practical example," *Metrologia*, vol. 51, no. 3, p. 154, 2014.

[15] A. Goodwin, K. Marsh, and W. Wakeham, *Measurement of the thermodynamic properties of single phases*. Elsevier, 2003.

[16] T. Sotani, J. Arabas, H. Kubota, M. Kijima, and S. Asada, "Volumetric behaviour of water under high pressure at subzero temperature," *High Temperatures - High Pressures*, vol. 32, no. 4, pp. 433–440, 2000.

[17] S. Asada, T. Sotani, J. Arabas, H. Kubota, S. Matsuo, and Y. Tanaka, "Density of water at subzero temperature under high pressure: measurements and correlation," *Journal of Physics: Condensed Matter*, vol. 14, no. 44, p. 11447, 2002.

[18] B. Guignon, C. Aparicio, and P. D. Sanz, "Specific volume of liquid water from (253 to 323) K and pressures up to 350 MPa by volumetric measurements," *Journal of Chemical & Engineering Data*, vol. 55, no. 9, pp. 3338–3345, 2010.

[19] O. Mishima, "Volume of supercooled water under pressure and the liquid-liquid critical point," *The Journal of chemical physics*, vol. 133, no. 14, p. 144503, 2010.

[20] G. Kell and E. Whalley, "Reanalysis of the density of liquid water in the range 0–150 °C and 0–1 kbar," *The Journal of Chemical Physics*, vol. 62, no. 9, pp. 3496–3503, 1975.

[21] B. F. Langer, "Design-stress basis for pressure vessels," *Experimental Mechanics*, vol. 11, no. 1, pp. 1–11, 1971.

[22] S. Lorefice, "Traceability and uncertainty analysis in volume measurements," *Measurement*, vol. 42, no. 10, pp. 1510–1515, 2009.

[23] S. Davidson, M. Perkin, and M. Buckley, *The measurement of mass and weight*. National Physical Laboratory, 2004.

[24] "Evaluation of measurement data-guide to the expression of uncertainty in measurement, JCGM 100: 2008 GUM 1995 with minor corrections," tech. rep., BIPM, IEC and IFCC, ILAC and ISO, IUPAC and IUPAP, OIML, Paris: Joint Committee for Guides in Metrology, France, 2008.

[25] V. Holten, C. Bertrand, M. Anisimov, and J. Sengers, "Thermodynamics of supercooled water," *The Journal of chemical physics*, vol. 136, no. 9, p. 094507, 2012.

[26] E. W. Lemmon and A. Goodwin, "Critical properties and vapor pressure equation for alkanes C_nH_{2n+2}: Normal alkanes with $n \leq 36$ and isomers for $n = 4$ through $n = 9$," *Journal of Physical and Chemical Reference Data*, vol. 29, no. 1, pp. 1–39, 2000.

[27] "http://webbook.nist.gov/chemistry/."

[28] E. W. Lemmon, M. O. McLinden, and W. Wagner, "Thermodynamic properties of propane. III. A reference equation of state for temperatures from the melting line to 650 K and pressures up to 1000 MPa," *Journal of Chemical & Engineering Data*, vol. 54, no. 12, pp. 3141–3180, 2009.

[29] P. J. Mohr, B. N. Taylor, and D. B. Newell, "Codata recommended values of the fundamental physical constants: 2010a)," *Journal of Physical and Chemical Reference Data*, vol. 41, no. 4, p. 043109, 2012.

[30] R. Span, *Multiparameter equations of state: an accurate source of thermodynamic property data*. Springer Science & Business Media, 2000.

[31] E. W. Lemmon, M. L. Huber, and M. O. McLinden, "NIST Standard Reference Database 23: Reference fluid thermodynamic and transport properties - REFPROP, version 9.1, standard reference data program;

National Institute of Standards and Technology: Gaithersburg, MD, 2013,"

[32] A. Cornfeld and H. Carr, "Experimental evidence concerning the law of rectilinear diameter," *Physical Review Letters*, vol. 29, no. 1, pp. 28–32, 1972.

[33] G. Venkatarathnam and L. Oellrich, "Identification of the phase of a fluid using partial derivatives of pressure, volume, and temperature without reference to saturation properties: Applications in phase equilibria calculations," *Fluid Phase Equilibria*, vol. 301, no. 2, pp. 225–233, 2011.

[34] T. M. Aminabhavi and G. Bindu, "Densities, viscosities, refractive indices, and speeds of sound of the binary mixtures of bis (2-methoxyethyl) ether with nonane, decane, dodecane, tetradecane, and hexadecane at 298.15, 308.15, and 318.15 K," *Journal of Chemical and Engineering Data*, vol. 39, no. 3, pp. 529–534, 1994.

[35] S. Ball and J. Trusler, "Speed of sound of *n*-hexane and *n*-hexadecane at temperatures between 298 and 373 K and pressures up to 100 MPa," *International Journal of Thermophysics*, vol. 22, no. 2, pp. 427–443, 2001.

[36] J. Boelhouwer, "Sound velocities in and adiabatic compressibilities of liquid alkanes at various temperatures and pressures," *Physica*, vol. 34, no. 3, pp. 484–492, 1967.

[37] M. F. Bolotnikov, Y. A. Neruchev, Y. F. Melikhov, V. N. Verveyko, and M. V. Verveyko, "Temperature dependence of the speed of sound, densities, and isentropic compressibilities of hexane + hexadecane in the range of (293.15 to 373.15) K," *Journal of Chemical & Engineering Data*, vol. 50, no. 3, pp. 1095–1098, 2005.

[38] T. S. Khasanshin and A. P. Shchemelev, "Sound velocity in liquid *n*-alkanes," *High Temperature*, vol. 39, no. 1, pp. 60–67, 2001.

[39] F. P. Nascimento, A. Mehl, D. C. Ribas, M. L. Paredes, A. L. Costa, and F. L. Pessoa, "Experimental high pressure speed of sound and density of (tetralin+*n*-decane) and (tetralin+*n*-hexadecane) systems and thermodynamic modeling," *The Journal of Chemical Thermodynamics*, vol. 81, pp. 77–88, 2015.

[40] Y. A. Neruchev, M. Bolotnikov, and V. Zotov, "Investigation of ultrasonic velocity in organic liquids on the saturation curve," *High temperature*, vol. 43, no. 2, pp. 266–309, 2005.

[41] S. Outcalt, A. Laesecke, and T. J. Fortin, "Density and speed of sound measurements of hexadecane," *The Journal of Chemical Thermodynamics*, vol. 42, no. 6, pp. 700–706, 2010.

[42] M. L. Paredes, R. A. Reis, A. A. Silva, R. N. Santos, and G. J. Santos, "Densities, sound velocities, and refractive indexes of tetralin + *n*-hexadecane at (293.15, 303.15, 313.15, 323.15, 333.15, and 343.15) K," *Journal of Chemical & Engineering Data*, vol. 56, no. 11, pp. 4076–4082, 2011.

[43] F. Plantier, A. Danesh, M. Sohrabi, J.-L. Daridon, F. Gozalpour, and A. C. Todd, "Measurements of the speed of sound for mixtures of methane + butane with a particular focus on the critical state," *Journal of Chemical & Engineering Data*, vol. 50, no. 2, pp. 673–676, 2005.

[44] D. J. Luning Prak, R. E. Morris, J. S. Cowart, L. J. Hamilton, and P. C. Trulove, "Density, viscosity, speed of sound, bulk modulus, surface tension, and flash point of direct sugar to hydrocarbon diesel (DSH-76) and binary mixtures of *n*-hexadecane and 2, 2, 4, 6, 6-pentamethylheptane," *Journal of Chemical & Engineering Data*, vol. 58, no. 12, pp. 3536–3544, 2013.

[45] J. A. Amorim, O. Chiavone-Filho, M. L. Paredes, and K. Rajagopal, "High-pressure density measurements for the binary system cyclohexane + *n*-hexadecane in the temperature range of (318.15 to 413.15) K," *Journal of Chemical & Engineering Data*, vol. 52, no. 2, pp. 613–618, 2007.

[46] T. Banipal, S. Garg, and J. Ahluwalia, "Heat capacities and densities of liquid *n*-octane, *n*-nonane, *n*-decane, and *n*-hexadecane at temperatures from 318.15 K to 373.15 K and at pressures up to 10 MPa," *The Journal of Chemical Thermodynamics*, vol. 23, no. 10, pp. 923–931, 1991.

[47] J. Boelhouwer, "*pvt* relations of five liquid *n*-alkanes," *Physica*, vol. 26, no. 11, pp. 1021–1028, 1960.

[48] J.-S. Chang, M.-J. Lee, and H.-m. Lin, "Densities of binary mixtures of hexadecane with m-xylene and tetralin from 333 K to 413 K and pressures up to 30 MPa," *Journal of Chemical & Engineering Data*, vol. 43, no. 2, pp. 233–237, 1998.

[49] A. K. Doolittle, "Specific volumes of *n*-alkanes.," *Journal of Chemical & Engineering Data*, vol. 9, no. 2, pp. 275–279, 1964.

[50] J. Dymond, K. Young, and J. Isdale, "p, ρ, T behaviour for n-hexane + n-hexadecane in the range 298 to 373 K and 0.1 to 500 MPa," *The Journal of Chemical Thermodynamics*, vol. 11, no. 9, pp. 887–895, 1979.

[51] J. H. Dymond and K. R. Harris, "The temperature and density dependence of the self-diffusion coefficient of n-hexadecane," *Molecular Physics*, vol. 75, no. 2, pp. 461–466, 1992.

[52] M. Glaser, C. Peters, H. Van Der Kool, and R. Lichtenthaler, "Phase equilibria of (methane + n-hexadecane) and (p, vm, t) of n-hexadecane," *The Journal of Chemical Thermodynamics*, vol. 17, no. 9, pp. 803–815, 1985.

[53] P. Gouel, "Specific volume of cycloalkanes and alkylbenzenes (C_6-C_{16})," *Bull. Cent. Rech. Explor.-Prod. Elf-Aquitaine*, vol. 2, pp. 211–225, 1978.

[54] M. A. Matthews, J. B. Rodden, and A. Akgerman, "High-temperature diffusion, viscosity, and density measurements in n-hexadecane," *Journal of Chemical and Engineering Data*, vol. 32, no. 3, pp. 317–319, 1987.

[55] P. Snyder and J. Winnick, "The pressure, volume and temperature properties of liquid n-alkanes at elevated pressures," in *Proceedings of the Symposium on Thermophysical Properties*, vol. 5, pp. 115–129, 1970.

[56] Y. Tanaka, H. Hosokawa, H. Kubota, and T. Makita, "Viscosity and density of binary mixtures of cyclohexane with n-octane, n-dodecane, and n-hexadecane under high pressures," *International journal of thermophysics*, vol. 12, no. 2, pp. 245–264, 1991.

[57] Y. Wu, B. Bamgbade, K. Liu, M. A. McHugh, H. Baled, R. M. Enick, W. A. Burgess, D. Tapriyal, and B. D. Morreale, "Experimental measurements and equation of state modeling of liquid densities for long-chain n-alkanes at pressures to 265 MPa and temperatures to 523 K," *Fluid Phase Equilibria*, vol. 311, pp. 17–24, 2011.

[58] A. Wurflinger, D. Mondieig, F. Rajabalee, and M. A. Cuevas-Diarte, "*pvt* measurements and related studies on the binary system nc," *Zeitschrift für Naturforschung A*, vol. 56, pp. 626–634, 2001.

[59] A. Zolghadr, M. Escrochi, and S. Ayatollahi, "Temperature and composition effect on CO_2 miscibility by interfacial tension measurement," *Journal of Chemical & Engineering Data*, vol. 58, no. 5, pp. 1168–1175, 2013.

[60] M. Baba, L. Dordain, J.-Y. Coxam, and J.-P. Grolier, "Calorimetric measurements of heat capacities and heats of mixing in the range 300-570 K and up to 30 MPa," *Indian Journal of Technology*, vol. 30, no. 11-12, pp. 553–558, 1992.

[61] M. S. Benson, P. S. Snyder, and J. Winnick, "Heat capacities of liquid *n*-alkanes at elevated pressures," *The Journal of Chemical Thermodynamics*, vol. 3, no. 6, pp. 891–898, 1971.

[62] M. Gollis, L. Belenyessy, B. Gudzinowicz, S. Koch, J. Smith, and R. Wineman, "Evaluation of pure hydrocarbons as jet fuels.," *Journal of Chemical and Engineering Data*, vol. 7, no. 2, pp. 311–316, 1962.

[63] A. F. A. Asfour, M. H. Siddique, and T. D. Vavanellos, "Density-composition data for eight binary systems containing toluene or ethylbenzene and C_8-C_{16} *n*-alkanes at 293.15, 298.15, 308.15, and 313.15 K," *Journal of Chemical and Engineering Data*, vol. 35, no. 2, pp. 192–198, 1990.

[64] A. Aucejo, M. C. Burguet, R. Munoz, and J. L. Marques, "Densities, viscosities, and refractive indices of some *n*-alkane binary liquid systems at 298.15 K," *Journal of Chemical and Engineering Data*, vol. 40, no. 1, pp. 141–147, 1995.

[65] I. Baños, F. Sánchez, P. Pérez, J. Valero, and M. Gracia, "Vapour pressures of butan-1-ol with *n*-hexadecane between 293.18 and 323.18 K. description of butan-1-ol+ *n*-alkane systems by ERAS model," *Fluid Phase Equilibria*, vol. 81, pp. 165–174, 1992.

[66] G. Calingaert, H. A. Beatty, R. C. Kuder, and G. Thomson, "Homologous series of alkanes," *Industrial & Engineering Chemistry*, vol. 33, no. 1, pp. 103–106, 1941.

[67] D. L. Camin, A. F. Forziati, and F. D. Rossini, "Physical properties of *n*-hexadecane, *n*-decylcyclopentane, *n*-decylcyclohexane, 1-hexadecene and *n*-decylbenzene," *The Journal of Physical Chemistry*, vol. 58, no. 5, pp. 440–442, 1954.

[68] J. Dymond, K. Young, and J. Isdale, "Transport properties of nonelectrolyte liquid mixtures – II. viscosity coefficients for the *n*-hexane + *n*-hexadecane system at temperatures from 25 to 100 °C at pressures up to the freezing pressure or 500 MPa," *International Journal of Thermophysics*, vol. 1, no. 4, pp. 345–373, 1980.

[69] M. M. El-Banna and M. M. El-Batouti, "Temperature dependence of the excess volumes of binary mixtures containing cyclohexane + some higher *n*-alkanes," *Canadian journal of chemistry*, vol. 76, no. 12, pp. 1860–1866, 1998.

[70] P. Espeau and R. Céolin, "A simple method to determine the specific volumes of liquids and melts as a function of the temperature: Application to four *n*-alkanes ($C_{16}H_{34}$, $C_{18}H_{38}$, $C_{19}H_{40}$ and $C_{21}H_{44}$) under saturating vapour pressure in the 298–573 K range," *Thermochimica acta*, vol. 445, no. 1, pp. 32–35, 2006.

[71] G. Findenegg, "Dichte und ausdehnungskoeffizient einiger flüssiger alkane," *Monatshefte für Chemie/Chemical Monthly*, vol. 101, no. 4, pp. 1081–1088, 1970.

[72] J. D. Gómez-Ibáñez and C.-T. Liu, "The excess volume of binary mixtures of normal alkanes," *The Journal of Physical Chemistry*, vol. 67, no. 6, pp. 1388–1391, 1963.

[73] G. H. Graaf, H. J. Smit, E. J. Stamhuis, and A. A. Beenackers, "Gas-liquid solubilities of the methanol synthesis components in various solvents," *Journal of Chemical and Engineering Data*, vol. 37, no. 2, pp. 146–158, 1992.

[74] F. Krafft, "Ueber neunzehn höhere normalparaffine C_nH_{2n+2} und ein einfaches volumgesetz für den tropfbar flüssigen zustand. i," *Berichte der deutschen chemischen Gesellschaft*, vol. 15, no. 2, pp. 1687–1711, 1882.

[75] J. Lauer and R. King, "Refractive index of liquids at elevated temperatures," *Analytical Chemistry*, vol. 28, no. 11, pp. 1697–1701, 1956.

[76] L. Mansker, A. Criser, A. Jangkamolkulchai, and K. Luks, "The isothermal compressibility of *n*-paraffin liquids at low pressures," *Chemical engineering communications*, vol. 57, no. 1-6, pp. 87–93, 1987.

[77] W. M. W. K. Plebanski, TA, "Dilatometric method for measuring the density of organic liquid at elevated temperatures," *Nauchn. Apparat*, vol. 1, pp. 47–59, 1986.

[78] A. J. Queimada, S. Quinones-Cisneros, I. M. Marrucho, J. A. Coutinho, and E. H. Stenby, "Viscosity and liquid density of asymmetric hydrocarbon mixtures," *International journal of thermophysics*, vol. 24, no. 5, pp. 1221–1239, 2003.

[79] A. I. Vogel, "38. Physical properties and chemical constitution. Part IX. Aliphatic hydrocarbons," *Journal of the Chemical Society (Resumed)*, pp. 133–139, 1946.

[80] J. Wu, Z. Shan, and A.-F. A. Asfour, "Viscometric properties of multicomponent liquid *n*-alkane systems," *Fluid Phase Equilibria*, vol. 143, no. 1, pp. 263–274, 1998.

[81] M. A. Abdi and A. Meisen, "Vapor pressure measurements of bis (hydroxyethyl) piperazine and tris (hydroxyethyl) ethylenediamine," *Journal of Chemical & Engineering Data*, vol. 43, no. 2, pp. 133–137, 1998.

[82] F. Eggertsen, E. Seibert, and F. Stross, "Volatility of high-boiling organic materials by a flame ionization detection method," *Analytical Chemistry*, vol. 41, no. 10, pp. 1175–1179, 1969.

[83] C. H. Lee, D. M. Dempsey, R. S. Mohamed, and G. D. Holder, "Vapor-liquid equilibria in the systems of *n*-decane/tetralin, *n*-hexadecane/tetralin, *n*-decane/1-methylnaphthalene, and 1-methylnaphthalene/tetralin," *Journal of Chemical and Engineering Data*, vol. 37, no. 2, pp. 183–186, 1992.

[84] P. L. Mills and R. L. Fenton, "Vapor pressures, liquid densities, liquid heat capacities, and ideal gas thermodynamic properties for 3-methylhexanal and 3, 4-dimethylpentanal," *Journal of Chemical and Engineering Data*, vol. 32, no. 2, pp. 266–273, 1987.

[85] D. L. Morgan and R. Kobayashi, "Direct vapor pressure measurements of ten *n*-alkanes in the C_{10}-C_{28} range," *Fluid Phase Equilibria*, vol. 97, pp. 211–242, 1994.

[86] H. Myers and M. Fenske, "Measurement and correlation of vapor pressure data for high boiling hydrocarbons," *Industrial & Engineering Chemistry*, vol. 47, no. 8, pp. 1652–1658, 1955.

[87] G. S. Parks, G. E. Moore, M. L. Renquist, B. F. Naylor, L. A. McClaine, P. S. Fujii, and J. A. Hatton, "Thermal data on organic compounds. XXV. Some heat capacity, entropy and free energy data for nine hydrocarbons of high molecular weight," *Journal of The American Chemical Society*, vol. 71, no. 10, pp. 3386–3389, 1949.

[88] C. Siitsman, I. Kamenev, and V. Oja, "Vapor pressure data of nicotine, anabasine and cotinine using differential scanning calorimetry," *Thermochimica Acta*, vol. 595, pp. 35–42, 2014.

[89] C. Viton, M. Chavret, E. Behar, and J. Jose, "Vapor pressure of normal alkanes from decane to eicosane at temperatures from 244 K to 469 K and pressures from 0.4 Pa to 164 kPa," *ELDATA: Int. Electron. J. Phys. Chem. Data*, vol. 2, pp. 215–224, 1996.

[90] J. S. Chickos and W. Hanshaw, "Vapor pressures and vaporization enthalpies of the *n*-alkanes from C_{21} to C_{30} at $t = 298.15$ K by correlation gas chromatography," *Journal of Chemical & Engineering Data*, vol. 49, no. 1, pp. 77–85, 2004.

[91] F. Francis and N. E. Wood, "CLXXXIV. The boiling points of some higher aliphatic *n*-hydrocarbons," *Journal of the Chemical Society (Resumed)*, vol. 129, pp. 1420–1423, 1926.

[92] M.-F. Grenier-loustalot, M. Potin-gautier, and P. Grenier, "Applications analytiques de la mesure des tensions de vapeur par saturation d'un gaz inerte cas des alcanes normaux et des polyethyleneglycols," *Analytical Letters*, vol. 14, no. 16, pp. 1335–1349, 1981.

[93] V. Piacente, D. Fontana, and P. Scardala, "Enthalpies of vaporization of a homologous series of *n*-alkanes determined from vapor pressure measurements," *Journal of Chemical and Engineering Data*, vol. 39, no. 2, pp. 231–237, 1994.

[94] K. Sasse, J. Jose, and J.-C. Merlin, "A static apparatus for measurement of low vapor pressures. experimental results on high molecular-weight hydrocarbons," *Fluid Phase Equilibria*, vol. 42, pp. 287–304, 1988.

[95] S. Young, "On the boiling points of the normal paraffins at different pressures," in *Proceedings of the Royal Irish Academy. Section B: Biological, Geological, and Chemical Science*, pp. 65–92, JSTOR, 1928.

[96] S. Dutour, J.-L. Daridon, and B. Lagourette, "Speed of sound, density, and compressibilities of liquid eicosane and docosane at various temperatures and pressures," *High Temperatures - High Pressures*, vol. 33, no. 3, pp. 371–378, 2001.

[97] Z.-V. O. N. Neruchev, YA, "Speed of sound and adiabatic compressibility of some *n*-parafines," *Ukrainian Journal of Physics*, vol. 12, pp. 1385–1387, 1967.

[98] C. Peters, J. Spiegelaar, and J. D. S. Arons, "Phase equilibria in binary mixtures of ethane + docosane and molar volumes of liquid docosane," *Fluid Phase Equilibria*, vol. 41, no. 3, pp. 245–256, 1988.

[99] N. Durupt, A. Aoulmi, M. Bouroukba, and M. Rogalski, "Heat capacities of liquid long-chain alkanes," *Thermochimica acta*, vol. 274, pp. 73–80, 1996.

[100] C. Atkinson, J. Larkin, and M. Richardson, "Enthalpy changes in molten *n*-alkanes and polyethylene," *The Journal of Chemical Thermodynamics*, vol. 1, no. 5, pp. 435–440, 1969.

[101] M. Thol and E. W. Lemmon, "Equation of state for the thermodynamic properties of trans-1, 3, 3, 3-tetrafluoropropene [R-1234ze(E)]," *International Journal of Thermophysics*, vol. 37, no. 3, pp. 1–16, 2016.

[102] Y. Zhou and E. W. Lemmon, "Equation of state for the thermodynamic properties of 1, 1, 2, 2, 3-pentafluoropropane (R-245ca)," *International Journal of Thermophysics*, vol. 37, no. 3, pp. 1–11, 2016.

[103] E. W. Lemmon and R. T. Jacobsen, "A new functional form and new fitting techniques for equations of state with application to pentafluoroethane (HFC-125)," *Journal of physical and chemical reference data*, vol. 34, no. 1, pp. 69–108, 2005.

Acknowledgments

First of all, I want to greatly thank Simona, Salvatore and Alberto for carefully following me during my research and giving me a lot of suggestions and teachings for my work.

Thanks to Andrea Capelli for the realization of the measuring cell and Davide Torchio for helping me for the weighing measurements. With them I thank all my colleagues at INRiM or rather my colleagues of "casa masse" for sharing with me these three years and the colleagues of the acoustic department.

I do want to thank Dr Eric Lemmon (or rather just Eric as he simply wants to be called) for my great American experience at NIST, for all that he has taught me and for his kindness.

I also thank Jill, Tom and Mark for being my Boulder family.

Of course, I must thank my family for supporting all my choices. And finally thank to Davide who supports, helps and encourages me always.